Evaluation of long-term changes of flood risk with deep learning and flood simulation

A Dissertation Submitted for the Doctoral Degree

Candidate: Chantsal Narantsetseg

Supervisor: Prof. Kojima Toshiharu

February 15, 2022

Laboratory of River and Hydrology

Graduate School of Engineering

Gifu University

Contents

List of Figures

List of Tables

CHAPTER 1. INTRODUCTION

1.1. Background

Various studies have been conducted on the effects of land use/land cover changes on various aspects such as disaster prevention, agriculture and water resources. For example, Priess *et al.* [1] investigated feedbacks between land use changes, which are simulated with the land use/land cover dynamics simulation model, and water demand in Central Mongolia, and concluded as the current extend of irrigated agriculture water demands exceed water availability. Moreover, Mandakh *et al.* [2] investigated the land use/land cover changes occurring as a result of human activities in Delgerkhaan Soum of Khentii Province in Eastern Mongolia using Landsat imageries, and defined the impacting factors of water surface area in Avarga Toson Lake area.

For studies of the impact of land use change on some events or phenomena, land use data form multiple periods are needed. One of the most commonly used data for studies of land use change is the result of land use classification with satellite images. Since the launch of Lansat-1 in 1972, satellite imagery has continued to be used to create land use data, because satellite imagery is easier available to provide up-to-date in wide-area. In Japan, EROS, JAXA [3] publishes "High-Resolution Land Use and Land Cover Map Products (HRLULC)" on JAXA's web page, which are produced from ALOS data such as ALOS/AVNIR-2, ALOS/PRISM and ALOS/PALSAR, and other spatial information. HRLULC has several versions since 2006. The latest version is Version 21.03 released in March 2021 with 12 categories and 10-m resolution during 2018 to 2020. Known example of global-scale land use/land cover map is GLCNMO2008 by Tateishi *et al.* [4] GLCNMO2008, which has 500-m special resolution, is produced using Terra and Aqua/MODIS. Data sources are from 2003 to 2013.

While a variety of land use data are available using satellite imagery, from regional to global scales, there is a relative lack of data on land use before the launch of Earth observation satellites. Another method to produced land use data without satellite imagery is to visually read topographic maps. In Japan, the Land Use Subdivision Mesh of National Land Numerical Information is well-known as the land use data produced by visual reading of topographical map. The Land Use Subdivision Mesh of National Land Numerical Information is so-called 100-m mesh, and it has been updated every few years since 1976. Another known example of land use map in Japan is "Saimitsu Suchi Jouhou" produced since 1981, which has 10-m spatial resolution, but available only for urban areas.

As for land use data before 1970 in Japan, there is LUIS [5]. LUIS has been developed nationwide, and at the Meiji/Taisho era, the middle of the Showa era and the end of the Showa era. LUIS is a valuable data set that provides a view of past land use and its evolution, which is not available in other land use data. However, its spatial resolution is as coarse as 2 km, and many studies have been published that have limited the target area and created new historical land use data. Ikemi *et al.* [6] created 100m-mesh land use data from 1/50,000 topographic maps of Fukuoka Prefecture in 1900 and 1950, and studied the spatial distribution of land use change and anthropogenic landform modification. Ohara *et al. [7]* created 500m mesh land use data for the Sapporo area (9 maps), Tokyo area (36 maps), and Osaka area (17 maps) between 1930 and 1970 from 1/50,000 topographic maps, and compared them with numerical elevation data (DEM) to discuss the relationship between land use change and topographic conditions. As described above, for the period before the 1970s, when detailed land use data did not exist, each researcher prepared the land use data in limited area, independently.

On the other hand, in addition to studies on the impact of land use change on some events/phenomena, studies on the impact of some events/phenomena on land use and population have also been conducted. Collenteur *et al.* [8] investigated to understand the impact of the occurrence of flood disasters on the spatial distribution of population dynamics in floodplain areas, and found that a trend of dampened population growth right after the flood followed by an accelerated growth a decade later. The impacts of flood events on floodplain development are so-called “Levee Effects ([9], [10]”, which has been attracting attention in recent years as complex mechanisms between hydrological and social processes in settled floodplain.

In Japan, since the Meiji era (1868-1912), there has been a great deal of river improvement, and it is thought that the land use around the river channel has changed greatly due to the Levee effects. Ito and Nakamura [11] constructed long-term land use data and levee length database by visual reading of the topographical maps from 1870 to 1990 in the lower Kiso river basin, and found that urbanization progressed in the specific area after the levee was established.

However, as mentioned above, it is difficult to obtain detailed land use data before 1970s, and the only way to obtain such data is to visually read topographic maps of only a limited area, as has been done in several studies. Moreover, it is difficult to assess how flood risks have changed due to the development of river infrastructure, rapid urbanization and land use changes, based only on flood cases with little information.

1.2. Research areas

The following study areas have been selected in this research to evaluate long-term changes of flood risk with deep learning and flood simulation for case studies including the region Gifu Prefecture, Japan. (Figure 1.1).

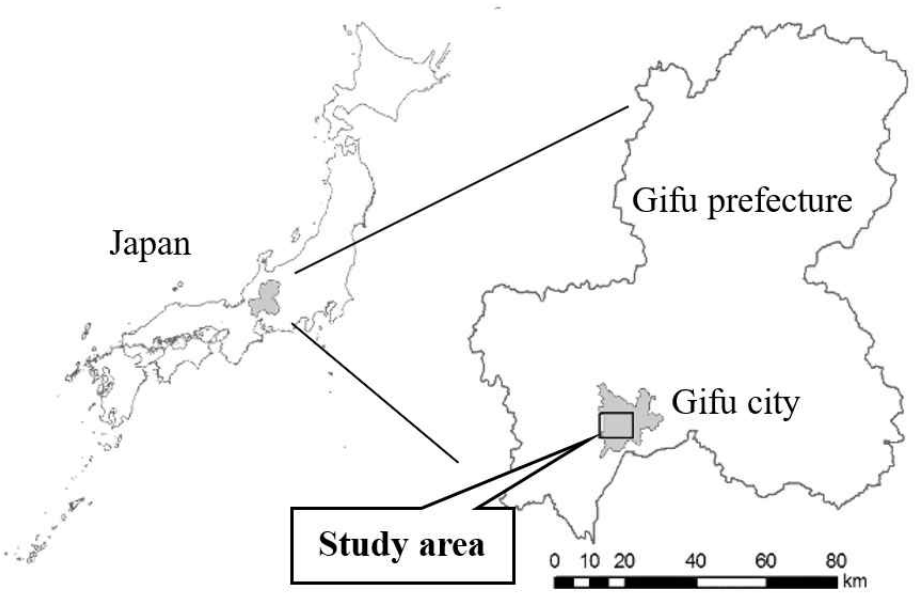

Figure 1.1 Location of the study area in Japan.

The right side of the Nagara River is a flatland, where is the area between the Nagara River, the Ijira River, the Toba River, and Dodogamine mountain. This area is nearly 234 hectares, and it was frequently damaged by flood until to finish the construction of levee to the Furu River and the Furu-Furu River in 1939. (Figure 1.2)

The right levee side of the Nagara River, around Gifu city where the land use significantly changed that as the almost paddy field was changed to the residential area, river width of each river is widening, and the route of each river is changing in the past hundred years. [12]

Figure 1.2 (b) shows the past topographical map, and Figure 1.3 (a) also shows the current topographical. Blue area is river area. Figure 1.2 (a) shows the past Nagara river was diverted to two branches such as the Furu river and the Furu-furu river. On the other hand, Figure 1.3 (a) shows the current Nagara river improved to the mainstream, and some river stream disappears due to river improvement.

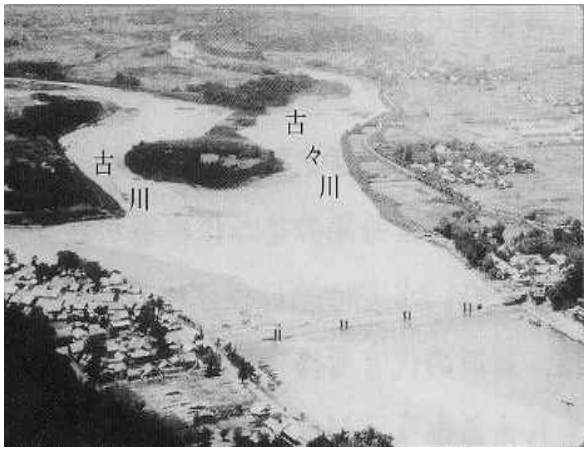

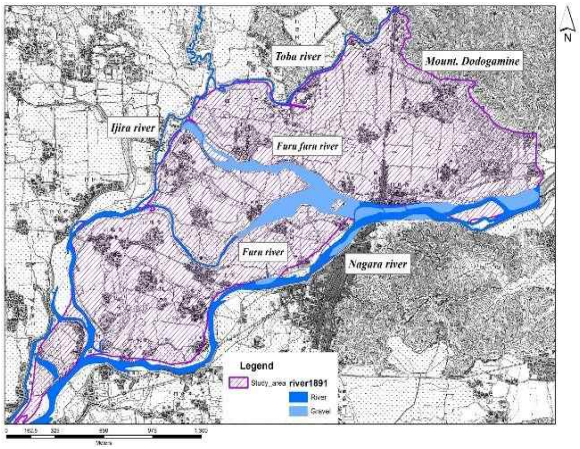

(a) Aerial photograph around the Nagara bridge (b) Topographical map

Figure 1.2 Study area former time (from 1891 till 1939).

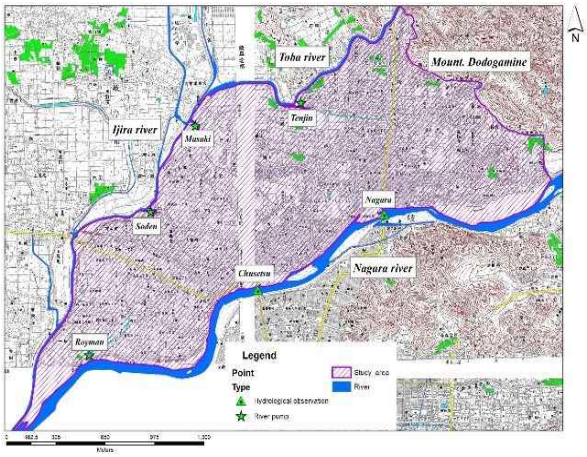

(a) Aerial photograph around the Nagara bridge (b) Topographical map

Figure 1.3 Study area current time (after finish construction of coffer bank in 1939)

1.3. Objectives and structure of the thesis

Main objective of this thesis is to evaluation of long-term changes of flood risk with deep learning and flood simulation. In order to achieve this goal, this dissertation consists of five chapters as below:

Chapter 1. Introduction, this chapter provides relevant background information on issues related to long-term changes in flood risk.

Chapter 2. In the third artificial intelligence boom that began around the 2000s, by doing so, it has become possible to realize a highly practical program, especially in recent years deep

learning has been rapidly developing and expanding to any research fields. Especially, CNN (Convolutional Neural Network) has been used in many cases for image recognition, discrimination and classification. However, while deep learning is being applied to satellite images, there are few examples of their application to topographical maps. Chapter 2 describes about developing and proposing of a classification method for topographical maps using deep learning for practical use.

Chapter 3. In former times, the flatland around the Kiso-River system, included Gifu City, was frequently damaged by inundation after heavy rainfall. The residential area was constructed at relatively higher and well-drained low land and protected by banks so-called "Waju-Tei." But in the current time, the new residential area is widening day by day. On the other hand, there are many mitigation factors of inundation risks, such as the construction of drainage pumps, channels and construction infrastructures for river improvements. Chapter 3 describes about the temporal changes of flood risks from the Meiji era to the current time in Gifu city are investigated with an old topographical map, GIS analysis, and flood simulation.

Chapter 4. Moreover, understanding of "Levee Effect", land use changes and flood risk by flood inundation simulation have not yet been fully investigated. Chapter 3 describes about assessment of long-term flood risk changes with 2D flood simulation and past land use data produced from old topographical maps. But chapter 4 describes about efficiency of the infrastructures such a river improvements and levee effect using 2D flood simulation.

Chapter 5. Conclusion, this chapter described the results summary of this research about evaluating flood risk with deep learning and flood simulation in long term change.

CHAPTER 2. DEVELOPMENT OF LAND USE CLASSIFICATION METHOD FROM TOPOGRAPHICAL MAPS WITH DEEP LEARNING

2.1. Introduction

Land use data is one of the most frequently used spatial information along with topographical data. A typical example of land use data in Japan is land use subdivision mesh data [13] of national land numerical information. This land use subdivision mesh data is a commonly 100m mesh from 1976, and is data that classifies the land use situation nationwide by classification of rice fields, other agricultural land, forests, wasteland, urban area, etc., and has maintained every few years.

Although it depends on the year of maintenance, it is mainly created by visual interpretation from 1:25,000 topographic maps and satellite images of the Geographical Survey Institute. Detailed numerical information [14] can be mentioned as more detailed digital land use information.

Detailed numerical information was created as a result of the residential land use trend survey conducted from 1981 to 1997, and is maintained for the three major metropolitan areas (metropolitan area, Chubu area and Kinki area) with a 10-m mesh. Since 2000, it has been released under the name of Numerical Map 5000 (Land Use) [15]. The land use subdivision mesh data of the national land numerical information is spatially more detailed, and the land use items in urban areas are also divided into general low-rise residential areas, dense low-rise residential areas, middle/high-rise residential areas, and commercial/ commercial land. However, it has the disadvantage that it is not maintained outside the three major metropolitan areas and cannot be applied to a wide area.

The National Land Use Database (LUIS) [16] shows past land use and its transition, which are not maintained by other land use data such as the Meiji/Taisho era, the middle and the end of the Showa era, and is maintained nationwide. This is valuable land use data, and is used for analysis of changes in landscape structure in groups [17] and estimation of past evaporation and scattering [18]. On the other hand, the spatial resolution is as coarse as 2 km, and many studies have been published that have created new past land use data by limiting the target area.

Matsubara *et al*. [19] in order to analyze land-use changes around the Keio University Hiyoshi Campus, used 1:20,000 "Mizoguchi" topographic map published in 1902 and the

1:25,000 "Kawasaki" topographic map published in 1914-1994. This study had read map symbols with a 50m mesh and had created land-use data.

Ikemi *et al.* [20] created 100m mesh land use data from 1:50,000 topographic maps of 1900 and 1950 for the Fukuoka prefecture area, and examined the transition of land use and the spatial distribution of artificial topographical changes. Ohara *et al.* [21] uses a 500m mesh of land use data for the Sapporo area (9 map width), Tokyo area (36 map width), and Osaka area (17 map width) from around 1930 to 1970 from a 1:50,000 topographic map. It was created and compared with digital elevation data (DEM) to discuss the relationship between land use changes and topographical conditions. In addition, Ito and Nakamura [22] created 100m mesh land use data from the 1:20,000 and 1:25,000 topographic maps of the Kiso River basin after the Meiji era, and considered changes in land use in the hinterland due to the construction of embankments. As described above, the current situation is that each researcher independently creates the data before the 1950s, when detailed land use data does not exist.

The main method for creating existing land use data is visual interpretation. One of the methods for creating land use data other than visual interpretation is land use classification using remote sensing images and satellite images. Since the launch of Landasat-1 in 1972, the use of satellite images for land use data creation has been under consideration due to the feature that the latest wide-area information can be easily obtained. As high-resolution land-use data that can be used in Japan, there is a high-resolution land-use cover map published by JAXA in Japan. [3]. It classifies the whole of Japan using high-resolution satellite images such as ALOS AVNIR-2, PRISM, and PLSAR. Currently, version 16.09 released in September 2016 has been released. Satellite images and remote sensing images are mainly classified on a pixel-by-pixel basis (pixel-based) using observation results from multiple wavelengths, while spatial information (textures) such as simultaneous occurrence matrices are used. For example, Donnie *et al.* [23], Franklin *et al.*, [24]and an object-based method of capturing pixels as a spatial set (segment or object) (Lobo *et al.*, [25], Kosaka *et al.* [26], Yamamoto *et al.* [27]) have been proposed.

On the other hand, in deep learning, which has been rapidly developing in recent years, there are many cases of using CNN (Convolutional Neural Network), which is particularly excellent in image recognition, discrimination, and classification.

Ito *et al.* [28] classified CNN classification using a data Landsat-5 (spatial resolution 30-m) and GLCNMO2008 [29] with a resolution of 500-m as learning/verification data. When 40,000 cropped images of each class were used for learning, the overall accuracy (OA) was 82.8%. In addition, Yoshihara *et al.* [30] extracted 4000 images of 25×25 pixels from Geoeye-

1 with a spatial resolution of 0.5 m and trained them with a CNN model. As a result, OA showed an accuracy of about 63%. There is. While the application of deep learning and machine learning to remote sensing images is advancing, there are few examples of application to existing topographic maps. Hirashima *et al.* [31] used CNN to identify map symbols on topographic maps as a method for creating training data for land use classification in aerial photographs, and extracted teacher data from aerial photographs centered on the positions of the identified map symbols. Then, CNN is used for two stages of extraction and classification of teacher data, such as classifying by CNN. However, regarding the method of directly creating land use data from existing maps, Iwasaki, Wayama [32] created a land use classification map of the old topographic map as one of the examples of use for deep learning map data. However, other than showing an accuracy of about 52 to 84%, there are almost no research examples assuming actual use.

When assuming actual use, it is necessary to show the accuracy of the created land use data. The accuracy of the subject attributes of land use data has not been discussed much but Yanashima [33] compared the detailed numerical information with public facilities (point vectors) of the national land numerical information, and found that 25% of the national land numerical information was detailed numerical information. Reported that the classification was inappropriate.

For land use data created from remote sensing images, according to Thomlinson *et al.* [34], has proposed criteria of 85% or more than 70% OA for classification each class. A standard of 70% or more for the classification accuracy of is proposed.

The above-mentioned GLCNMO2008 [4] is 77.9% for OA when the number classification class is 20, 94.4% when integrated into 8 classes, and high-resolution land use cover map for Japan [3] shows 78.0% of OA when integrated into 10 classification classes. And the accuracy of the dataset is disclosed.

As mentioned above, the classification accuracy of the land use data currently used is about 80%. As reported by Kojima and Takara [35], the classification accuracy depends on the spatial resolution, and the accuracy decreases as the resolution becomes coarser. In addition, if the classification classes divided into grassland and forest are integrated into one classification class called vegetation, the misclassification between grassland and forest will be correctly classified, so the classification accuracy is also in the number of classification classes. Although it depends, 80-85% or more can be proposed as practically usable accuracy considering the criteria of Thomlinson et al. [34].

Although there are some research examples for creating land use data from existing maps by deep learning, it seems that they have not been put into practical use.

Land use data creation using deep learning can be applied to future reduction of land use data creation costs, old topographic maps for which detailed land use data has not been created, overseas maps, etc.

In this research, aiming for practical use in the future, the numerical map 25000 (map image) issued by the Geographical Survey Institute, which is relatively homogeneous data, is used as the map image for classification. A preliminary study will be conducted using the land use subdivision mesh of the national land numerical information as the true value.

In the future, we plan to use the findings obtained in this study to develop overseas maps for which there is no available digital data, and classification of old topographic maps.

2.2. Methods

2.2.1 Topographical map and land use data

The map image data to be classified includes the CD-ROM version of "Nagoya (published in January 1, 2007)" and "Gifu (published January 1, 2009)" out of the numerical map 25000 (map image) published by the Geographical Survey Institute.

The numerical map 25000 (map image) is a digitized version of the 1:25,000 topographic map issued by the Geographical Survey Institute, and the CD-ROM version is distributed collectively for each primary mesh, but the publication dates are different. "Nagoya (published in January 1, 2007)" is significantly different from Mt. Ryozen (secondary mesh code 523673) published in December 1988 to Suzuka Pass (secondary mesh code 523622) published in November 2006.

The pixel value of the numerical map 25000 (map image) is an index color of values from 0 to 255, but in this research, it is converted to RGB color in consideration of the application to old topographic maps and digitized paper maps. In addition, the coordinates were converted to the UTM coordinate system, and the pixel size was set to 2 m.

As the true value of land use, the land use subdivision mesh data of the national land numerical information was used. Land use subdivision mesh data has been updated every few years since 1976. In this research, land use mesh data were used according to the year of publication: The 1991 version (L03-b-91), the 1997 version (L03-b-97), the 2006 version (L03-b-06), and the 2009 version (L03-b-09).

Considering that it takes time to create land use data, we decided to use the land use data issued immediately after the year of publication of the topographic map. Table 2.1 shows the combination of the secondary mesh code of the topographic map, the year of issue, and the corresponding land use data.

Table 2.1 Correspondence table of secondary mesh code of map image, publication year of map image and land use data

Meshcode	Year of publication	Landusedata	Meshcode	Year of publication	Landusedata	Meshcode	Year of publication	Landusedata
523600	2000	L03-b-06	523656	2004	L03-b-06	533630	2004	L03-b-06
523061	2005	L03-b-06	523657	2005	L03-b-06	533631	2007	L03-b-09
523602	1995	L03-b-97	523660	2006	L03-b-06	533632	2001	L03-b-06
523603	2005	L03-b-06	523661	2006	L03-b-06	533633	2008	L03-b-09
523604	2004	L03-b-06	523662	1998	L03-b-06	533634	2008	L03-b-09
523607	2005	L03-b-06	523663	1998	L03-b-06	533635	2006	L03-b-06
523610	2001	L03-b-06	523664	1998	L03-b-06	533636	2006	L03-b-06
523611	2005	L03-b-06	523665	1998	L03-b-06	533637	2006	L03-b-06
523612	1995	L03-b-97	523666	2002	L03-b-06	533640	2004	L03-b-06
523613	1995	L03-b-97	523667	2002	L03-b-06	533641	2007	L03-b-09
523614	2005	L03-b-06	523670	2004	L03-b-06	533642	2001	L03-b-06
523616	2003	L03-b-06	523671	2004	L03-b-06	533643	2008	L03-b-09
523617	2003	L03-b-06	523672	1998	L03-b-06	533644	2008	L03-b-09
523620	2000	L03-b-06	523673	1988	L03-b-91	533645	2006	L03-b-06
523621	1999	Lb3-b-06	523674	1998	L03-b-06	533646	2006	L03-b-06
523622	2006	L03-b-06	523675	1998	L03-b-06	533647	2006	L03-b-06
523623	2000	L03-b-06-	523676	2002	L03-b-06	533650	2004	L03-b-06
523624	1998	L03-b-06	523677	2002	L03-b-06	533651	1998	L03-b-06
523626	2005	L03-b-06	533600	2006	L03-b-06	533652	2007	L03-b-09
523627	2002	L03-b-06	533601	2006	L03-b-06	533653	2008	L03-b-09
523630	2004	L03-b-06	533603	2006	L03-b-06	533654	2007	L03-b-09
523631	2005	L03-b-06	533603	2007	L03-b-09	533655	2006	L03-b-06
523632	2005	L03-b-06	533604	2002	L03-b-06	533656	2006	L03-b-06
523633	2000	L03-b-06	533605	2001	L03-b-06	533657	2006	L03-b-06
523634	1995	L03-b-97	533606	1999	L03-b-06	533660	1998	L03-b-06
523635	2000	L03-b-06	533607	1998	L03-b-06	533661	1997	L03-b-97
523636	2002	L03-b-06	533610	2007	L03-b-09	533662	1989	L03-b-91
523637	2003	L03-b-06	533611	2006	L03-b-06	533663	2004	L03-b-06
523640	2005	L03-b-06	533612	2006	L03-b-06	533664	1991	L03-b-91
523641	2006	L03-b-06	533613	2006	L03-b-06	533665	1991	L03-b-91
523642	2004	L03-b-06	533614	2002	L03-b-06	533666	2007	L03-b-09
523643	1997	L03-b-97	533615	2002	L03-b-06	533667	2007	L03-b-09
523644	2001	L03-b-06	533616	1998	L03-b-06	533670	1998	L03-b-06

523645	2002	L03-b-06	533617	1998	L03-b-06	533671	1997	L03-b-97
523646	2005	L03-b-06	533620	2006	L03-b-06	533672	1989	L03-b-91
523647	2002	L03-b-06	533621	2007	L03-b-06	633673	1997	L03-b-97
523650	2005	L03-b-06	533622	2006	L03-b-06	533674	1991	L03-b-91
523651	2006	L03-b-06	533623	2006	L03-b-06	533675	1991	L03-b-91
523652	2006	L03-b-06	533624	2001	L03-b-06	533676	2006	L03-b-06
523653	1993	L03-b-97	533625	2001	L03-b-06	533677	2007	L03-b-09
523654	2002	L03-b-06	533626	2001	L03-b-06			
523655	2001	L03-b-06	533627	2002	L03-b-06			

The mesh data provided by the Geographical Survey Institute has a different coordinate system for each map version, but all of have been converted to the UTM coordinate system.

2.2.2. Extraction of training/validation data

An image of 32 × 32, 64 × 64, 128 × 128 pixels was extracted from the map image centering on the barycentric coordinates of each mesh of the land use subdivision mesh data, and used as training data and verification data. Since the map image is geometrically corrected to a spatial resolution of 2 m, 64 x 64 pixels is equivalent to 128 m x 128 m, which is almost the same as the mesh size of the land use subdivision mesh data. Table 2.2 shows the correspondence between the land use type of land use subdivision mesh data and the adopted classification class.

Table 2.2 Correspondence between land use type and classification class of land use subdivision mesh data

Code	Class	1991, 1997	2006	2009
1	Paddy	Rice field		
2	Field	Other agricultural land		
3	Forest	Forest		
-	-	Wasteland		
4	Urban	Building site		
-	-	Highway traffic site		Road
-	-			Railroad
-	-	Other sites		
5	River and lake	Rivers and lakes		
-	-	Beach		
-	-	Sea of water		
-	-	Golf course		
-	-	-	Out of analysis range	

The classification classes were set to 5 classes: Paddy, Field (other agricultural field), Forest, Urban, River and lake, considering the number of sample data that can be acquired and whether or not they can be distinguished from the map image. As for the data for verification

of classification accuracy, 500 sets for each of the above classes, a total of 2,500 sets, were randomly extracted from all areas of the map images "Nagoya" and "Gifu". As for the training data, 30,000 sets for each class were randomly selected so that they would not overlap with the verification data, for a total of 150,000 sets. At the time of learning, in order to verify the effect of the number of training data, 500 to 20,000 sets were randomly extracted from 30,000 sets and used as training data. (Section 2.3, 2.4) In addition, in order to verify the appropriate number of samples in each class, we prepared a separate training data set with the total number of samples in the five classes set at 50,000. For "rivers and lakes" and "other agricultural land" with 64 x 64 pixels, 500 samples were visually selected for each to verify the effect of the learning data extraction method.

2.2.3 Decsription of CNN

A CNN with the structure shown in Figure 2.1 was constructed using Python 3.7.9, Keras 2.3.1 and Tensorflow 1.14.0. CNNs that convolve images are considered to be more suitable for classifying map images because they are easier to detect spatial features of images than other technologies that use images as one dimension.

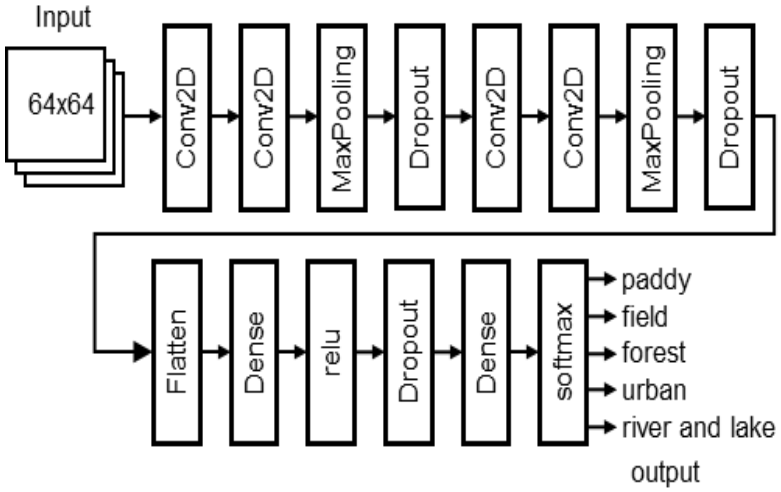

Figure 2.1 CNN structure. Conv2D: Convolutional layer, MaxPooling: Pooling layer, Dropout: Dropout, Flatten:, Dense: Fully connected layer, relu, softmax: Activation function.

Adadelta was used as the optimization algorithm. In the input layer, the pixel value of RGB image normalized to 0 to 1 was input. In the final layer, the Softmax function with the output value of each class set to 0 to 1 was used, and the Categoral Cross Entropy error function was used as the loss function. The Softmax function is an activation function that sets the total value of all outputs to 1.0, and determines that the class with the highest output value is the classification class of the image. ReLU (Rectified Linear Unit) was used as the activation

(2.1)

function of the intermediate layer. If the t - th true value of class i is y_i^t and the corresponding output value is $\hat{y}_i^t$, the loss function L is expressed by the following equation.

$$L = -\sum_{t}^{N}\sum_{i}^{M} y_i^t \log \hat{y}_i^t$$

Here, N is the total number of training data (or verification data), and M is the number of classification classes. CNN learning is optimized to minimize L. The hyperparameters were adjusted manually.

2.2.4. Classification accuracy assessment

During training, 10% of the training data is randomly extracted, and the correct answer rate (Val_accuracy) and loss function L (Val_loss) during training as verification data, and in the remaining 90% of the training data is monitored together with the correct answer rate (accuracy) and loss function L (loss).

Val_Accuracy evaluated here uses Validation data in which samples are randomly extracted for each learning, so it is difficult to make a quantitative comparison with other learning results. Therefore, we decided to save the CNN coefficient estimated every 5 times of learning (epoch) and perform quantitative evaluation using the above-mentioned 2,500 sets of verification data. The classification accuracy evaluation is based on the error discrimination matrix (Error Matrix, Confution Matrix), and the overall accuracy (OA; same as the above-mentioned accuracy rate), the Kappa coefficient (Kappa), and the accuracy of each class (PA; Producer's Accuracy, UA; User's Accuracy) [36] was used.

The accuracy of land use data such as national land numerical information and detailed numerical information actually used in Japan has not been discussed well, but the report by Hanashima [32] suggests that it is about 75% in a bad place. In this study, 85% of OA is adopted as the standard for practical use in consideration of the standard of Thomlinson et al. [34].

2.3. Results and discussion

2.3.1. Image size

Figure 2.2 shows the classification accuracy when the number of learning data in each class is 10,000 and the input image is 32 × 32, 64 × 64, 128 × 128 pixels. The coefficients were saved every 5 learning times, and the classification accuracy was evaluated using the verification data.

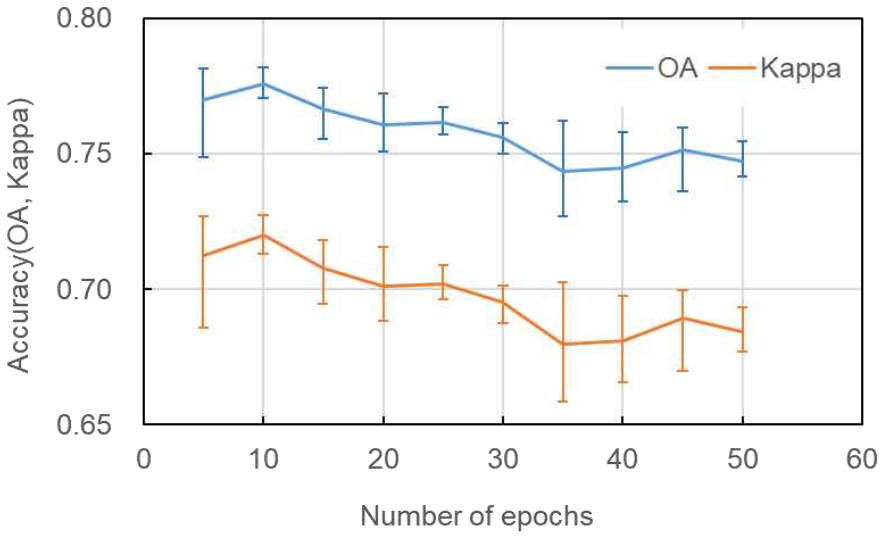

(a) 32 x 32 pixels (10,000 learning data)

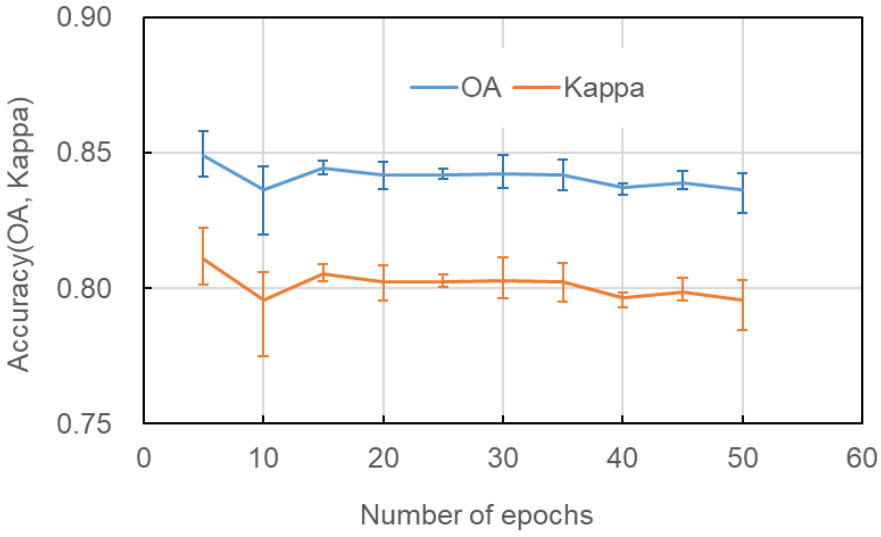

(b) 64 x 64 pixels (10,000 learning data)

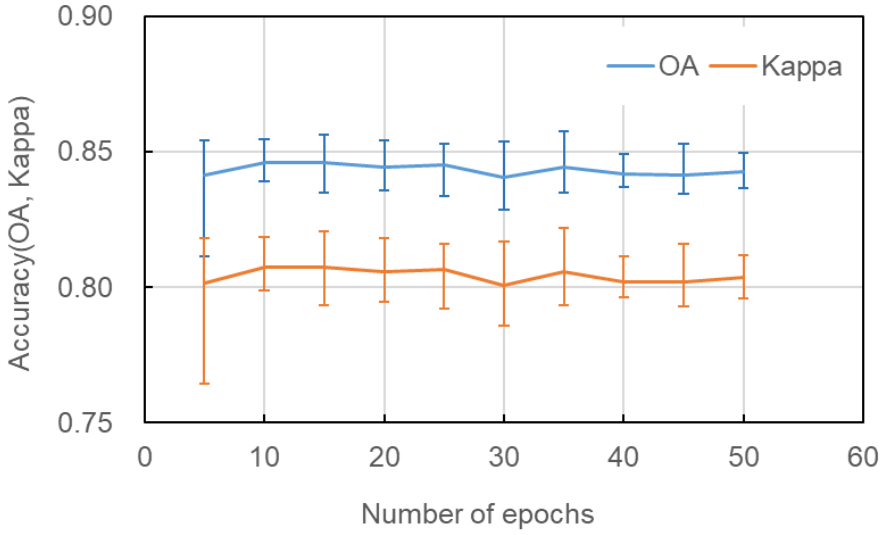

(c) 128 x 128 pixels (10,000 learning data)

Figure 2.2 Relationship between input image size, number of learnings and classification accuracy

Since Adadelta, which is a stochastic gradient descent method, is used for optimization, the learning results are slightly different each time. Therefore, learning was performed 3 to 5 times, and the average value is shown in the figure. The error bars are the maximum and minimum values. With 32 × 32 pixels, when the number of learning times was 10, the average value of OA was 77.6% and the maximum value of OA was 78.2%, showing the best accuracy. The accuracy tended to decrease gradually as the number of learnings increased. With 64 × 64 pixels, when the number of learnings was 5, the average value of OA was 84.9% and the maximum value of OA was 85.8%, showing the best accuracy. The result was that the accuracy was the best when the number of learnings was 5 and the accuracy was the worst when the number of learnings was 10. It seems that the average value decreased because one of the results showed very poor accuracy of OA = 82.0% for 10 learning times. Looking at the maximum value, there was not much change after the 10th learning, and the average value tended to gradually decrease. With 128 × 128 pixels, the average value of OA was 84.6% when the number of learnings was 10, which was the best accuracy, but the maximum value of OA was 85.8% when the number of learnings was 35 times. The change due to the number of learnings was small compared to the results of other image sizes, but the average value tended to decrease slightly as the number of learnings increased.

Figure 2.3 shows the relationship between the classification accuracy and the input image size in the number of learnings, which shows the most accurate average value for each input image size.

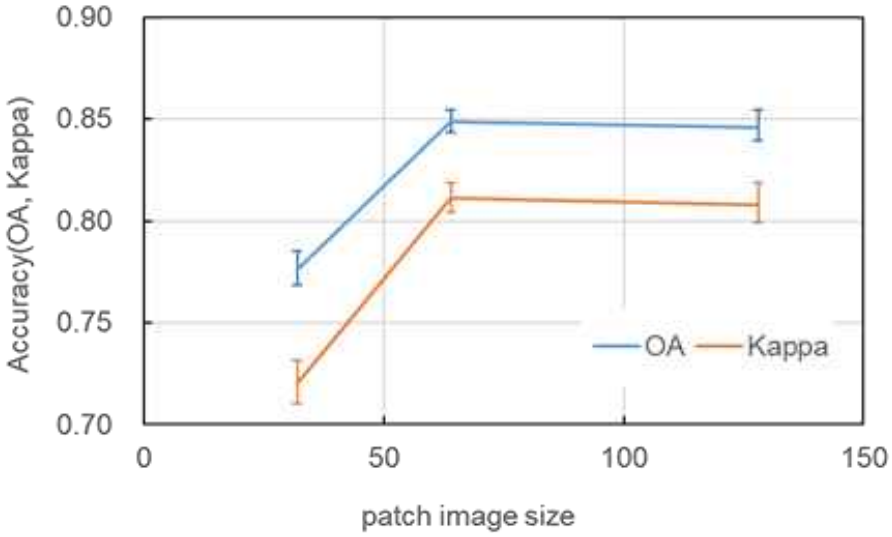

Figure 2.3 Relationship between input image size and classification accuracy.

Although the accuracy is greatly improved with 32 × 32 pixels, there is not much difference in classification accuracy between 64 × 64 pixels and 128 × 128 pixels, but 64 × 64 pixels is slightly higher accuracy. It is considered that the input image size is optimal depending on the size and distribution of map symbols. With 32 x 32 pixels, important map symbols may not be included in one input image, which is considered to have reduced accuracy.

On the other hand, if the input image is large, it is considered that the map image of the class other than the land use of the national land numerical information, which is the true value, is mixed in the input image and the accuracy is lowered. To solve this problem, in addition to increasing the number of training samples and performing reinforcement learning, it is conceivable to use a method such as fuzzy classification [37] that outputs the classification judgment by the area ratio of the target section.

In this study, we will use 64 × 64 pixels, which show the best accuracy.

2.3.2. Number of learning

Figure 2.4 shows the relationship between the number of trainings and the classification accuracy when the number of training data is 500 and 30,000 with 64 × 64 pixels as the input image. Considering this together with Figure 2.2 (b), where the number of training data is 10,000, the number of trainings at which the highest accuracy occurs is approximately 5 to 10 times, depending on the number of data, and thereafter, as the number of trainings increases, the number of trainings increases. It can be seen that the accuracy is gradually decreasing.

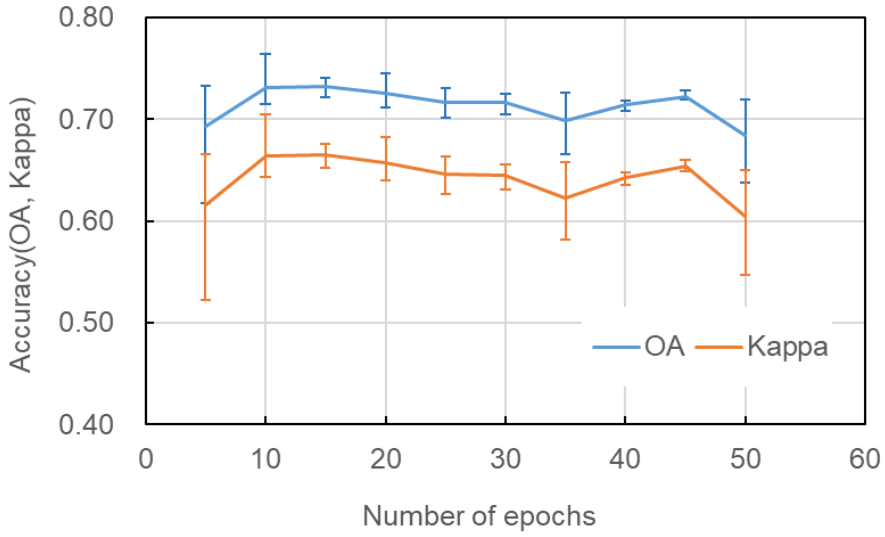

(a) Number of learning data for each class 500

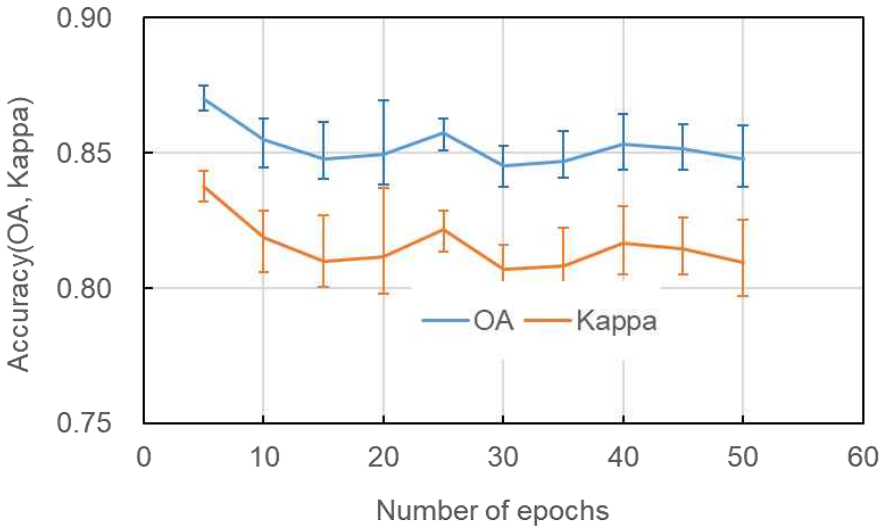

(b) Number of learning data for each class 30,000

Figure 2.4 Relationship between the number of learnings and classification accuracy.

Figure 2.5 shows the correct answer rate (Accuracy) and loss function (Loss) based on the learning data during training, and the correct answer rate (Val_Accuracy) and loss function (Val_Loss) based on the validation data when the number of training data in each class is 10,000.

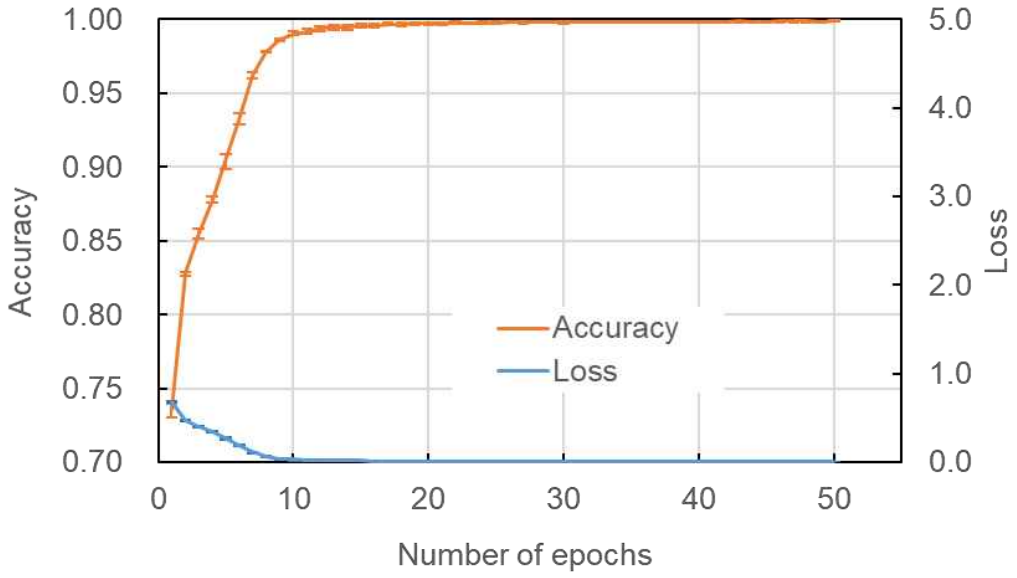

(a) Learning data

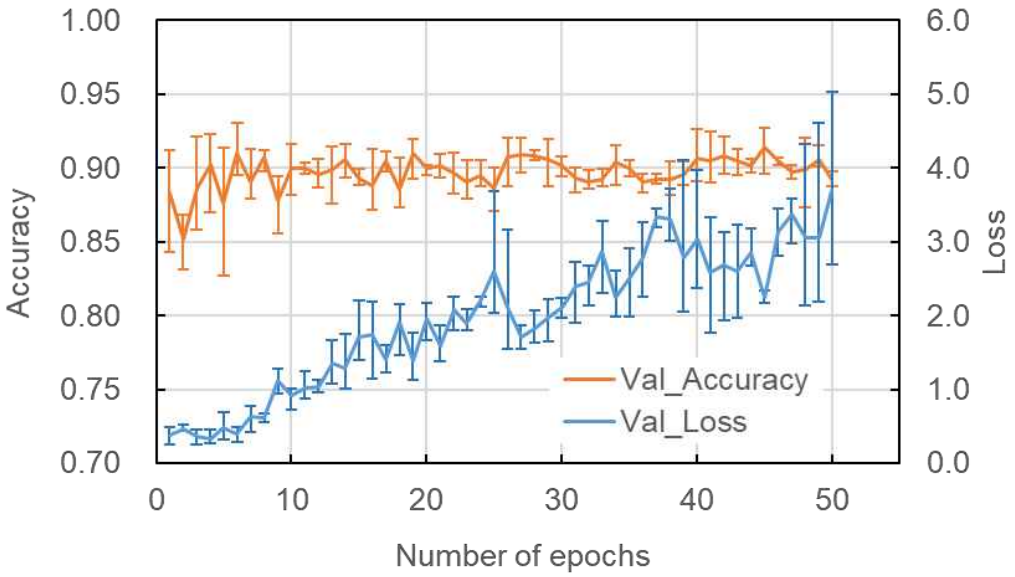

(b) Validation data

Figure 2.5 Relationship between the number of learnings and the correct answer rate/loss function

Similarly, the average value of the learning results of multiple times is shown, and the error bars are the maximum and minimum values. The correct answer rate based on the learning data reaches almost 100% when the number of learnings is about 20 times, and the loss function also reaches almost 0 when the number of learnings is 10 times (see Figure 2.5(a)). If it matches the training data excessively, the possibility of so-called "overfitting" is suggested. In the evaluation using the validation data shown in Figure 2.5 (b), the accuracy rate (Val_Accuracy) was almost 90% after 5 learnings, showing almost no change. On the other hand, the loss function (Val_Loss) gradually increases after the number of learnings is 7, and it can be seen that the estimation error increases. The reason why the loss function deteriorates even though the correct answer rate does not change is that the class showing the maximum value in the output value of the final layer does not change, but the difference from the others is considered to become small. Therefore, the correct answer rate and classification accuracy did not decrease significantly up to the number of learnings of 50, but if the number of learnings was further increased, the classes showing the maximum value would be replaced, and there is a possibility that the number would decrease sharply. This increase in the loss function is considered to be the cause of the decrease in accuracy as the number of learnings seen in Fig. 2.2 and Fig. 2.4 increases. From the above, it is considered appropriate to study about 5 to10 times within the scope of this study.

2.3.3. Learning data extraction method

The problem of multiple classification classes coexisting within the object of image classification has long been a problem. When one pixel is classified, a pixel in which multiple classification classes coexist is called a mixel, and a method for separating the classes in the mixel has been studied [38] [39]. A similar problem arises in this study, where the classification target is an image with N × N pixels. There may be multiple land uses in each mesh of the 100m mesh national land numerical information set as the true value in this study, or incorrect land use may be assigned. Therefore, in this study, we compared and considered the classification accuracy when sample extraction was performed arbitrarily by the following visual interpretation.

As shown in Fig. 2.6, in "river areas and lakes", there are cases where the image to be classified is almost the water surface, and there are cases where the river passes through the image but there is almost no water surface.

We compared the classification accuracy when 500 samples of images with a water surface of 40% or more were selected and used as training data, and when 500 samples were randomly extracted and used as training data. All land uses other than rivers and lakes were randomly extracted from 500 samples and used as learning data.

The average classification accuracy was 71.7% for OA and 65.1% for Kappa coefficient when only images with a water surface of 40% or more were used as training data, but 73.2% for OA when all random training data were acquired., Kappa coefficient averaged 66.5%, showing better accuracy when learning data was acquired at random.

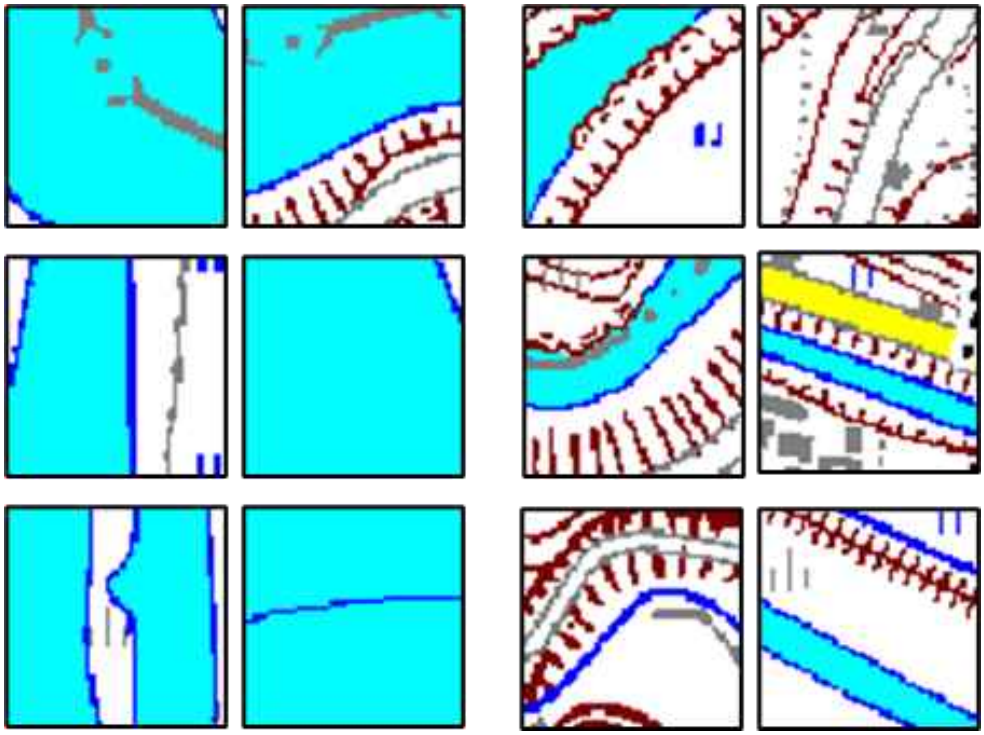

(a) Water surface 40% or more (b) Water surface less than 40%

Figure 2.6 Example of input image of "River area and lake" class.

On the other hand, it cannot be said that the use of satellite imagery for land use data was also misleading, but that "other agricultural lands" are relatively larger than the main residential areas, paddy field and wetlands.

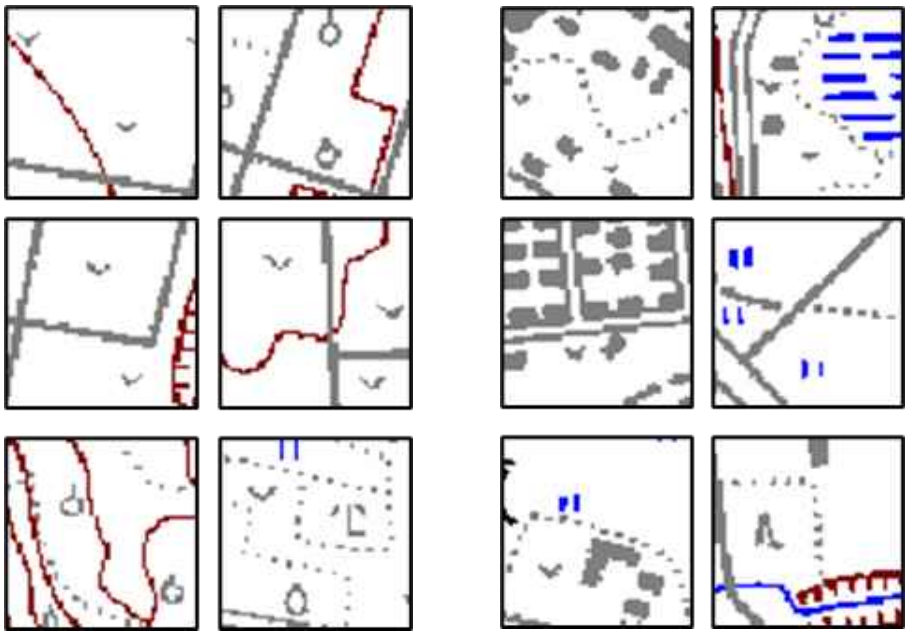

(a) Correctly agricultural land (b) Not agricultural land

Figure 2.7 Example of input image for "Other agricultural land" class.

Figure 2.7 (a) is an example of being correctly classified as "other agricultural land" such as fields/pastures, orchards, wastelands, and bamboo grove, and Figure 2.7 (b) is classified as other agricultural land in the national land numerical information. However, it is an example that can be read as other than that on the map image. Similar to rivers and lakes, 500 samples that can be visually read as "other agricultural land" were extracted and classified, and the average was 74.4% for OA and 68.0% for Kappa coefficient. The accuracy was improved compared to the result using the training data.

The following are possible causes for this. If only 40% or more of the water surface is used as the learning data, the classification accuracy will decrease because the rivers and lakes with less than 40% of the water surface will be learned so that they will not be classified correctly. On the other hand, if the learning data is created by excluding the samples that are not agricultural land, the learning noise of the agricultural land classification that has existed so far is reduced, and it is considered that the classification accuracy of the correct agricultural land is improved.

In this way, the method of extracting learning data affects the classification accuracy. As in the case of other agricultural land studies, it is expected that the classification accuracy will be improved by visually confirming the map symbols and extracting the learning data. On the other hand, if only samples with specific characteristics are extracted, such as the results of studies on rivers and lakes, the classification accuracy may decrease. Note that even in other agricultural lands, for example, if only the areas where the map symbols of fields and pastures are shown are extracted, other map symbols such as orchards, bamboo grove, and whale fields may not be correctly classified.

2.3.4. Number of training samples

Figure 2.8 shows the change in classification accuracy when the number of training data in each class is 500 to 30,000 samples.

Figure 2.8 Relationship between the number of learning samples in each class and classification accuracy

With 1,000 samples, the average accuracy was 77.3% in OA and 71.7% in Kappa, which did not reach the practical classification accuracy, but when 10,000 samples, the average accuracy was 84.9% in OA and 81.1% in Kappa, which almost reaches a practical level. At 15,000 samples, the average accuracy was 86.0% in OA, the lowest accuracy was 85.0%, and even the lowest value shows a practical level of OA.

When the number of training samples is further increased, the improvement in accuracy slows down to 86.8% on average for OA when the number of samples is 20,000 and 87.2% on average for OA when the number of samples is 30,000. Table 2.3 shows an example of the classification results with 10,000 samples.

In this example, the OA is 85.5%, and the classification accuracy of each class is more than 70% for both PA and UA. It has been shown that when the number of training samples in each class is the same, it is possible to obtain an almost practical level of accuracy by sampling 10,000 or more in each class.

Table 2.3 Example of error discrimination matrix when the number of training samples in each class is 10,000. Pdy: paddy, Fld: field, Frst: forest, Ubn: urban, Riv: river and lake.

		Referenced					Sum	UA (%)
		PDY	FLD	FRST	UBN	RIV		
Classified	PDY	394	30	9	24	11	468	84.2
	FLD	55	422	29	45	21	572	73.8
	FRST	14	7	454	2	5	482	94.2
	UBN	27	33	2	422	10	494	85.4
	RIV	10	8	6	7	453	484	93.6
Sum		500	500	500	500	500	2500	
PA (%)		78.8	84.4	90.8	84.4	90.6		

OA = 85.8%, Kappa=82.3%

On the other hand, in the optimization problem, it is well known that when the number of training samples is biased, the classification result is biased to the class with a large number of training samples, and the classification accuracy decreases. Figure 2.9 shows the number of learning samples for rice fields 7,844, the number of other agricultural land samples 1,559, the number of forest samples 29,737, and the number of building land samples according to the number of land use meshes included in "Nagoya" and "Gifu". The classification accuracy is shown when the number of samples in each class is 10,000, and the total number of samples is 50,000. As in Fig. 2.2, it can be seen that the accuracy is the best when the number of learnings is 5, and the accuracy does not improve even if the number of learnings is increased further. The accuracy was 61.2% on average for OA and 51.5% on average for Kappa, showing a lower classification accuracy than when the sample size of each class was unified to 500.

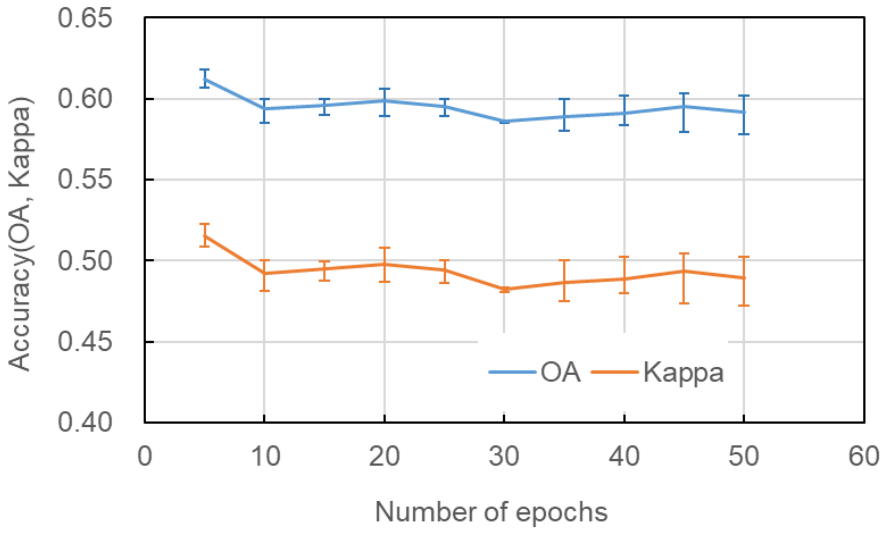

Figure 2.9 Relationship between the number of learnings and classification accuracy.

Table 2.4 shows an example of the error discrimination matrix with 5 learnings. Compared to Table 2.3, the PA of forests and rice fields with a large number of learning samples shows high values, while the cases where other classes are misclassified as forests and rice fields increase, so each UA shows a low value.

Table 2.4 Example of error discrimination matrix when the number of training samples in each class is not unified. Pdy: paddy, Fld: field, Frst: forest, Ubn: urban, Riv: river and lake.

		Referenced					Sum	UA (%)
		Pdy	Fld	Frst	Ubn	Riv		
Classified	Pdy	429	90	5	45	41	610	70.3
	Fld	11	175	3	14	12	215	81.4
	Frst	46	166	491	19	83	805	61.0
	Ubn	14	69	1	422	364	870	48.5
	Riv	0	0	0	0	0	0	0.0
Sum		500	500	500	500	500	2500	
PA (%)		85.8	35.0	98.2	84.4	0.0		

OA = 60.7%, Kappa=50.9%

For other agricultural lands with a small number of learning samples, only 215 meshes out of 2,500 meshes were discriminated as other agricultural lands, and the UA showed a relatively high value. However, meshes, which are true values and other agricultural land, are often misclassified as rice fields and forests, and PA showed a low value of 35.0%. The number of learning samples for rivers and lakes was 4,036, which is not extremely small compared to the number of samples for other agricultural lands, but the result was that even one mesh was not classified. Although the detailed values are different, the accuracy of rivers and lakes was low in other examples as well. As shown in Fig. 2.6, the cause of this is that rivers and lakes have very different forms: lakes and large rivers where most of the mesh is water surface, and small and medium-sized rivers where the ratio of water surface in the mesh is low. This is probably because there are two land use classes. Conversely, if the number of learning samples is sufficient and the number of samples in each class is well-balanced, land use with different map symbols such as paddy fields, fields/pastures, and tea fields will be aggregated into one class.

2.3.5. Ensemble average of learning results

As mentioned above, optimization by the stochastic gradient descent method, which is usually used in deep learning, randomly produces slightly different learning results even if the same data is used. The accuracy is improved by integrating these slightly different learning results. In general, if the output value of class i in a mesh t is $\hat{y}_i^t$ ($i = 1 \cdots n$), the classification class of that mesh is shown by Equation 2.2.

$$\underset{i \in \{1,M\}}{\arg\max}\, \hat{y}_i^t \tag{2.2}$$

Here, when there are n learning results and the output value of the j the learning result class i is indicated by $\hat{y}_{i,j}^t$ (j = $1 \cdots n$),

Here, the new methods, a), b), c) are proposed by following:

i) A method in which the class showing the maximum value out of n learning results is used as the classification class of mesh t (argmax)

$$\underset{i \in \{1,M\}}{\arg\max} \left\{ \max_{j \in \{1,n\}} \hat{y}_{i,j}^t \right\} \tag{2.3}$$

ii) A method that sums the output values of n learning results and sets the class showing the maximum of the total output values as the classification class of mesh t. (Weighted Average Voting)

$$\underset{i \in \{1,M\}}{\arg\max} \left\{ \sum_{j=1}^{n} \hat{y}_{i,j}^t \right\} \tag{2.4}$$

iii) A method of the classification classes determined by each of the n learning results, the mode is the classification class of mesh t. (Max voting)

$$\underset{j \in \{1,n\}}{\mathrm{mode}} \left\{ \underset{i \in \{1,M\}}{\arg\max}\, \hat{y}_{i,j}^t \right\} \tag{2.5}$$

Figure 2.10 shows the relationship between the number of integrated learning results and the classification accuracy when the number of learning samples in each class is 10,000.

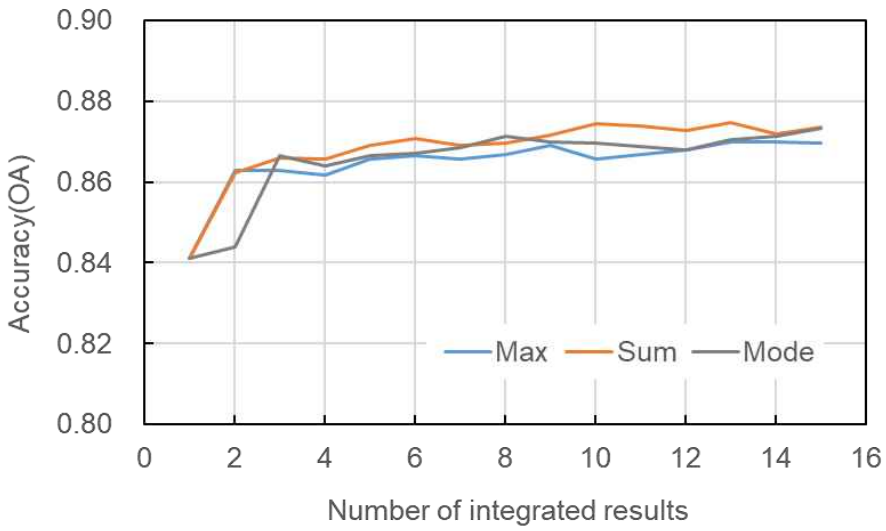

Figure 2.10 Relationship between the number of integrated learning results and classification accuracy.

It was shown that the OA, which was initially 84%, improved to 86% or more by integrating three or more learning results. There was no clear difference in which of the three integration methods was superior.

2.3.6. Spatial evaluation

Spatial evaluation of land use classification results.

As an example, where each class is arranged in a well-balanced manner and there are few areas not subject to classification such as "other land" and "seawater area", the secondary mesh code 533602 (1:25,000 topographic map named "Nagahama") and, as an example of not extracting CNN training data, secondary mesh code 523731 (map name "Okazaki"; published in 2002) was trained with 30,000 training samples for each class. Figure 2.11 shows the result of ensemble average of the learning results.

Here, we have shosen research area which, Okazaki and Nagahama by this reason.

- There is a large water area.
- All land use is well-balanced.

Reasons for Okazaki map is selected from the map (mesh number 5237) other than the maps for which the training data was acquired (mesh number 5336, 5236).

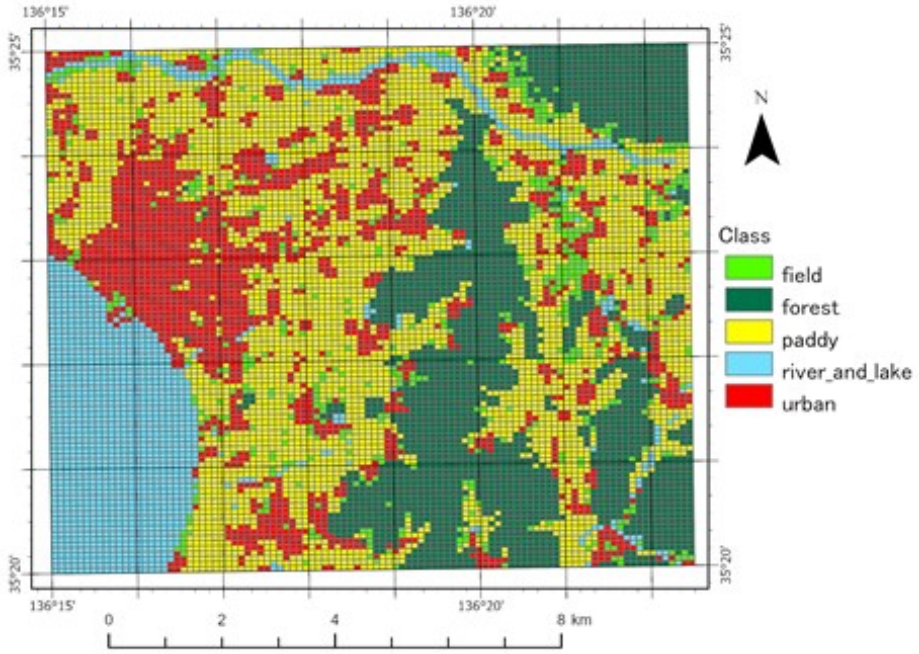

(a) Nagahama

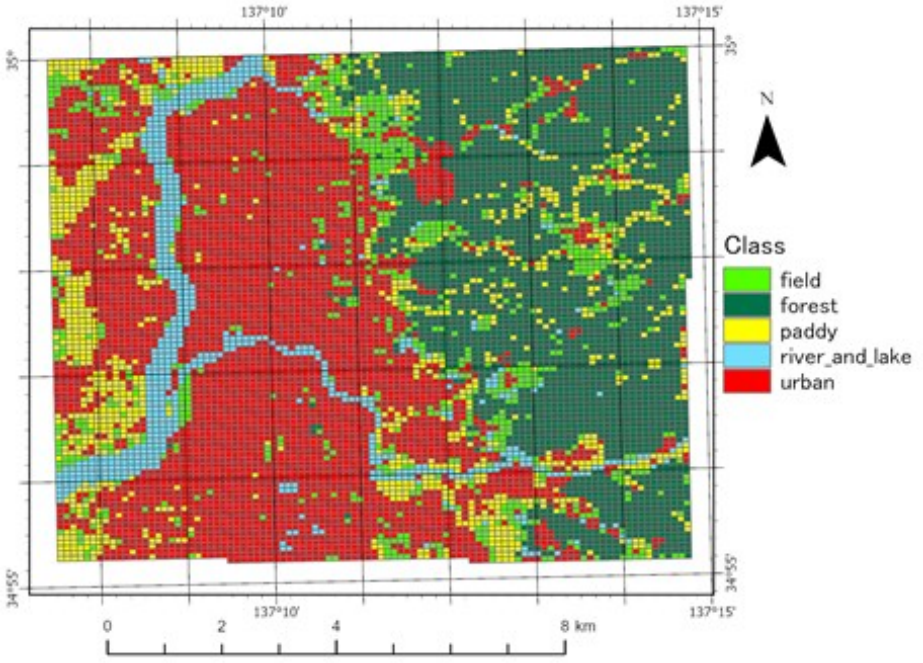

(b) Okazaki

Figure 2.11 Classification results by deep learning. Sample size 30,000. Integration of 5 classification results by Max Voting method.

Figures 2.12 and 2.13 show the 2006 version of the national land numerical information land use subdivision mesh (L03-b-06) and the numerical map 25000 (map image) in the same area. The land use types "wasteland", "transport", and "other" that exist in the land use subdivision mesh data do not exist in the deep learning classification class, in Figure 2.11

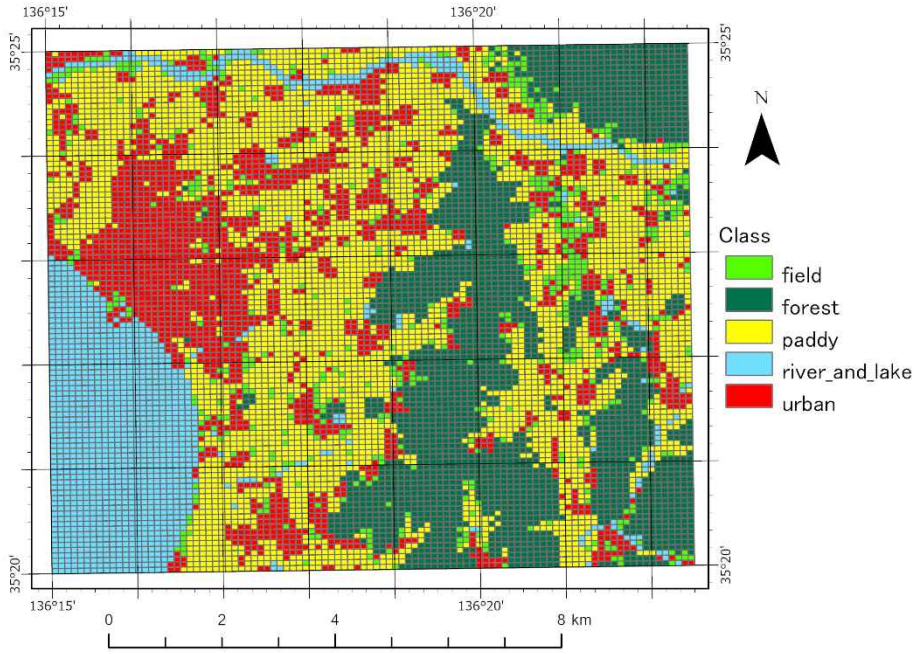

(a) Nagahama

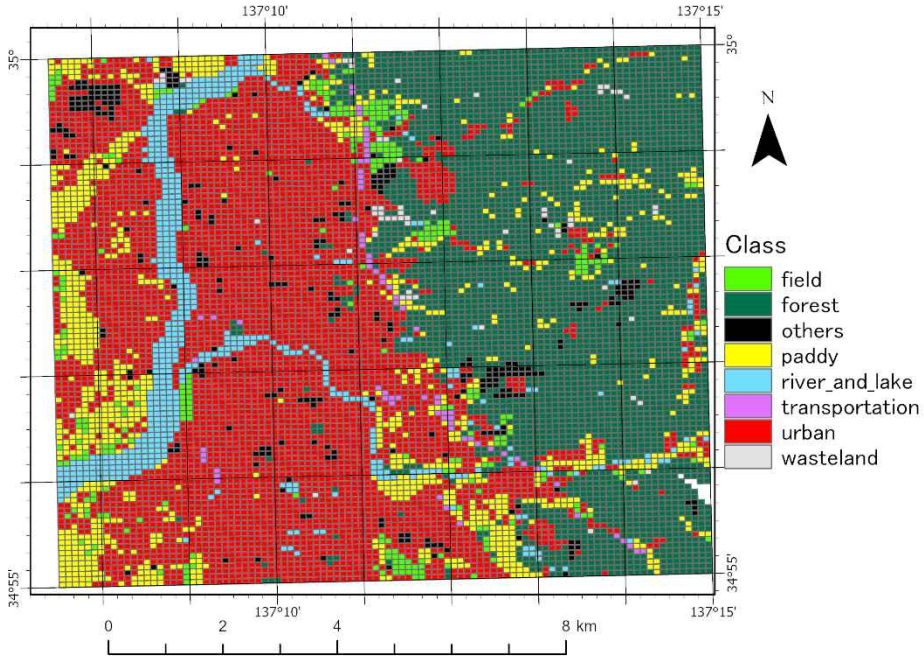

(b) Okazaki

Figure 2.12 National Land Numerical Information Land Use Subdivision Mesh Data.

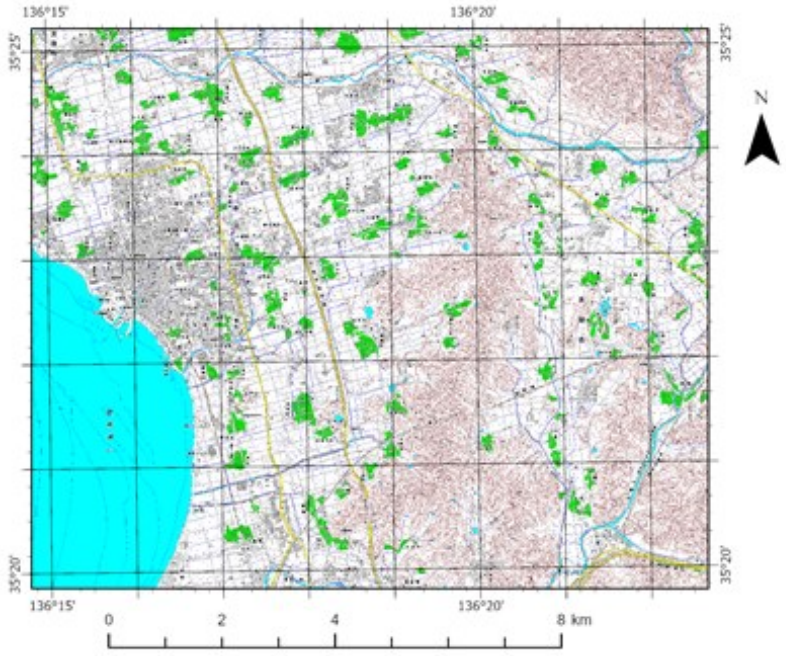

(a) Nagahama

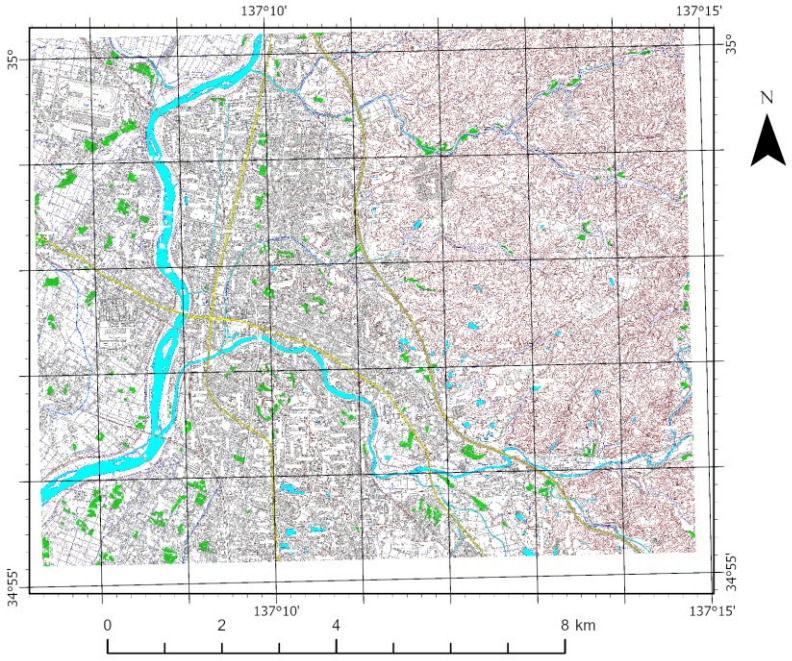

(b) Okazaki

Figure 2.13 Numerical map 25000 (map image).

Although it is classified as another land use, it seems that it is classified very accurately as a whole. Especially in river areas and lakes, both lakes and river areas existing in the area are well classified. Tables 2.5 and 2.6 show the error discrimination matrix of the classification

results in this area. One secondary mesh, that the land use subdivision mesh (100 m mesh) in one map of the 1: 25,000 topographic map is 100 × 100 10,000 mesh.

Table 2.5 Error discrimination matrix in secondary mesh code 533602

		Referenced					Sum	UA(%)
		PDY	FLD	FRST	UBN	RIV		
Classified	PDY	3418	10	76	104	9	3617	94.5
	FLD	144	132	156	38	18	488	27.0
	FRST	34	4	2186	6	0	2230	98.0
	UBN	127	8	38	1637	8	1818	90.0
	RIV	40	0	24	2	1248	1314	95.0
Sum		3763	154	2480	1787	1283	9467	
PA(%)		90.8	85.7	88.1	91.6	97.3		

OA = 91.1%, Kappa=87.8%

Table 2.6 Error discrimination matrix in secondary mesh code 523731

		Referenced					Sum	UA(%)
		PDY	FLD	FRST	UBN	RIV		
Classified	PDY	763	73	26	81	25	968	78.8
	FLD	15	228	3	15	3	264	86.4
	FRST	170	283	2621	71	41	3186	82.3
	UBN	84	135	14	3709	30	3972	93.4
	RIV	10	32	5	26	482	555	86.8
Sum		1042	751	2669	3902	581	8945	
PA(%)		73.2	30.4	98.2	95.1	83.0		

OA = 87.2%, Kappa=81.3%

About 95% of "Nagahama (533602)" and about 90% of "Okazaki (523731)" are the land use types corresponding to rice fields, other agricultural land, forests, building land, river land and lakes. In "Nagahama", OA is 91.1% and Kappa is 87.8%, which are very accurate classifications. Even in "Okazaki", the OA is 87.2% and the Kappa coefficient is 81.3%, which is slightly inferior to Nagahama, but it can be said that it has reached a practical level. Regarding the classification accuracy of each class, rivers and lakes showed good classification

accuracy in both "Nagahama" where a wide range of lakes exist and "Okazaki" where there are no large lakes. As shown in Fig. 2.6, it is considered that good accuracy can be shown by collecting learning data with two types of features in a well-balanced manner.

On the other hand, in other agricultural lands, there was a tendency that UA was low in "Nagahama" and PA was low in "Okazaki" compared to other classes. Since other agricultural lands are classes that include various map symbols, the classification accuracy is considered to be inferior to those of other classes. In addition, PA is high in "Nagahama" included in the area where the training data was acquired, and it is considered that the meshes of other agricultural land are classified almost accurately by the true value. Also, in "Okazaki", since a specific map symbol contained in other agricultural land is hardly included in the learning data, it is not possible to accurately classify the specific map symbol, and the PA of other agricultural land is low.

The Atsumi Peninsula to Mikawa region of Aichi Prefecture, which includes "Okazaki," is a production center for oranges, and there are more map symbols for "orchards" than "Gifu" and "Nagoya," which may be a factor in misclassification. As mentioned above, it is necessary to be careful about the acquisition of learning data of the "other agricultural land" class in which multiple map symbols are mixed, but other than that, a topographic map different from the area where the learning data was acquired is sufficient. Practical level classification results were obtained.

2.4. Summary

In this chapter, we aimed to put into practical use a method for classifying existing maps including map symbols by using deep learning. Within the scope of this study, which is to create a land use map equivalent to about 100 m mesh in five classification classes for a map image equivalent to 1:25,000, the overall accuracy (OA) is constantly 85% or more. We were able to propose a practical level land use classification method that can be shown. Even in the application result to the area different from the acquisition area of the learning data, the accuracy of 85% or more can be shown by OA, the applicability to 1:25,000 map images all over Japan, and the update of land use data. The findings obtained in the details of the practical classification procedure are as follows.

- ✓ In the applicable range of this method, learning using 64 × 64 pixels, which corresponds to a mesh of about 100 m, is suitable. If the size is increased, the information obtained will increase, but the misjudgment by the mixer will increase.

- ✓ The optimal number of learning times is about 5 times. When learning 10 times or more, the value of the loss function increases significantly, and the effect of overfitting can be seen.
- ✓ There are some meshes classified into different land use classes in the land use subdivision mesh data of the national land numerical information. In particular, other agricultural lands are often misclassified as rice fields and wetlands, so care must be taken when using them as the true value of land use classification.
- ✓ Other agricultural land is a land use class that includes a large number of map symbols, and it is necessary to extract each map symbol in a well-balanced manner and create learning data.
- ✓ The number of learning samples should be the same for each class to some extent. If the number of training samples in each class is not balanced, the classification accuracy will decrease even if the total number of samples is large.
- ✓ In order to show the practical level of classification accuracy, it seems that the number of samples in one class needs to be 10,000 or more.
- ✓ There was no significant difference in the results of the three ensemble average methods, and the accuracy improved regardless of which method was used.

In this study, CNN was trained using the training data acquired in the areas of Nagoya (primary mesh number 5236) and Gifu (primary mesh number 5336) of the numerical map 1:25000. The learned CNN is applied to another area (secondary mesh number 523731) and it is verified that sufficient classification accuracy can be obtained, but the influence of regional land use and map symbol is also suggested.

In the future, it will be necessary to apply it to map images nationwide and study regional bias and bias of the types of map symbols included in the learning data to further improve accuracy.

CHAPTER 3. FLOOD SIMULATION WITH OLD AND CURRENT TOPOGRAPHICAL MAPS

3.1. Introduction

3.1.1. Background

A stone monument about a warning for residence in the tsunami-damaged area became a popular topic after the tsunami hazard by the Great East Japan Earthquake, 11th March of 2011. It is also on the news that old location name at the landslide-damaged area in Yagi, Asaminami district, Hiroshima is evidence of frequent land-slides as “八木蛇落悪谷” the 20th August of 2014. It is essential to know the past disaster risks in the residential area for natural disaster mitigation.

Flooding, it being flash, due to rising groundwater, coastal, and due to the opening or breaking of a dam or reservoir is a life-threatening natural hazard all over the world; too much rainfall within a short period of time and consequent high river discharge results in floods which subsequently creates significant infrastructure problems for areas and a substantial economic deficits in production as well as extensive damages to existing property, goods and even loss of human lives along with siltation of reservoirs and hence limit the capacity of existing dams to control floods. Flood hazards management involves prediction, preparation, prevention, mitigation, and post-disaster management activities, hence inspiring various researches from evacuation measures, hydrology and floodplain analysis, flood risk assessment creation of terrain models for floodplain mapping, the stimulation of the impacts of flood retarding structures on streamflow and many more.

In former times, the flatland around the Kiso-River system, included Gifu City, was frequently damaged by inundation/flood after heavy rainfall. Large paddy fields worked as a flood control reservoir. The residential area was constructed at relatively higher and well-drained low land and protected by banks so-called “Waju-Tei.” Currently, former paddy fields change to the new residential area. On the other hand, there are many mitigation factors of inundation risks, such as the construction of drainage pumps and channels.

3.1.2. Research object

The object of this chapter is an experiment to evaluate the flood risks from the past to present using the past and present topographical maps in Gifu City. For that we shall try to identify the areas at risk of flooding in long term, to analyze the urban expansions are relevant to current and future flood risks, to outline policies to be applied in such areas in order to decrease and manage flood risks and development of an information system for decision-makers for residents of that risky places.

3.1.3. Research flow

In order to reach the purpose of the study, the following flow of research has to be undertaken by Figure 3.1, this research will be run on GIS analysis and hydrological analysis. GIS applications are in land use mapping, digitizing several layers and defining is paddy field can decrease flood risk or not, hydrological data is in define total inundation water volume of Nagara river and hydrograph for to simulate flood inundation.

Flood risk evaluation with GIS analysis will be based on land use data of the old and current time by GIS data processing with total inundation water volume from hydrological data processing.

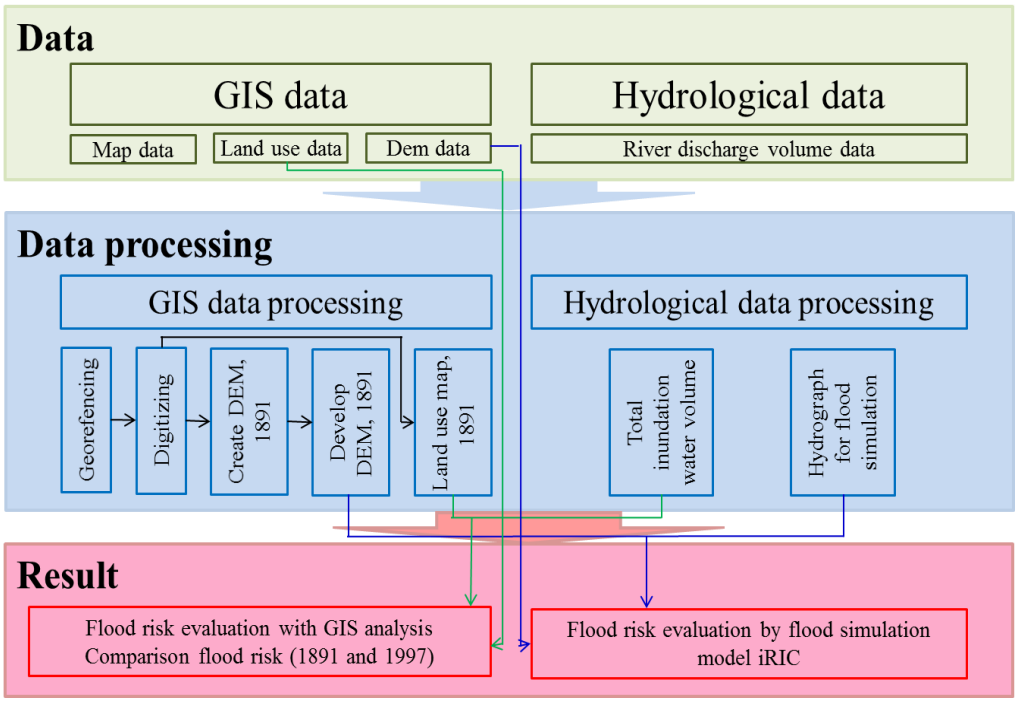

Figure 3.1 Research flow

Flood risk evaluation by flood simulation model iRIC will be based on hydrograph for flood simulation from hydrological data processing with DEM data of the old and current time by GIS data processing.

3.2 Datasets and data processing

3.2.1. Description of GIS data

a) Map data

In modern mapping, a topographic map is a type of map characterized by large-scale detail and quantitative representation of relief, using contour lines but, historically, using a variety of methods. Traditional definitions require a topographic map to show both natural and man-made features. The Geographical Survey Institute of Japan is responsible for the base mapping of Japan. Standard map scales are 1:25,000, 1:50,000, 1:200,000 and 1:500,000 [40]

In this chapter, those topographic map data and their sources are using for spatial analyze of study area below in Table 3.1 and Figure 3.2.

Table 3.1 List of the topographical map data

Product	Source	Scale	Surveyed
1891	Imperial Japanese Land Survey (大日本帝国陸地測量部)	1/20,000	1891
1920	Imperial Japanese Land Survey (大日本帝国陸地測量部)	1/25,000	1920
1947	Geographical Survey Institute of Japan (国土地理院)	1/25,000	1947
1970	Geographical Survey Institute of Japan (国土地理院)	1/25,000	1970
1992	Geographical Survey Institute of Japan (国土地理院)	1/25,000	Northern side in 1994 Gifu eastern side in 1992
1997	Geospatial Information Authority of Japan (国土地理院)	1/25,000 Digital Map	Gifu southern side in 2000 Northern side in 2000 Gifu eastern in 1997

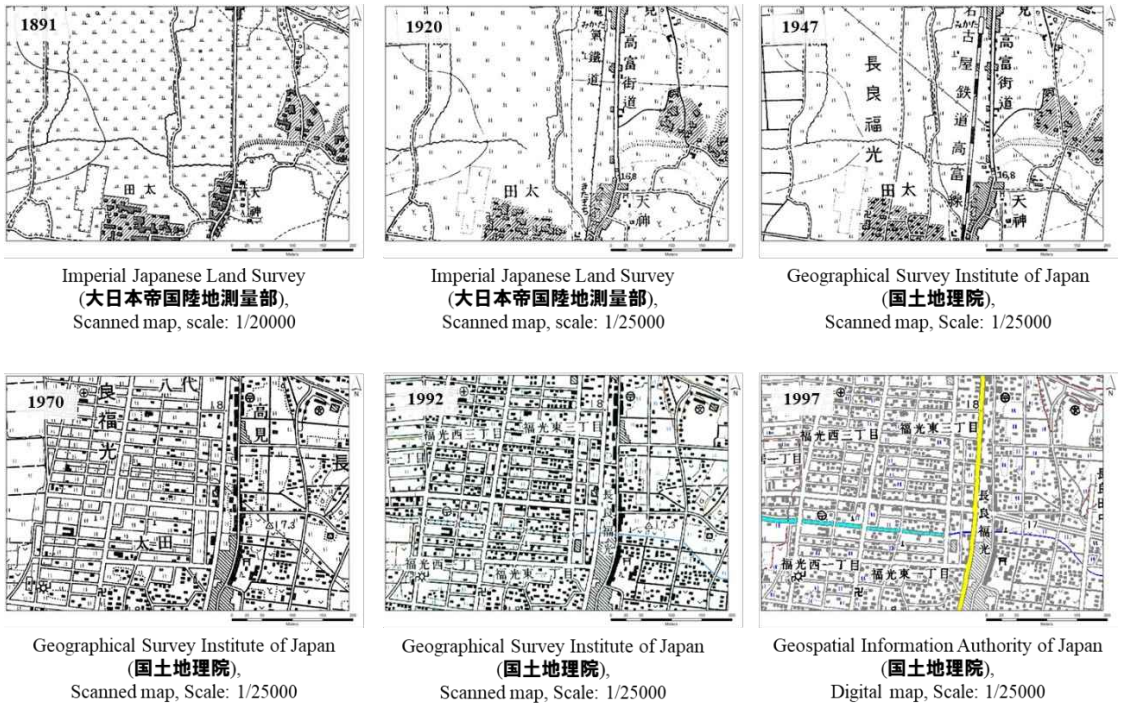

Imperial Japanese Land Survey (**大日本帝国陸地測量部**), Scanned map, scale: 1/20000

Imperial Japanese Land Survey (**大日本帝国陸地測量部**), Scanned map, scale: 1/25000

Geographical Survey Institute of Japan (**国土地理院**), Scanned map, Scale: 1/25000

Geographical Survey Institute of Japan (**国土地理院**), Scanned map, Scale: 1/25000

Geographical Survey Institute of Japan (**国土地理院**), Scanned map, Scale: 1/25000

Geospatial Information Authority of Japan (**国土地理院**), Digital map, Scale: 1/25000

Figure 3.2 Topographical map data

b) DEM data

A digital elevation model (DEM) is a digital file consisting of terrain elevations for ground positions at the regularly spaced horizontal interval. It represents only height information without any further definition about the surface [41].

For this study, a DEM data used for the simulation model to evaluate current and former time flood risk. High-resolution DEM data (5m) had published by Geological Survey Institute, Japan acquired by airborne LIDAR system and included the shape of flood protection banks, as shown in Figure 3.3.

But former time, such high technologies was not inventing usually in 1891, so created DEM by digitized objects which including information with elevation from old topographical maps 1981 by GIS software.

Figure 3.3 DEM image, current time

c) Land use data

Land use data is used to evaluate of inundation depth by land use change in the long term. Current time`s vegetation and land use map were downloadable from the Natural Environment GIS database, published by Biodiversity center of Japan, Ministry of the Environment.[42]. This map is developed with the surveying from 1993–2003.

The land use categories identified were: bare soil, cultivated area, forest, garden, grassland, paddy field, urbanized area, water bodies, etc. The attributes used for each of the land use categories are shown in Figure 3.4 and Figure 3.5.

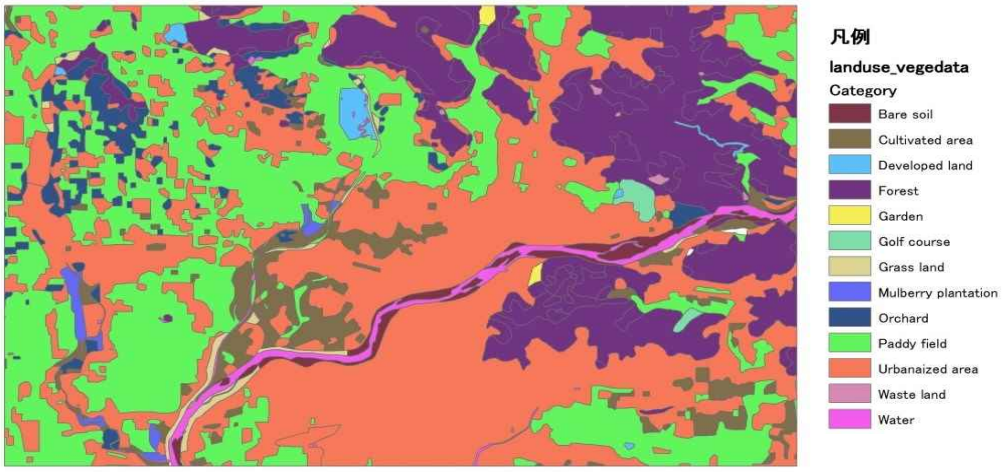

Figure 3.4 Land use data, 2004

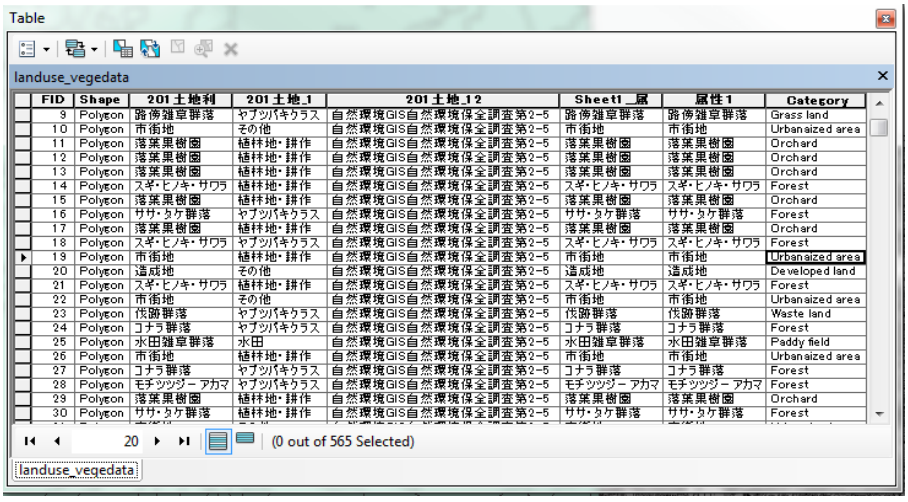

FID	Shape	201土地利	201土地_1	201土地_12	Sheet1_属	属性1	Category
9	Polygon	路傍雑草群落	ヤブツバキクラス	自然環境GIS自然環境保全調査第2-5	路傍雑草群落	路傍雑草群落	Grass land
10	Polygon	市街地	その他	自然環境GIS自然環境保全調査第2-5	市街地	市街地	Urbanaized area
11	Polygon	落葉果樹園	植林地・耕作	自然環境GIS自然環境保全調査第2-5	落葉果樹園	落葉果樹園	Orchard
12	Polygon	落葉果樹園	植林地・耕作	自然環境GIS自然環境保全調査第2-5	落葉果樹園	落葉果樹園	Orchard
13	Polygon	落葉果樹園	植林地・耕作	自然環境GIS自然環境保全調査第2-5	落葉果樹園	落葉果樹園	Orchard
14	Polygon	スギ・ヒノキ・サワラ	植林地・耕作	自然環境GIS自然環境保全調査第2-5	スギ・ヒノキ・サワラ	スギ・ヒノキ・サワラ	Forest
15	Polygon	落葉果樹園	植林地・耕作	自然環境GIS自然環境保全調査第2-5	落葉果樹園	落葉果樹園	Orchard
16	Polygon	ササ・タケ群落	ヤブツバキクラス	自然環境GIS自然環境保全調査第2-5	ササ・タケ群落	ササ・タケ群落	Forest
17	Polygon	落葉果樹園	植林地・耕作	自然環境GIS自然環境保全調査第2-5	落葉果樹園	落葉果樹園	Orchard
18	Polygon	スギ・ヒノキ・サワラ	ヤブツバキクラス	自然環境GIS自然環境保全調査第2-5	スギ・ヒノキ・サワラ	スギ・ヒノキ・サワラ	Forest
19	Polygon	市街地	植林地・耕作	自然環境GIS自然環境保全調査第2-5	市街地	市街地	Urbanaized area
20	Polygon	造成地	その他	自然環境GIS自然環境保全調査第2-5	造成地	造成地	Developed land
21	Polygon	スギ・ヒノキ・サワラ	植林地・耕作	自然環境GIS自然環境保全調査第2-5	スギ・ヒノキ・サワラ	スギ・ヒノキ・サワラ	Forest
22	Polygon	市街地	その他	自然環境GIS自然環境保全調査第2-5	市街地	市街地	Urbanaized area
23	Polygon	伐跡群落	ヤブツバキクラス	自然環境GIS自然環境保全調査第2-5	伐跡群落	伐跡群落	Waste land
24	Polygon	コナラ群落	ヤブツバキクラス	自然環境GIS自然環境保全調査第2-5	コナラ群落	コナラ群落	Forest
25	Polygon	水田雑草群落	水田	自然環境GIS自然環境保全調査第2-5	水田雑草群落	水田雑草群落	Paddy field
26	Polygon	市街地	植林地・耕作	自然環境GIS自然環境保全調査第2-5	市街地	市街地	Urbanaized area
27	Polygon	コナラ群落	ヤブツバキクラス	自然環境GIS自然環境保全調査第2-5	コナラ群落	コナラ群落	Forest
28	Polygon	モチツツジ－アカマ	ヤブツバキクラス	自然環境GIS自然環境保全調査第2-5	モチツツジ－アカマ	モチツツジ－アカマ	Forest
29	Polygon	落葉果樹園	植林地・耕作	自然環境GIS自然環境保全調査第2-5	落葉果樹園	落葉果樹園	Orchard
30	Polygon	ササ・タケ群落	植林地・耕作	自然環境GIS自然環境保全調査第2-5	ササ・タケ群落	ササ・タケ群落	Forest

Figure 3.5 Attribute data of survey for land use around Gifu city

3.2.2. GIS data processing

A Geographical Information System (GIS), was used in several aspects of this study. First, it was used to overlay maps for spatially represented old and current maps. Second, to digitize several layers for define land usage and assume their areas, and finally to create DEM from the old topographical map and develop created DEM with other elevation objects such flood protecting bank (levee), river and paddy field area for analyzing flood simulation model. I describe each of these activities below.

Georeferencing

A spatial reference is a series of parameters that define the coordinate system and other spatial properties for each dataset in the geodatabase. It is typical that all datasets for the same area use a standard spatial reference definition.

One of the defining features of GIS is its ability to combine spatially referenced data. An occurring frequency issue is the need to combine spatial data from different sources that use different spatial reference system. Scanned map datasets don't typically contain spatial reference information. To use raster dataset in conjunction with spatial data, you may need to align or georeferenced them to a map coordinate system. A map coordinate system is defined using map projection. (Map projection - a method by which the curved surface of the earth is portrayed on a flat surface) Coordinate systems enable geographic datasets to use common locations for integration. A coordinate system is a reference system used to represent the

locations of geographic features, imagery, and observations, such as the Global Positioning System (GPS) locations, within a common geographic framework.

In this study georeferenced as having the best potential to define mitigation site using 6 different year`s topographical maps such as below:

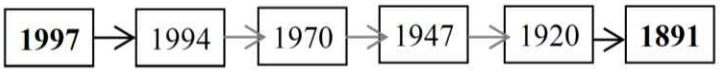

Digital map (1997) is containing spatial reference information (coordinate grid, geodesy points…etc.,) that should use by Ground Control points for georeferencing. But on the other scanned map datasets did not contain the same spatial reference information in the same place as a digital map 1997. Thus, spatial reference information is using for general grounds points in raster dataset for georeferencing. But mostly natural and social objectives changed in Gifu city during the past 100 years, those changes are made troubles to georeferenced the map 1891. So, we used other maps such as 1920, 1947, 1970, 1992 years for to overlay 1997 and 1891.

Data representation

Digitizing is the process by which coordinates from a map, image, or other sources of data are converted into a digital format in a GIS [43]. This process becomes necessary when available data is gathered in formats that cannot be immediately integrated with other GIS data. For research, using ArcGIS 10.0 software on-screen digitizing method, which involves scanning a map or image into a computer, then traces the points, lines, and polygons. In this study had digitized layers of from topographical maps 1891. (Table 3.2, Figure 3.6.)

Table 3.2 Digitized layers and their description

Digitized layers		Layer type	Description of layers	
			Number of shape	Characteristics
Study area		Polygon	1	23471545.39m^2
River		Polygon	1	1731618.97m^2
Counter line		Polyline	375	7.5-300m height
Height points		Point	116	98-417.6m height
Flood protection	One side	Polyline	113	66457.4m
	Double-sided	Polyline	47	46261.22m

bank	Rocky bank	Polyline	12	79.63m
Land use type	Paddy field	Polygon	21	4321409.36m^2
	Urban	Polygon	68	2698371.26m^2
	Others	Polygon	176	15863656.45m^2

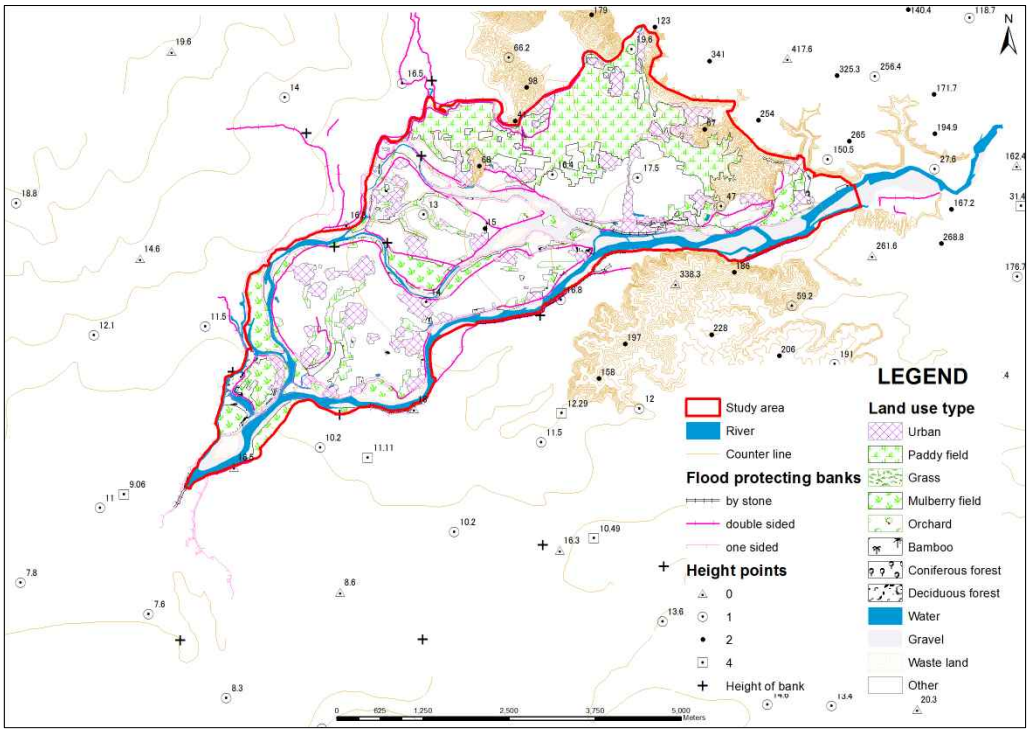

Figure 3.6 Digitized layers

Creation Digital Elevation Model, 1891

There are a number of interpolation methods in creating a DEM using contour line and height points digitized from the topographic map were illustrated and explained. In this research, I selected create DEM by following methods as figures. (Figures 3.7-3.10).

a) Labeling contour map. Contour lines and height points are a familiar way of representing surfaces on maps and quickly interpret the shape of the terrain.

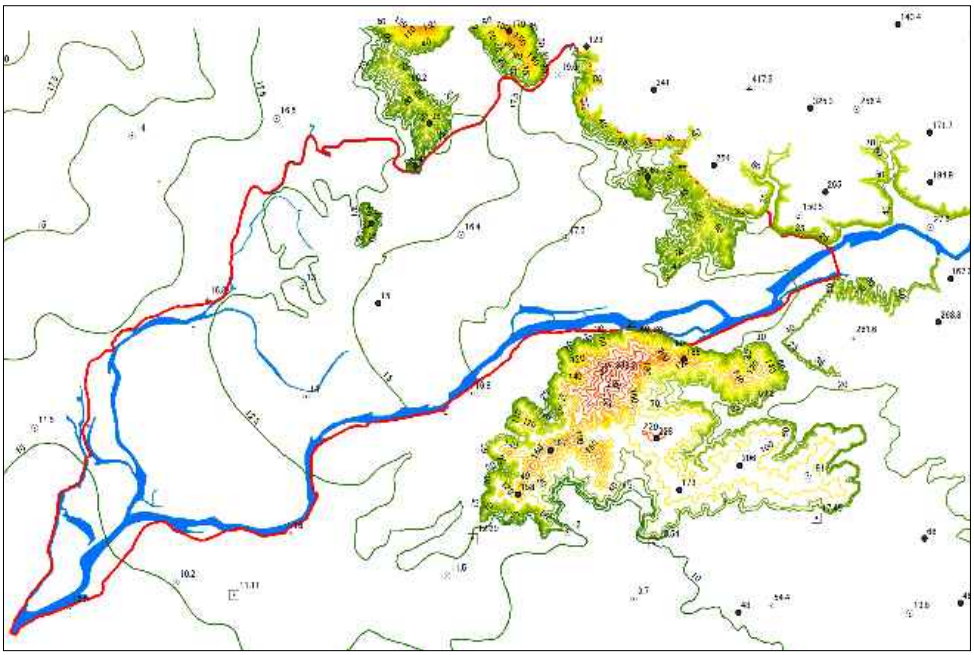

Figure 3.7 Labeling contour map

A contour line connects a series of points of equal elevation, and it is used to illustrate relief on a map. For example, numerous contour lines that are too close with another contour line, usually at a hilly or mountainous terrain. When they far apart, they indicate a gentler slope. Also, the contour is a line through all cross points with equal height (or other) values.

In order to output a more detailed DEM, need to digitize the contours with 7.5-300 m of height, elevation points are with 98-417.6m height. Alternatively, sample points can also be collected from a ground survey using GPS. The more sample points collected and used, the more accurate the output will be in representing the earth's surface.

b) Create a TIN model. A triangulated irregular network (TIN) surface can be generated from either surface source measurements or by converting another functional surface to a TIN surface from counter line, and points, which contain elevation information. A TIN is an efficient way of representing continuous surfaces as a series of linked triangles. Figure 3.11.

In ArcGIS software, you can create TIN by the command "Create TIN'' from ArcToolbox/3D Analyst Tools/TIN management.

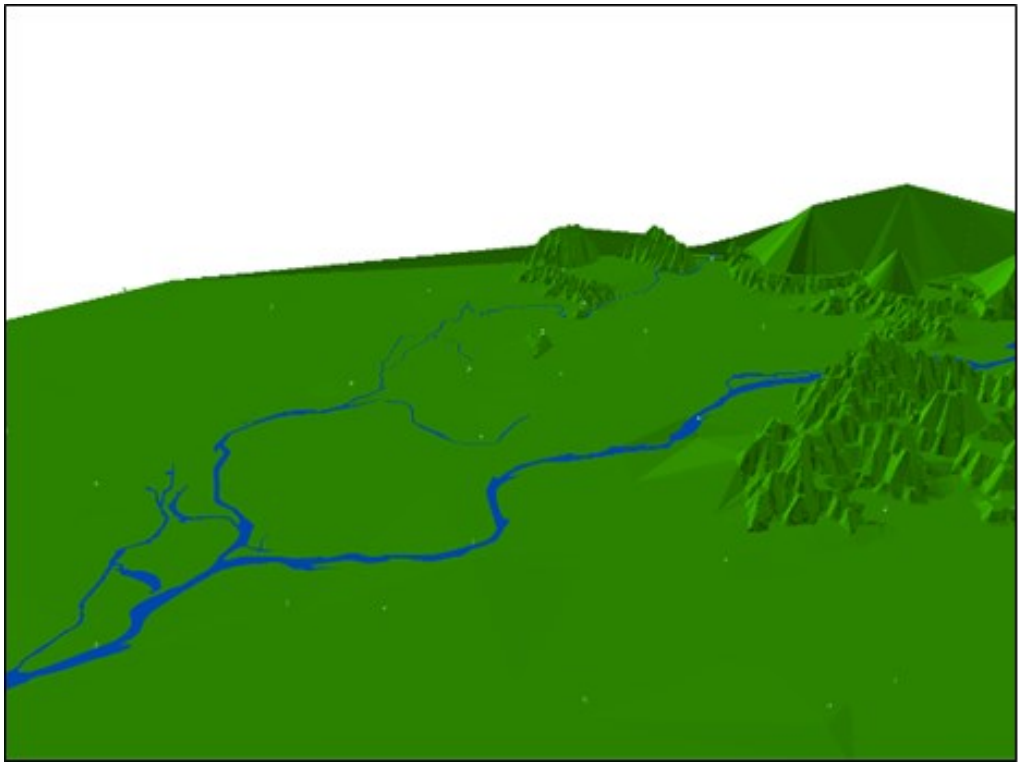

Figure 3.8 TIN model

c) Elevation points. For create DEM, we needed nodes from TIN into an output feature class and produces a 2D or 3D point feature class whose points are extracted from nodes of the input TIN.

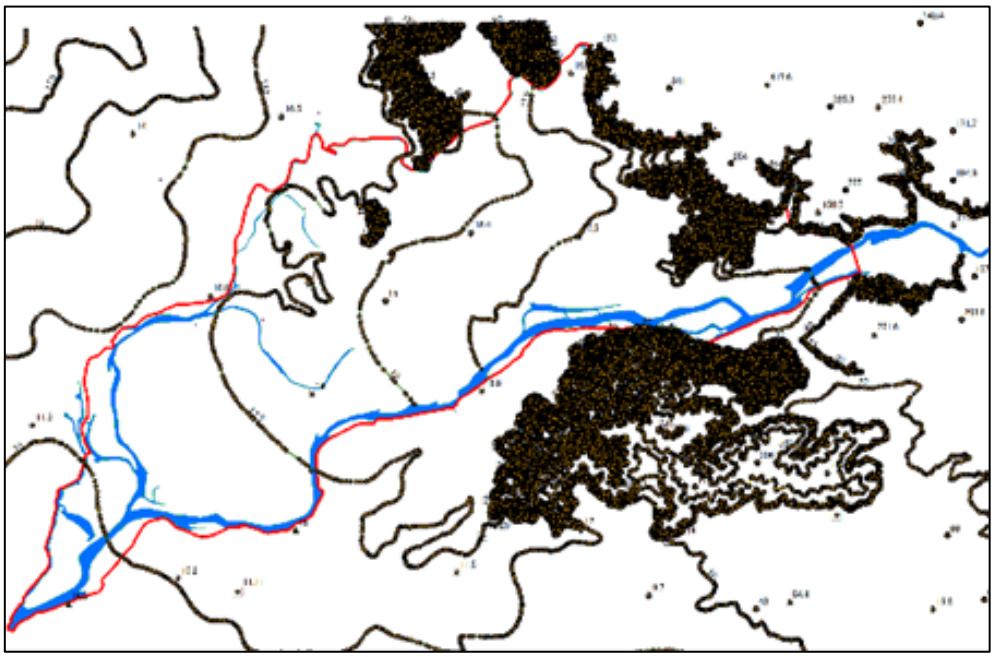

Figure 3.9 Elevation points

d) Create DEM (Interpolation using elevation points) Some of the most common interpolation methods include Inverse Distance Weighted (IDW) interpolation, Spline, & Kriging. These are all available in ArcGIS 10.0 software.

IDW [44] is the method, which should be used when the set of points is dense enough to capture the extent of local surface variation needed for analysis. It estimates cell values by averaging the values of sample data points in the neighborhood of each processing cell. The closer a point is to the center of the cell being estimated, the more influence or weight it has in the averaging process. The higher the distance, the less influence the cell has on the output value.

Figure 3.10 Created DEM, 1891

DEM development for a flood simulation model

Contour line and elevation points are containing in created DEM 1891 as figure 3.13. In real life, there have many natural and human-made things are locating on the earth. So, I need to develop that old DEM by levee, paddy fields and river valley too.

For this section, I tried to overlay old DEM data with some objects containing height information by the following method as figures 3.11-3.15. In topographical map 1891 is contained levee, land use types such as paddy fields and urbanized area so on.

a) Line data of flood protecting the bank. Here, I am digitized levee by polyline from topological map 1891. (Table 3.2, Figure 3.11)

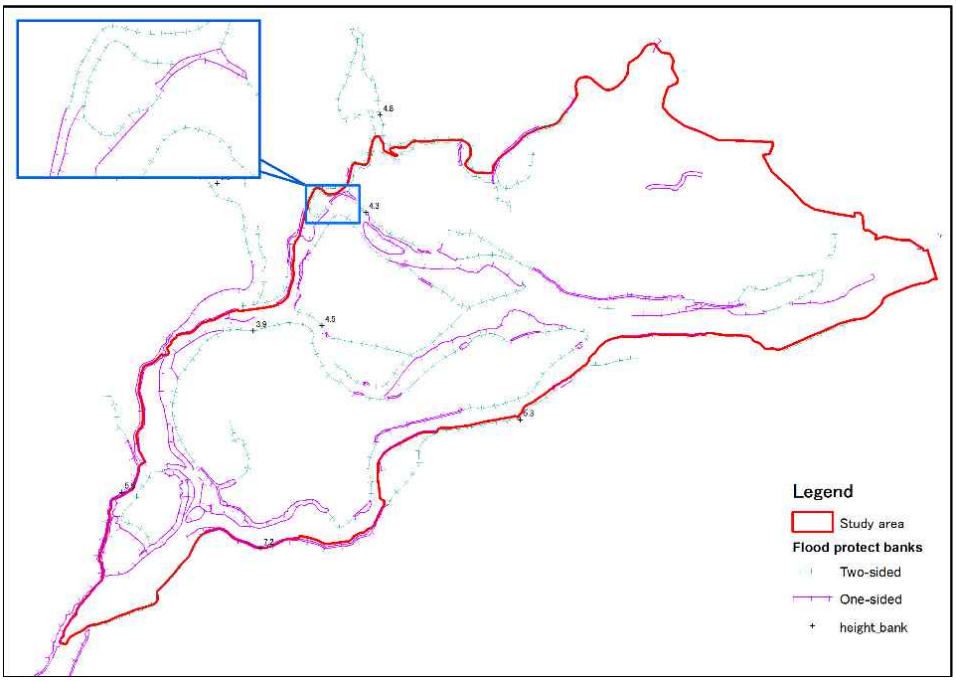

Figure 3.11 Flood protecting bank

b) Create a buffer zone 15m. In the old topographical map, the average width of the levee was 15m. So, in this step, I created a buffer zone by 15m from each bank of river. (Figure 3.12)

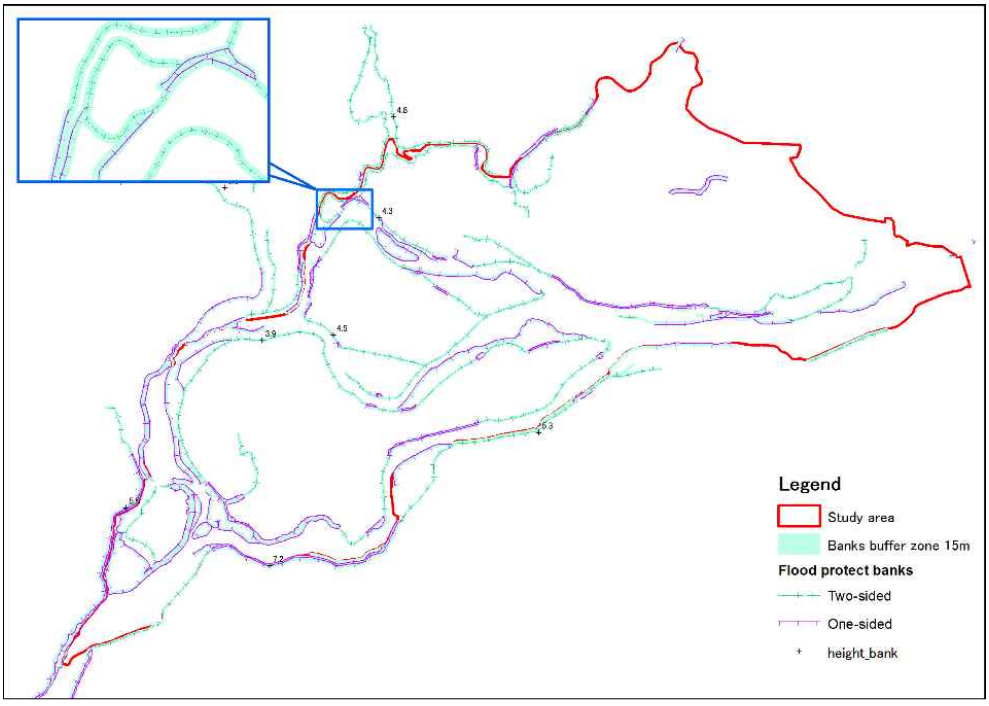

Figure 3.12 Created buffer zone by 15m

c) Set elevation 5m. In this step, the average height of levee was 5m in Meiji era. So, I edited attribute data of levee by 5 m height elevation. Then convert that data to raster data. (Figure 3.13)

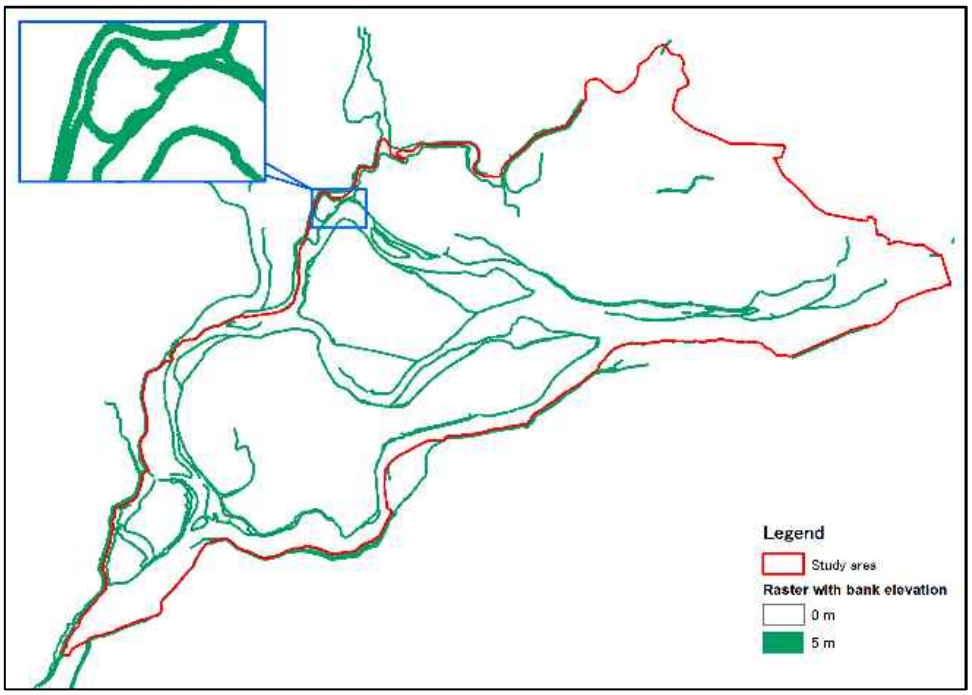

Figure 3.13 Convert to raster data containing elevation information

d) Unit raster data. The last step is to unit two raster data, which created DEM data and converted raster data containing height information of levee. (Figure 3.14)

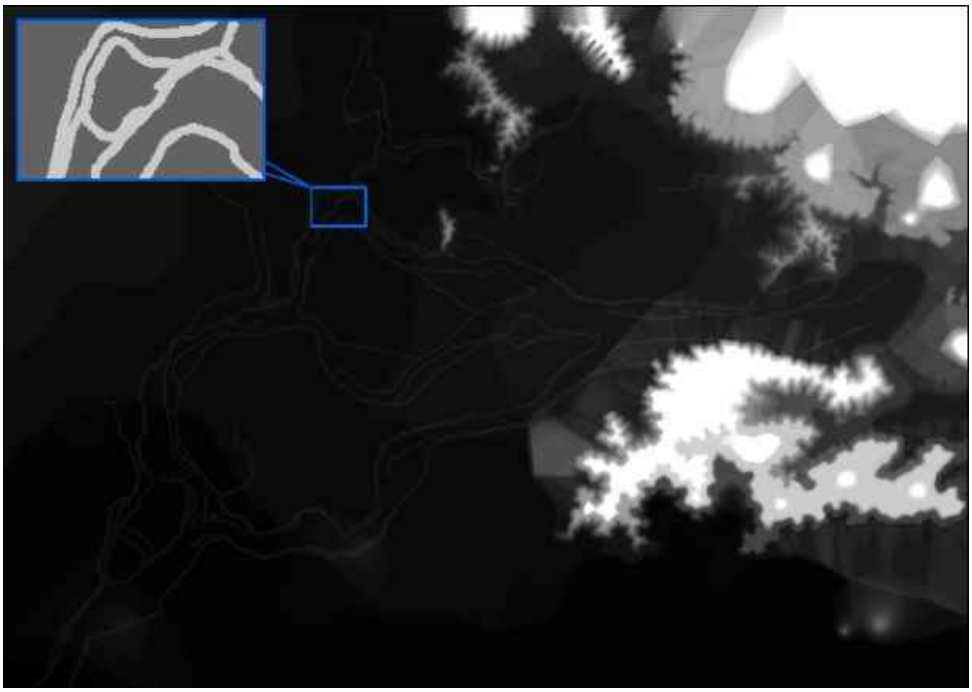

Figure 3.14 DEM data with 5 m high flood protecting the bank

By that method, other conditions (1 m deeper of the river, and 0.5m more in-depth of paddy fields) are converted their raster. In the result, DEM in 1891 is developed by the height information (Figure 3.15): Levee – 5m high, Paddy field – 0.5m deep and River–1 m deep

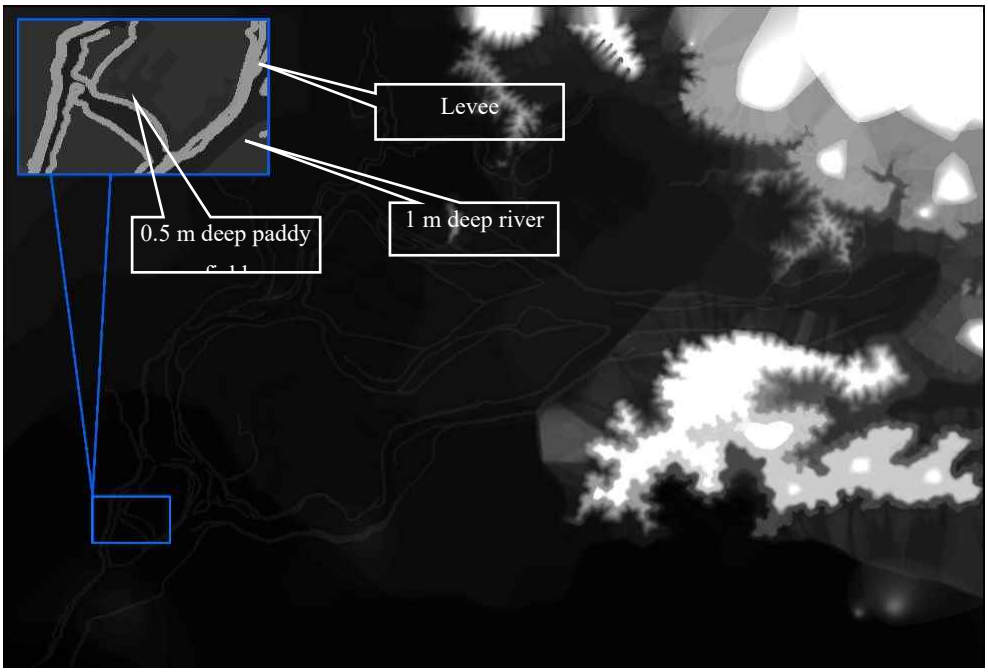

Figure 3.15 Developed DEM by the height information

Creation land use map

Land use involves the management and modification of natural environment or wilderness into built environment such as settlements and semi-natural habitats such as arable fields, pastures, and managed woods. It also has been defined as “the arrangements, activities, and inputs people undertake in a certain land cover type to produce, change or maintain it”. [45]. In that section, I created land use maps of former times and current times by the current land use data and to digitized land use polygon data from the topographical map, 1981. You can see from figure 3.16 and figure 3.17, and land usage is changing to urbanized are too fast.

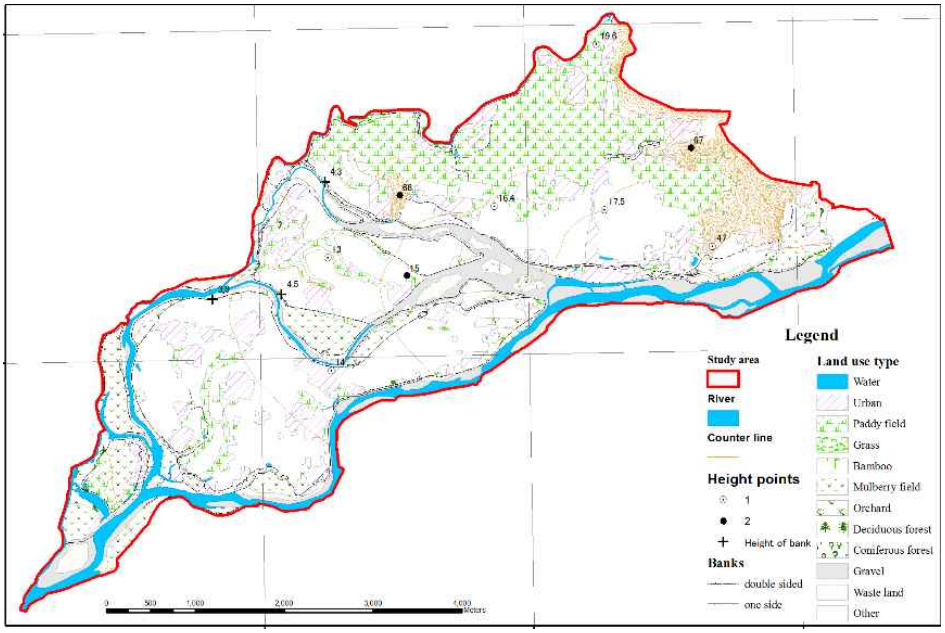

Figure 3.16 Land use map, 1891

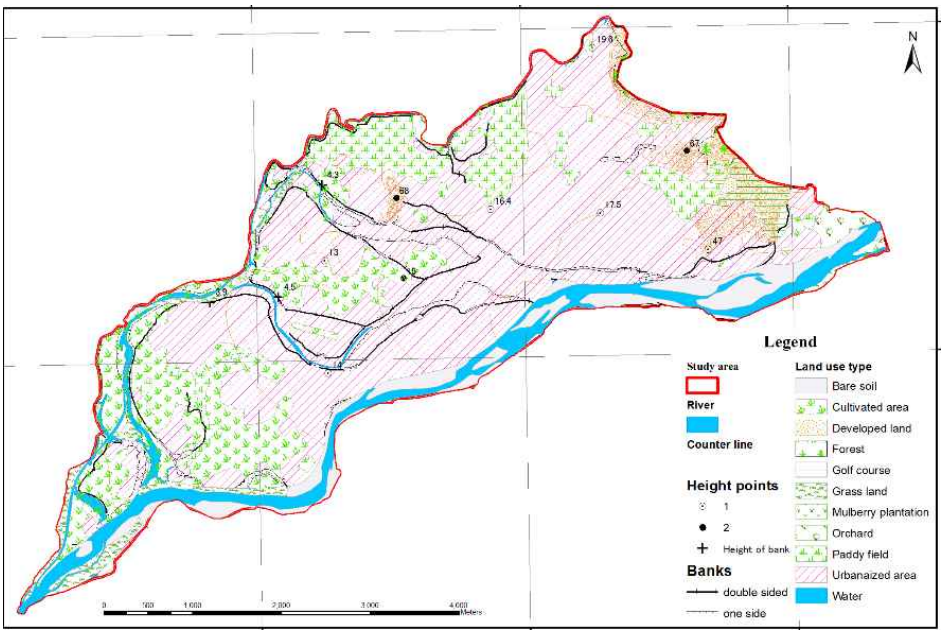

Figure 3.17 Land use map, current time

3.2.3. Hydrological data

This study is using a database [46] of the river discharge volume and water level data from Chusetsu-bridge point data of the Nagara river for hydrological analysis. Figure 3.18 shows the web page of the Chusetsu observing station.

Figure 3.18 Database based on webpage

In this database, Nagara-bridge point is observing only water level data, but Chusetsu-bridge point is observing both of water level data from 1976 and river discharge volume data from 2002. I used the Chusetsu point data to estimate probable hydrological discharge value.

Hydrological data processing

a) Total inundation water volume

The total floodwater volume in this research is decided with the hydrograph of Basic High Water as follows:

Basic high water is the maximum river discharge volume used in the flood control plan such as construction of dam and banks. The basic high water for the Nagara river (Chusetsu point), which is decided under the comprehensive judgment with hydrological statistics, historical flood and model simulation, is 8900m^3/s as Figure 3.19. [47]

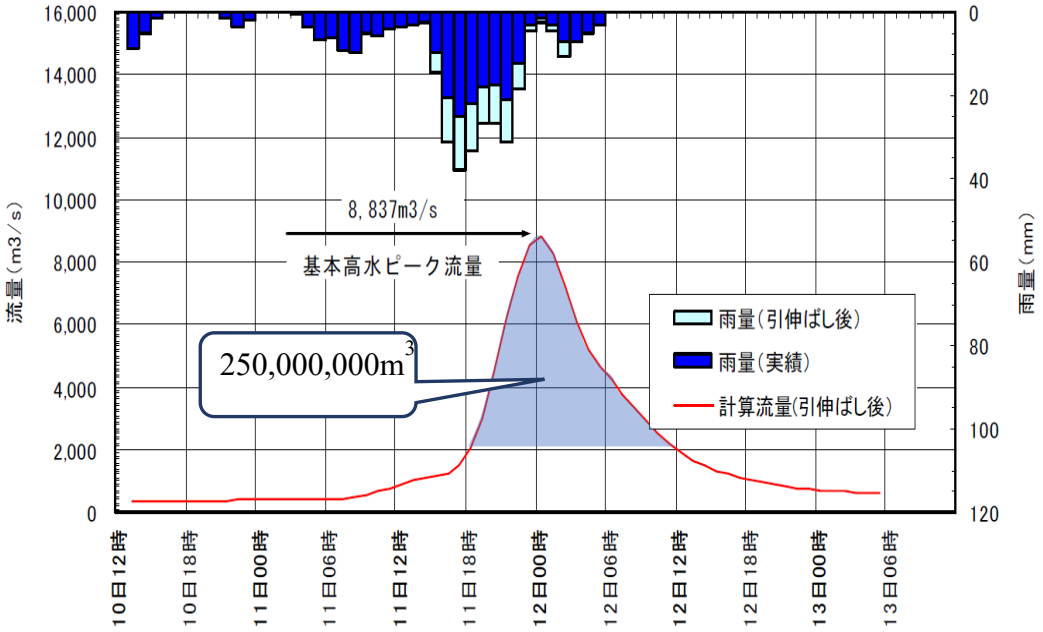

Figure 3.19 Hydrograph to decide peak discharge volume of basic high water level.

I assumed as the flood situation that the whole of the discharge volume larger than 2000m^3/s overflow to flood plain. Total inundation water volume is estimated with the summation of the discharge volume larger than 2000m^3/s in the hydrograph of the necessary high water. It is defined as 250,000,000 m^3.

b) Hydrograph for flood simulation

The hydrographs for flood simulation by iRIC is decided with hydrological frequency analysis. First, the annual maximum hourly discharge data from 2002 to 2012 at Chusetsu point is evaluated as Table 3.3.

Table 3.3 List of annual maximum peak discharge

Year	Annual maximum discharge (m^3/s)
2002	5334.34
2003	2374.18
2004	7666.87
2005	2158.62
2006	3309.36
2007	2654.77
2008	1409.24

2009	2423.78
2010	2770.68
2011	2661.89
2012	2102.23

The Weibul formula is applied as plotting position formula to this hydrological data as Table 3.4.

Table 3.4 List of annual maximum discharge and probabilities by plotting position formula

	Annual maximum discharge (m^3/s)	*p (i)*
1	1409.24	0.08333
2	2102.23	0.16667
3	2158.62	0.25000
4	2374.18	0.33333
5	2423.78	0.41667
6	2654.77	0.50000
7	2661.89	0.58333
8	2770.68	0.66667
9	3309.36	0.75000
10	5334.34	0.83333
11	7666.87	0.91667

The following 3 probability distribution functions are applied. [48]

a) Gumbel distribution

$$f(x)=\frac{1}{a}\exp\left\{-\frac{x-c}{a}-\exp\left(-\frac{x-c}{a}\right)\right\} \tag{3.1}$$

where, x is valuable, a and c is the parameters.

b) 2-parameter log-normal distribution

$$f(x)=\frac{1}{x\zeta\sqrt{2\pi}}\exp\left\{-\frac{1}{2}\left(\frac{\ln x-\lambda}{\zeta}\right)^2\right\} \tag{3.2}$$

where parameter log-normal x, $\zeta$is the standard deviation of x.

c) 3-parameter log-normal distribution

$$f(x)=\frac{1}{x\zeta\sqrt{2\pi}}\exp\left\{-\frac{1}{2}\left(\frac{\ln(x-c)-\lambda}{\zeta}\right)^2\right\} \tag{3.3}$$

where c is a lower limit value, which is defined as Equation 3.4.

$$c=\frac{x_1x_N-x_m{}^2}{x_1+x_N-2x_m} \tag{3.4}$$

The fitting parameters of each distribution function are estimated with the graphical estimation method as follows:

a) Gumbel distribution

a = 1942.3

c = 0.00058297

b) 2-parameter log-normal distribution

ζ= 0.58885

λ = 7.9521

c) 3-parameter log-normal distribution

c = 997.37

ζ = 0.90987

λ = 7.4375

Also fitting accuracies of each distribution function are evaluated as follows (see Figures 3.20 to 3.23):

a) Gumbel distribution: SLSC = 0.02670

b) 2-parameter log-normal distribution: SLSC=0.01803

c) 3-parameter log-normal distribution: SLSC=0.01395

3-paremeter log-normal distribution shows the best fitting accuracy. So, I use this distribution to estimate the probable discharge volume.

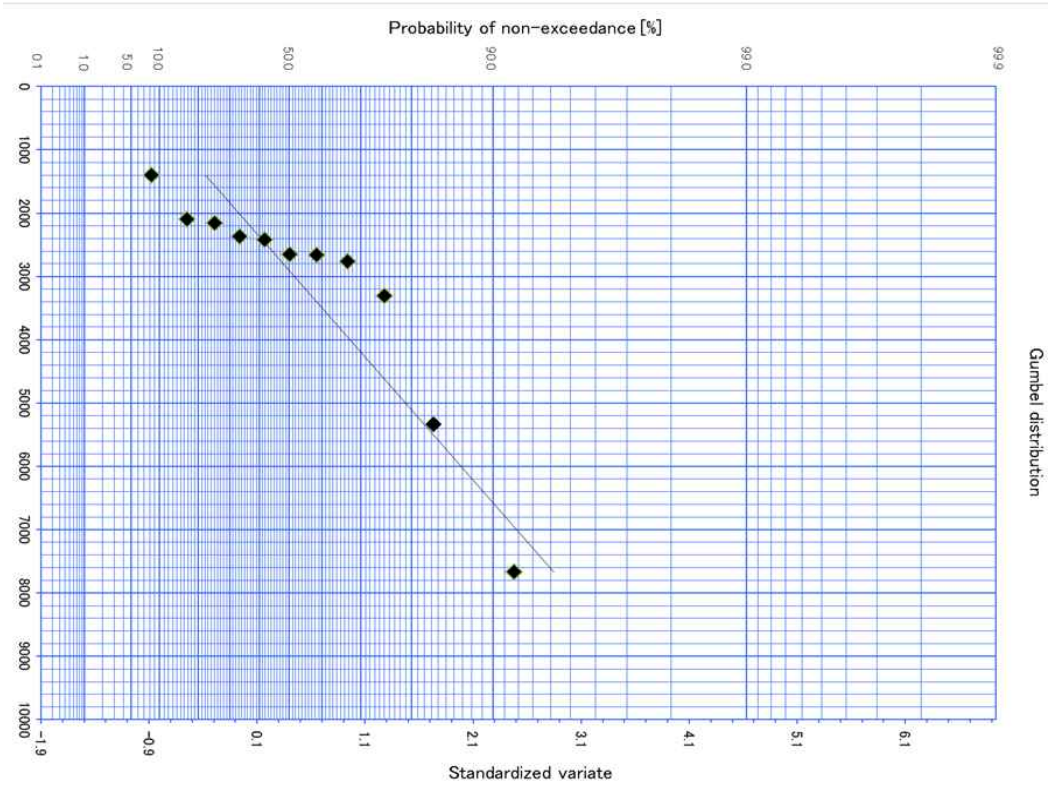

Figure 3.20 Probable plotting sheet of Gumbel distribution

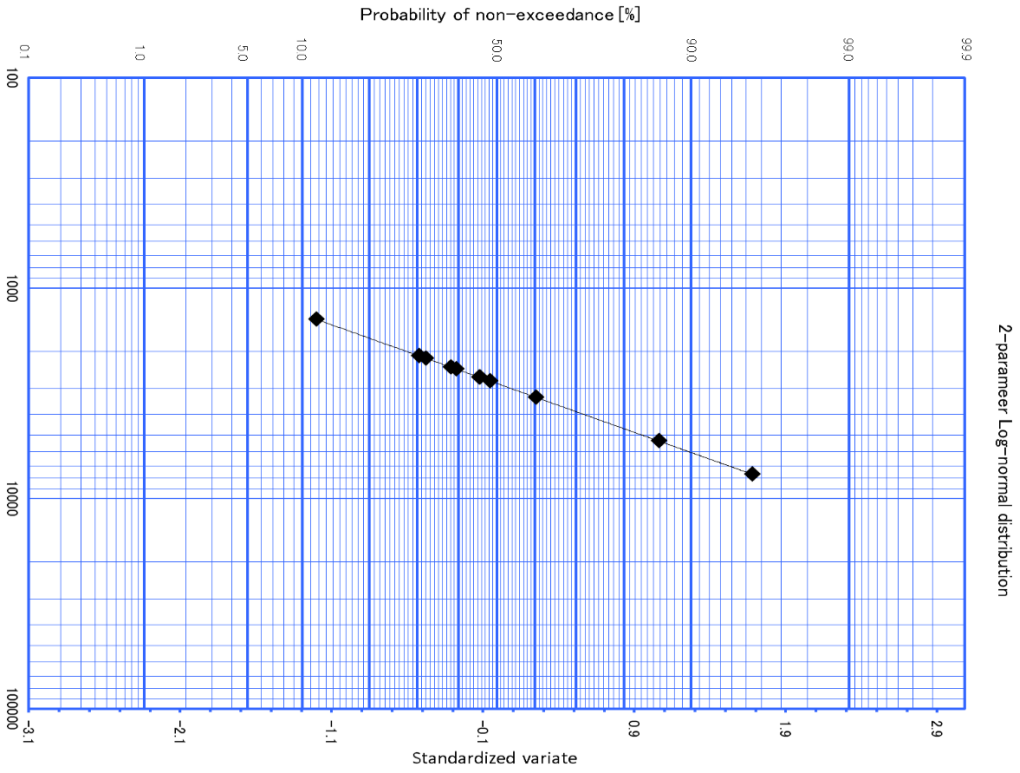

Figure 3.21 Probable plotting sheet of 2-parameter log-normal distribution.

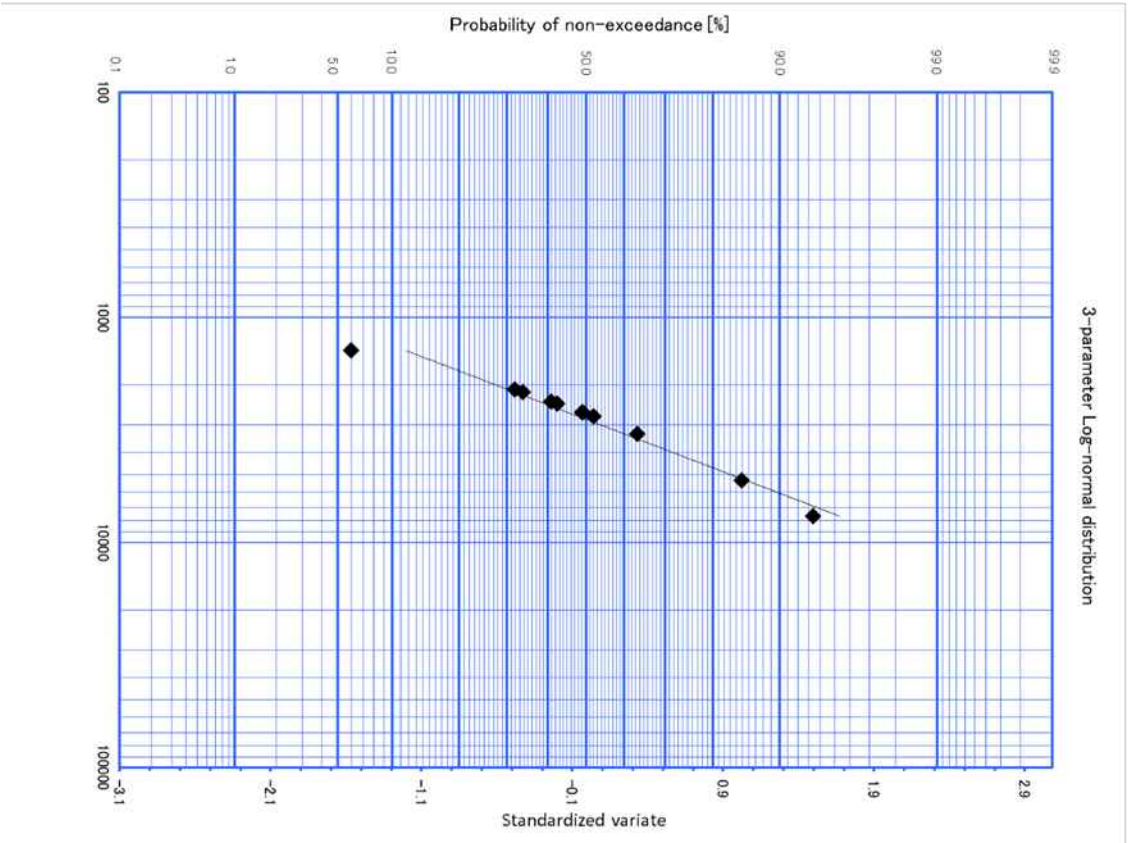

Figure 3.22 Probable plotting sheet of 3-parameter log-normal distribution.

The probability peak discharge of return period T=5 years is estimated as Q=3653m^3/s with the above hydrological frequency analysis.

For the flood simulation, the simulation hydrograph is decided as follows: for time series pattern, the observed hydrograph from 18 September 2012 to 20 September 2012. I cut the data to shorten the total simulation time as Figure 3.24. Finally, I get the hydrographs for flood simulation with iRIC, to edit the discharge volume to fit the peak discharge to Q=3653 m^3/s as Figure 3.25.

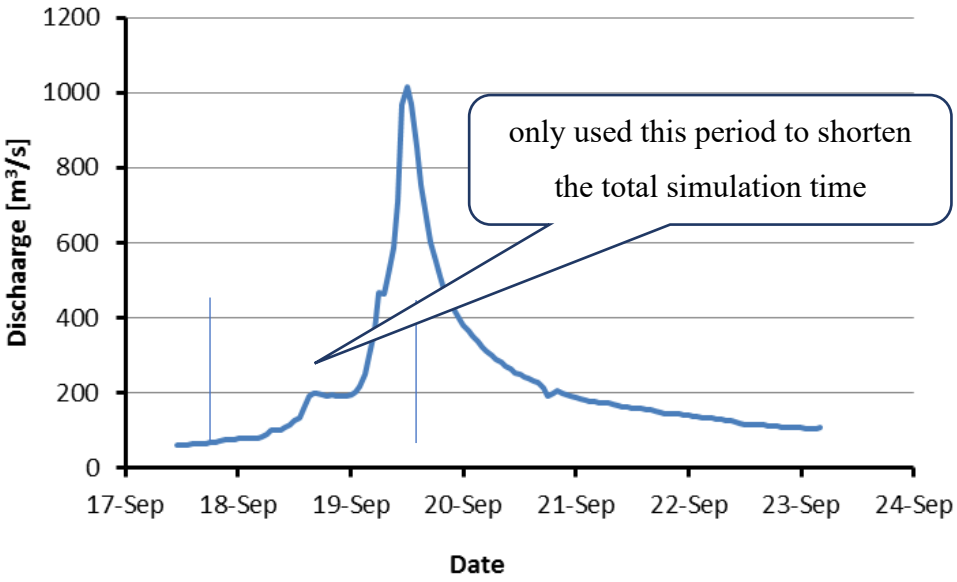

Figure 3.23 Original observed hydrograph

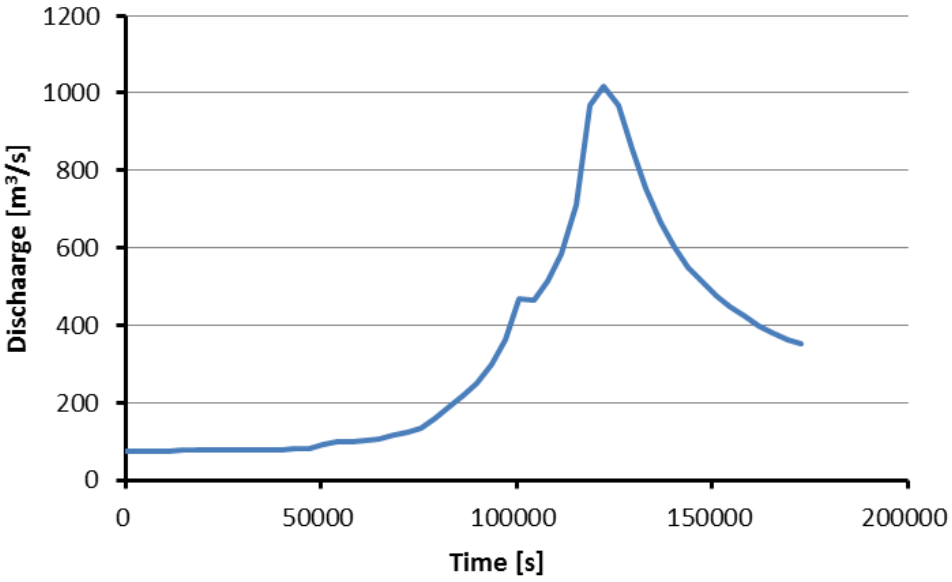

Figure 3.24 Shorten hydrograph.

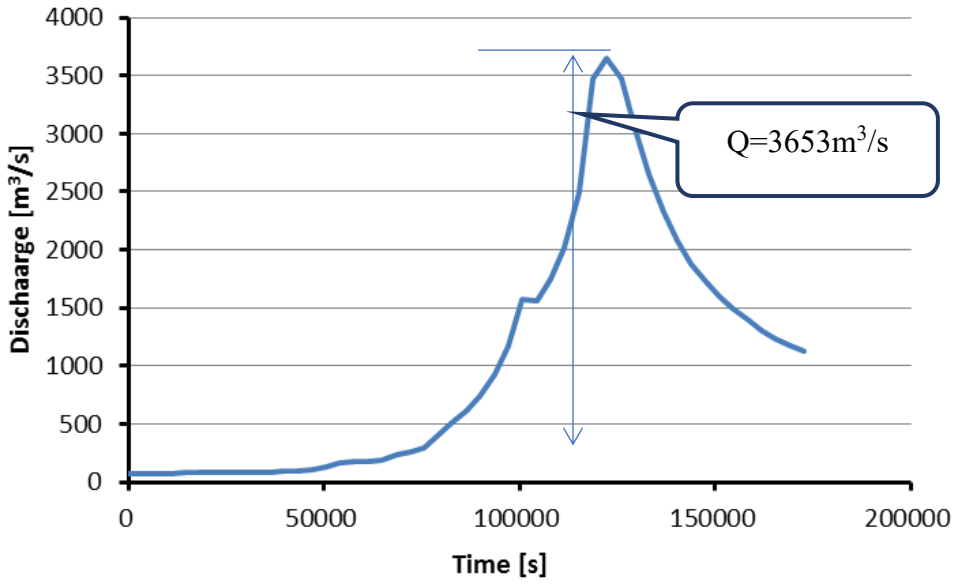

Figure 3.25 Final hydrograph.

3.3. Flood risk evaluation by a flood simulation model

3.3.1. General Introduction of iRIC flood model

The essential operation and startup procedures of Nays2D Flood, which is compiled with iRIC, Nays2D Flood simulates two-dimensional plane river flow and riverbed deformation. It was developed by Professor Yasuyuki Shimizu of Hokkaido University.[49]. The International River Interface Cooperative (iRIC) software application provides an integrated river simulation environment. iRIC provides a comprehensive, unified environment in which data necessary for river analysis solvers (hereafter: solvers) can be compiled, rivers can be simulated, and analytical results can be visualized.

In this chapter, iRIC Nays 2D Flood, an analytical solver for calculation of unsteady two-dimensional plane flow and riverbed deformation using boundary-fitted coordinates within general curvilinear coordinates is used to flood inundation simulation. iRIC Nays 2D Flood requires topographic data and calculation conditions to perform flooding calculation. The general operation for iRIC simulations is performed on the Windows system, with the following continuity and momentum equations of two-dimensional unsteady flow in the Cartesian co-ordinate system be expressed as [50]:

Continuity equation:

$$\frac{\partial h}{\partial t}+\frac{\partial(hu)}{\partial x}+\frac{\partial(hv)}{\partial y}=r \tag{3.5}$$

Momentum equations:

$$\frac{\partial(uh)}{\partial t}+\frac{\partial(hu^2)}{\partial x}+\frac{\partial(huv)}{\partial y}=-hg\frac{\partial H}{\partial x}-\frac{\tau_x}{\rho}+D^x \tag{3.6}$$

$$\frac{\partial(vh)}{\partial t}+\frac{\partial(huv)}{\partial x}+\frac{\partial(hv^2)}{\partial y}=-hg\frac{\partial H}{\partial y}-\frac{\tau_y}{\rho}+D^y \tag{3.7}$$

$$\frac{\tau_x}{\rho}=C_f u\sqrt{u^2+v^2} \tag{3.8}$$

$$\frac{\tau_y}{\rho}=C_f v\sqrt{u^2+v^2} \tag{3.9}$$

$$D^x=\frac{\partial}{\partial x}\left[\nu_t\frac{\partial(uh)}{\partial x}\right]+\frac{\partial}{\partial y}\left[\nu_t\frac{\partial(uh)}{\partial y}\right] \tag{3.10}$$

$$D^y=\frac{\partial}{\partial x}\left[\nu_t\frac{\partial(vh)}{\partial x}\right]+\frac{\partial}{\partial y}\left[\nu_t\frac{\partial(vh)}{\partial y}\right] \tag{3.11}$$

$$\nu_t=\frac{\kappa}{6}u_* h \tag{3.12}$$

$$C_f=\frac{gn^2}{h^{1/3}} \tag{3.13}$$

where: h = water depth

t = time

u = depth-averaged velocity components in x direction

v = depth-averaged velocity components in y direction

r = rainfall

g = gravity acceleration

H = water height

τ_x = bed shear stress in x direction

τ_y = bed shear stress in y direction

C_f = bed friction coefficient

ν_t = eddy viscosity

ρ = water density

κ = Karman constant (= 0.4)

u_* = shear velocity

n = Manning's roughness coefficient

3.3.2. Calibration

Performance of the iRIC model was applied to simulate the Nagara river floodplain, which is flatland on the right side of the Nagara River, where is the area between the NagaraRiver, the Ijira River, the Toba River, and Mont. Dodogamine. The simulation has focused on the applicability of water flow and flood propagation by using flow conditions in the year of 2011.

Computational conditions. Figure 3.29 shows the computational grids and the land-cover category map. Grid cell size is about 40 x 40 m. The boundary condition of upper-side is non-discharge. The boundary conditions of the right and left, and lower-side are free to discharge. The test hydrograph is entered from the inflow point on the upper-side boundary, as shown in Figure 3.26. Red and blue areas are land-cover categories for the definition of roughness coefficients. Blue indicates river stream area, in where roughness coefficient n is defined as 0.01. The red area is another land cover type, in where n is defined as 0.03. Other computational conditions are shown in Table 3.5.

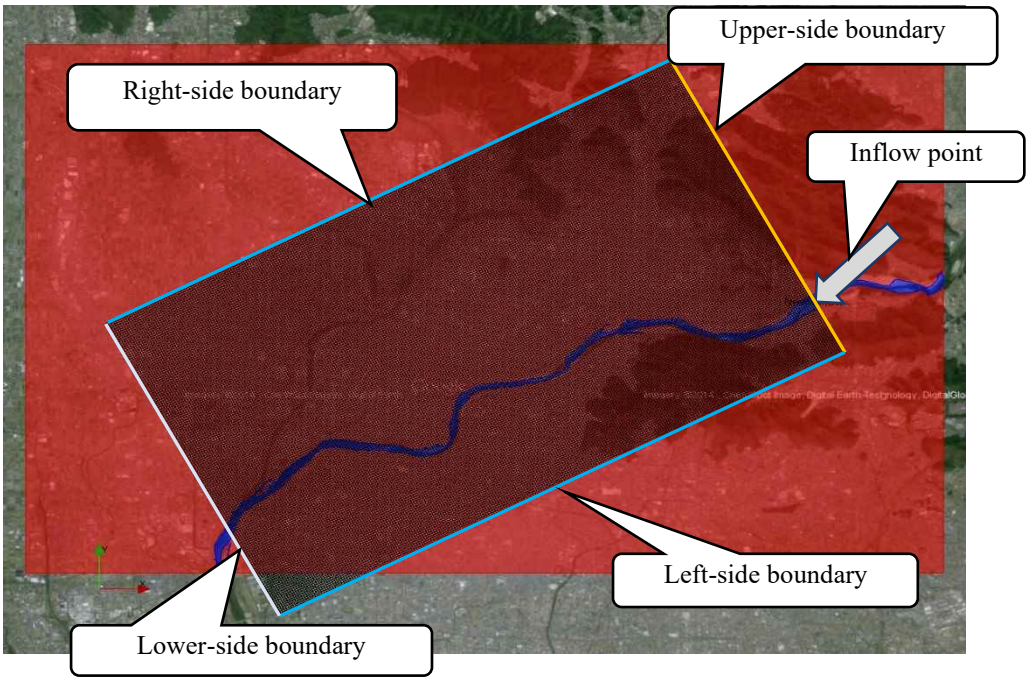

Figure 3.26 Illustration of the computational grids and boundaries.

Table 3.5 Other computational conditions

Precipitation	0 mm/h
Initial water depth	0 m
Computational time step	0.01 sec
Difference method	CIP method

3.4 Results and discussions

Simulation cases

The following cases are simulated in this study.

a) Case 1

Target date: Modern age

Topography: 5-m DEM published by GSI

b) Case 2

Target date: Modern age

Topography: 5-m DEM published by GSI with the artificial crevasse on the levee around the Nagara bridge.

c) Case 3

Target date: Meiji era

Topography: 5-m DEM made from the old topographical map

Case 1

The simulated results with modern DEM without artificial crevasse on the levee are as follows. Figure 3.27 and Figure 3.28 are the simulated inundation depths before and after the overflow. The figures show the overflow occurs from nearby Kinka bridge, marked with a white circle in Figure 3.29 and figure 3.30 are the simulated inundation depth at 118,800sec and 128400 sec, respectively. These figures are also clearly shown the overflow from nearby Kinka bridge. Figure 3.31 is the simulated maximum inundation depth during the simulation period in Case-1. Those figures are show the inundation flood mainly damages to the south side of the Nagara River from near Kinka bridge. It seems that the modern river infrastructure developments and flood control systems have an excellent performance to prevent flood.

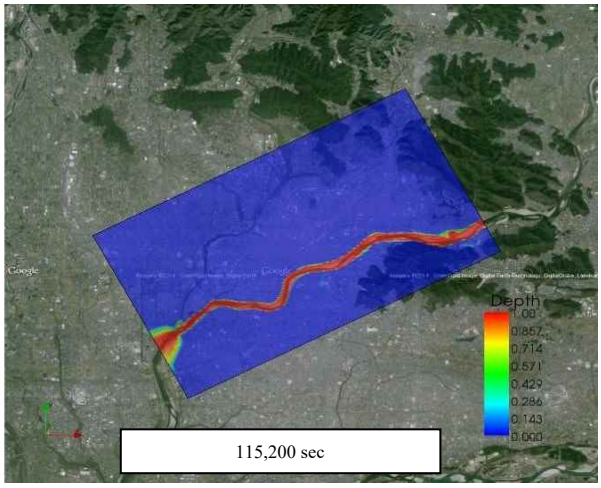

Figure 3.27 Simulated inundation depths at 115,200 sec in Case 1.

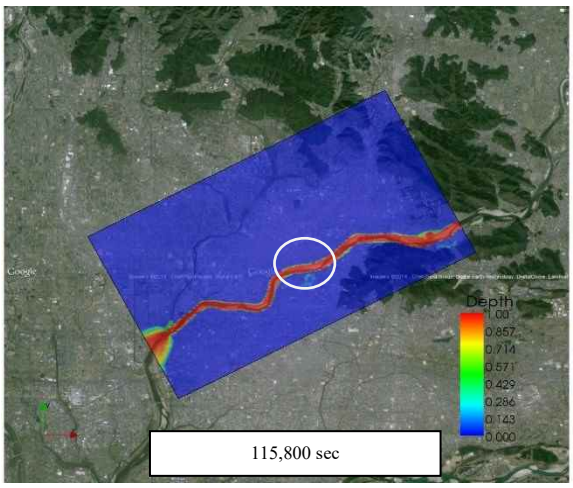

Figure 3.28 Simulated inundation depths at 115,800 sec in Case 1.

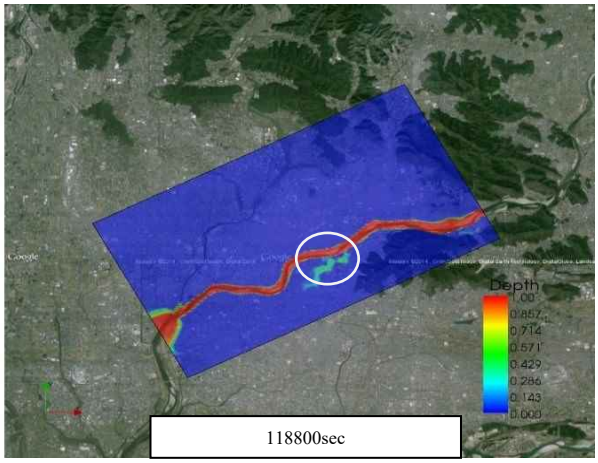

Figure 3.29 Simulated inundation depths at 118,800 sec in Case 1.

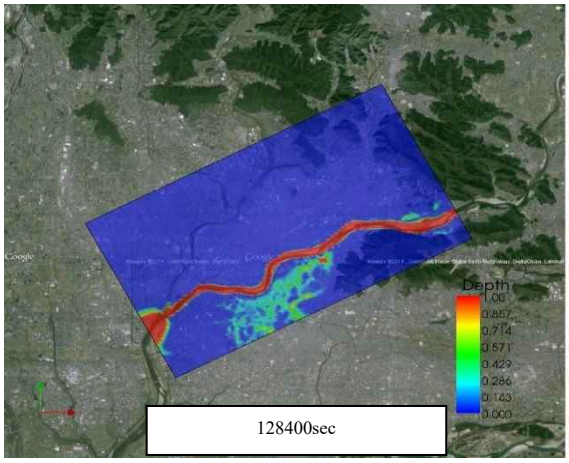

Figure 3.30 Simulated inundation depths at 128,400 sec in Case 1.

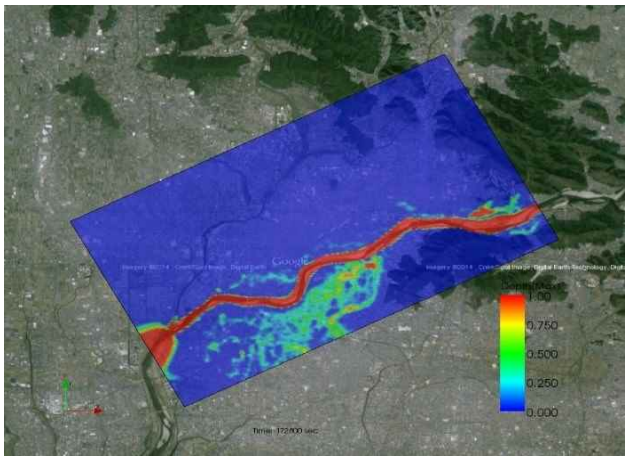

Figure 3.31 Simulated maximum inundation depths in Case 1.

Case 2

The simulated results with modern DEM with artificial crevasse at the levee near Nagara bridge are as follows. This artificial crevasse was created for determining the risk of inundation in the case if levee shall break due to natural disasters such as disasters, floods and other accidents. Figure 3.32 shows DEM image around Nagara bridge and Figure 3.33 shows an artificial crevasse on the levee by a red circle, which edited levee height for evaluate inundation risk when levee will break.

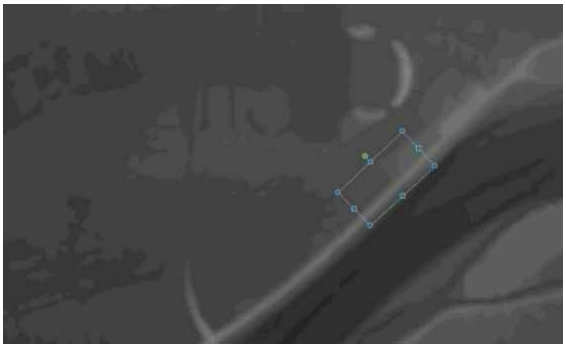

Figure 3.32 DEM image around the Nagara bridge

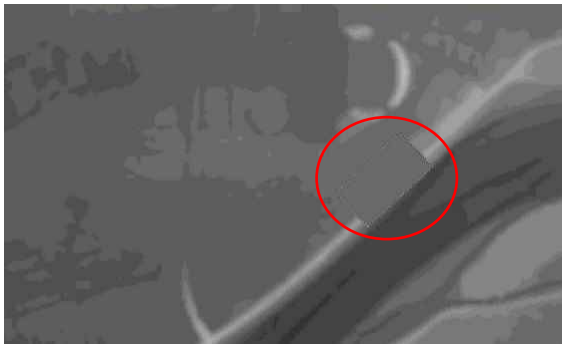

Figure 3.33 Edited levee height for evaluate inundation risk with an artificial crevasse.

Figure 3.34 – Figure 3.39 are showing the simulation inundation before and after depths the overflow from the artificial crevasse on the levee. The figures show the overflow occurs from the artificial crevasse, where is shown in the white circle of Figure 3.35. The timing of overflow occurrence is before the peak discharge time (show Figure 3.38).

Figure 3.36 shows the timing of overflow from the upper stream, where is not crevasse.

Figure 3.37 shows the simulated inundation depth at 128,400 sec. Figure 3.39 shows the simulated maximum inundation depth in Case 2. It seems the effect of old levee around Nishi-Nakashima to Danno-Shima in Figure 3.39. The flood inundation damages both of the northern and south side of the Nagara River in the case with the artificial crevasse (the Case 2).

However, in the case without artificial crevasse (the Case 1), the only south part of the Nagara river is damaged by flood inundation. It is indicated that the river infrastructures as levee make an excellent performance to protect the low land from flood disaster in the modern age.

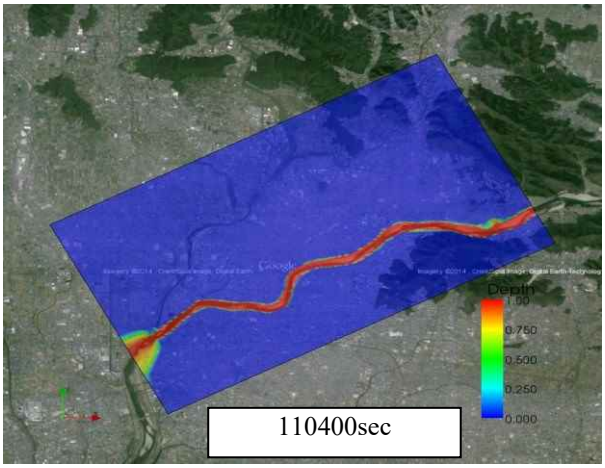

Figure 3.34 Simulated inundation depths at 110,400 sec in Case 2.

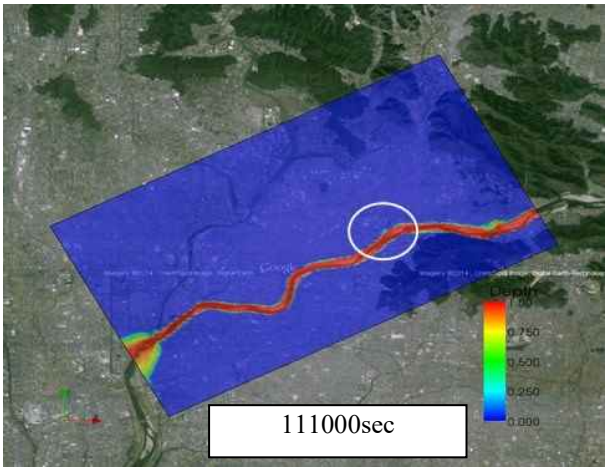

Figure 3.35 Simulated inundation depths at 111,000 sec in Case 2.

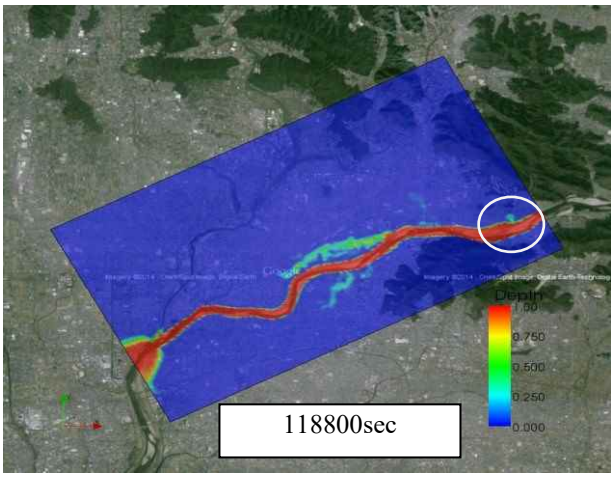

Figure 3.36 Simulated inundation depths at 118,800 sec in Case 2.

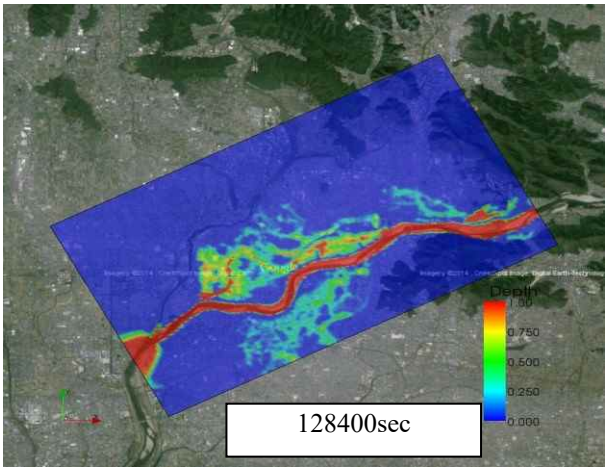

Figure 3.37 Simulated inundation depths at 128400 sec in Case 2.

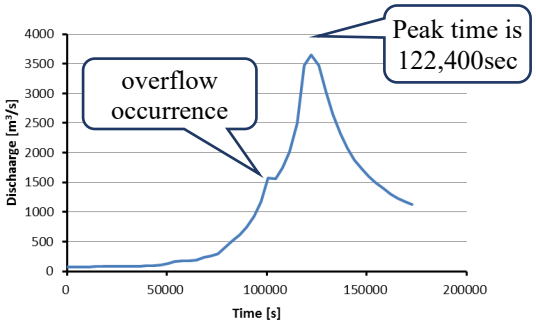

Figure 3.38 Input hydrograph and illustration of overflow occurrence timing.

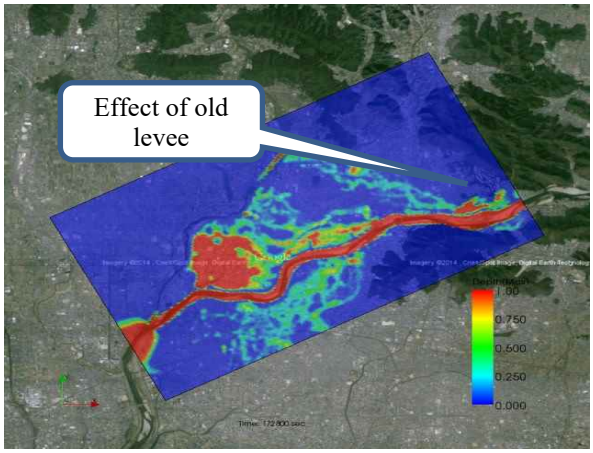

Figure 3.39 Simulated maximum inundation depths in Case 2.

Case 3

The simulated results with Meiji era DEM are as follows. The input water volume from the upper stream does not flow down through the river stream and overflow at the Obusa area (see Figure 3.40). This overflow point is the almost same as the results with the modern DEM. Figure 3.41 and Figure 3.42 are the simulated flood inundation at 76,800 sec and 160,800 sec, respectively.

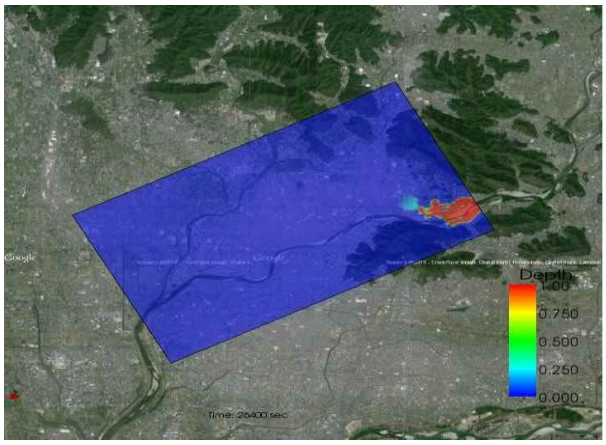

Figure 3.40 Simulated inundation depths at 26,400 sec in Case 3.

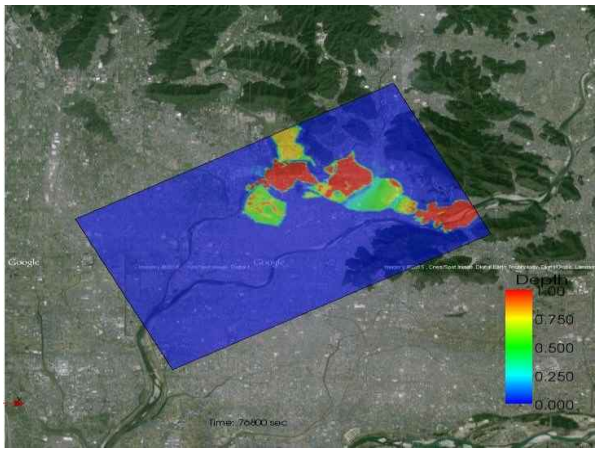

Figure 3.41 Simulated inundation depths at 76,800 sec in Case 3.

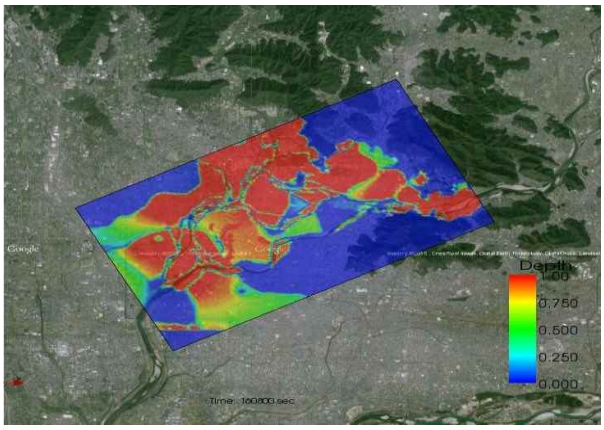

Figure 3.42 Simulated inundation depths at 160,800 sec in Case 3.

These figures show that the expanse of the simulated flood inundation area is affected by interpolated elevation data and levee. The Meiji era DEMs are produced by interpolation of the contour line from an old map. The contour lines on flatlands are apart from each other. Therefore, miss interpolation often occurs as Figure 3.43. Especially, streamlines should have the lowest elevation around there. This miss interpolation causes the damming around the Obusa area in Figures 3.40 to 3.42. It is one of the critical issues of the evaluation of flood risk with old topographical maps.

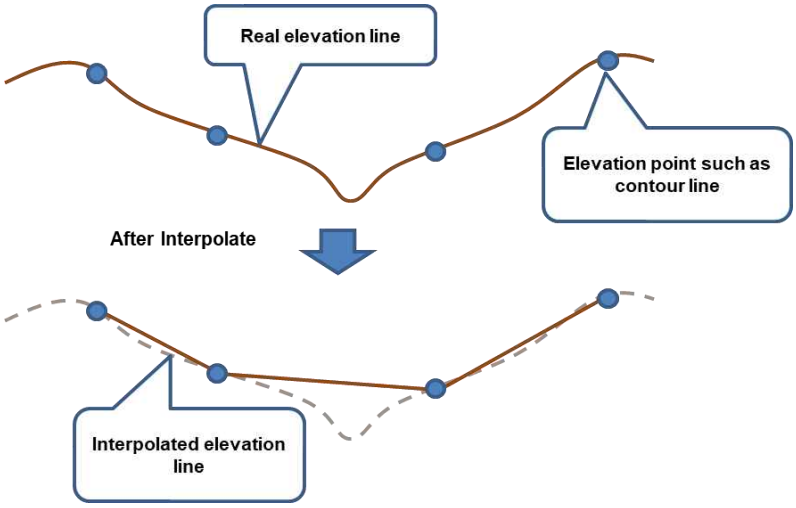

Figure 3.43 Illustration of the topographical interpolation error with contour lines.

3.5. Summary

In this chapter, the temporal changes of flood risks from the Meiji era to the current time in Gifu city are investigated with an old topographical map, GIS analysis, and flood simulation. The findings in this research are summarized as follows:

1) Land use changes are investigated by the comparison of the old map and current map. The area of paddy fields in the target area decreased by 30% from the Meiji era to the current time.

2) The flood simulation with the iRIC and 5-m DEM published by Japanese GSI is attempted using a sample hydrograph. It is showed that the iRIC and 5-m DEM have a good effect on the simulation of flood inundation.

3) The DEM in Meiji era is produced by the interpolation technique with the contour lines from the old topographical map. However, the interpolation with contour lines could not produce good DEM, which is suitable for flood simulation. In a normal map, elevations on the river bed are uncertain. Therefore, the interpolated river bed is often not smooth from up to downstream, as the mentioned results in this research. In the simulation results, the discharge from upstream is blocked by the irregular grid, and the unexpected overflow occurs in the upstream. It is showed that iRIC and high-resolution DEM has an excellent performance to simulate the flood inundation. The improvement of the interpolation technique from contour lines is one of the essential tasks for the evaluation of flood inundation risks with old topographical maps.

CHAPTER 4. ASSESSMENT OF LONG TERM FLOOD RISK CHANGES IN GIFU CITY

4.1. Introduction

Heavy rainfall within a short period and consequent high river discharge are results in floods which subsequently creates huge infrastructure problems for areas, such huge economic deficits in production as well as damages to existing property and goods, even loss of human lives. In about hundred years ago the flat-land around the Kiso Three Rivers system (the catchment areas of the Kiso River, Nagara River, and Ibi River are called "the Kiso Three River system") included Gifu City, Gifu Prefecture of Japan, was frequently damaged by inundation after heavy rainfall. Our research aims to evaluate flood risk changes by river improvement in the Kiso Three River system fin the past hundred years. For that reason, we simulated in several times on flood inundation in the large, medium and low scale case in the urban area of Gifu city with 2D flood inundation model, and compared the distribution of flood depth. The results, the flood inundation area in the urban area for small scale flood disaster dramatically is reduced from 3.82 km² in the past time to 0.48 km² in the current time with the progress of river infrastructure improvement. However flooded area in the urban area for large and middle scale disaster show the almost same. It is suggested that flood risks in urban area are dramatically improved for only a small disaster.

Gifu Prefecture was a frequent flood occurred area where damaged by the Kiso Three Rivers system since a long time ago. For this reason, river improvements and infrastructures are constructed on the branches of the Kiso Three river system from the 1900s to the current, which after construction the damage of the flood dramatically decreased. Although the risk of floods has reduced due to river improvements, it is finding that there are significant fluctuations in population and land use from 1920 to 2015. Such the phenomenon that the development of floodplain advances by embankment and development of levee is called "Levee Effect," and several studies have been conducted ([8]; [10]). However, in these studies, only studies using primary social data such as qualitative analysis and short-term population change are being conducted. On the other hand, Ito and Nakamura [Nakamura 2018], constructed long-term land use data and levee length database and found that urbanization progressed in the specific area after the levee was established.

However, it is not enough to evaluate how flood risks have been changing by the river infrastructure improvement, the rapid urbanization and land use changes, using 2D flood

inundation simulation. In this research, the authors investigate flood risk changes in the past 100 years with 2D flood inundation simulation analysis considered 100 years ago, and current topographical and river infrastructure situations. Also, land use changes have been evaluated and compared with simulated flood risks in order to investigate the relationship the levee development and urbanization and flood risk changes.

4.2. Research data

4.2.1 Topographical map and terrain information

Flood inundation analysis needs land surface topography. However, there is no data like the numerical elevation model in the 1900s. For this reason, we read terrain information from the topographic map and interpolate the elevation value to create a numerical elevation model from old maps. A numerical elevation model of the current time is created in the same way.

Here, we used the 1:20,000 scale topographical maps from 1891 to 1893 (Meiji 24 to 26 in Japanese calendar) surveyed by The Ministry of the Imperial Japanese Land survey to produce the past topographical map in Meiji era (mainly in 1891), and also used the 1:25,000 topological maps from 2002 to 2009 (Heisei 21 to 26 in Japanese calendar) corresponded by the Geospatial Information Authority of Japan to produce the current topographical map in Heisei era (mainly in 2009).

Based on the topographical maps of Figures 4.1 and 4.2, the terrain information such as contour line, reference points for ground surveying, height points, and levee shape was digitized to shapefile using ArcGIS software. The details of digitized terrain information are shown in Table 4.1.

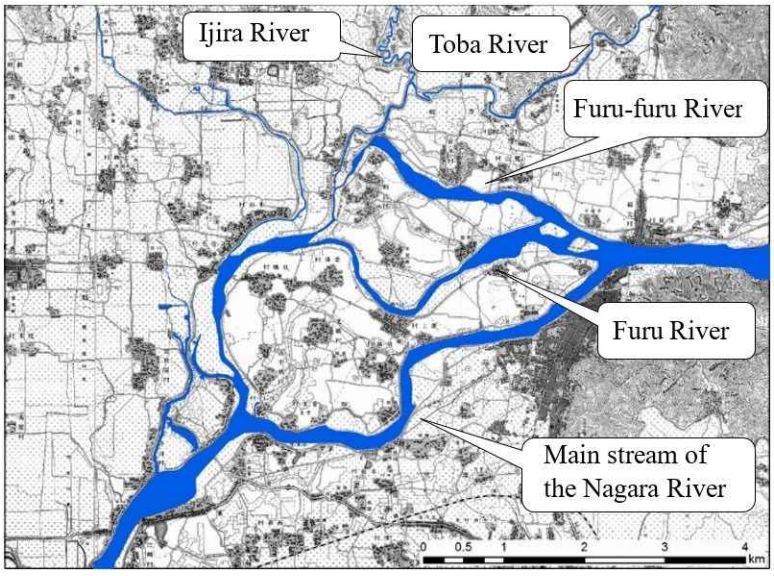

Figure 4.1 Topographical data in 1891 (Meiji era).

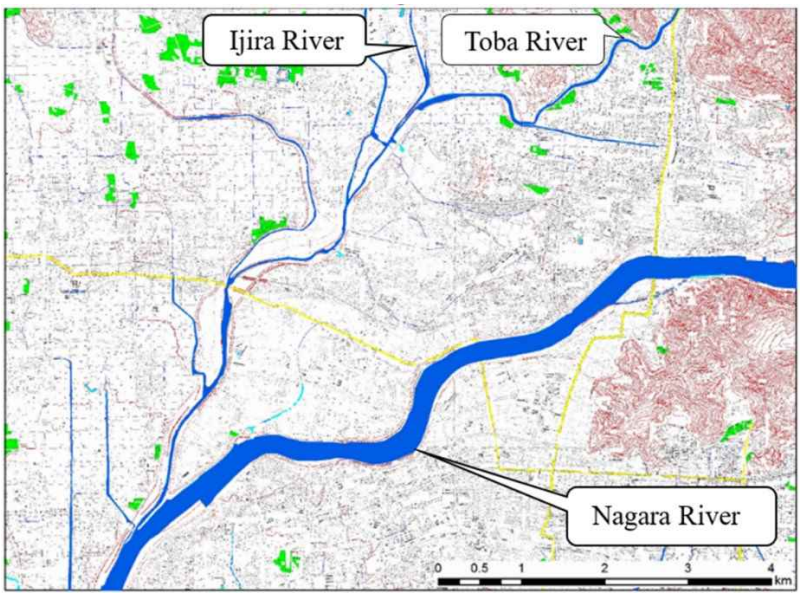

Figure 4.2 Topographical data in 2009 (Heisei era).

Table 4.1 Digitized Symbols.

Terrain symbol	Symbol sample on map	Layer symbol	Layer type
Contour			polyline
Levee	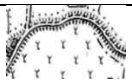		polyline
River			polygon
Reference point			point
Height points	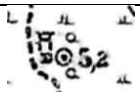		point

Here, height point shows the height from the average elevation around the point and often indicates the height of levee top from the ground height. Contour lines are digitized under 40 m asl because the whole urban area of Gifu city is locating less than 20 m. Flood inundation analysis does not need high mountain topography.

It is challenging to create a numerical elevation model, because of contour lines and reference points are not written in the river in the old topographic map. So, the contour lines which are interrupted in the river were joined in order to compensate for the elevation value in

the river. Moreover, surrounding rivers other than the Nagara River and the Ijira River were also digitized, but small rivers that do not affect the flooding calculation were omitted.

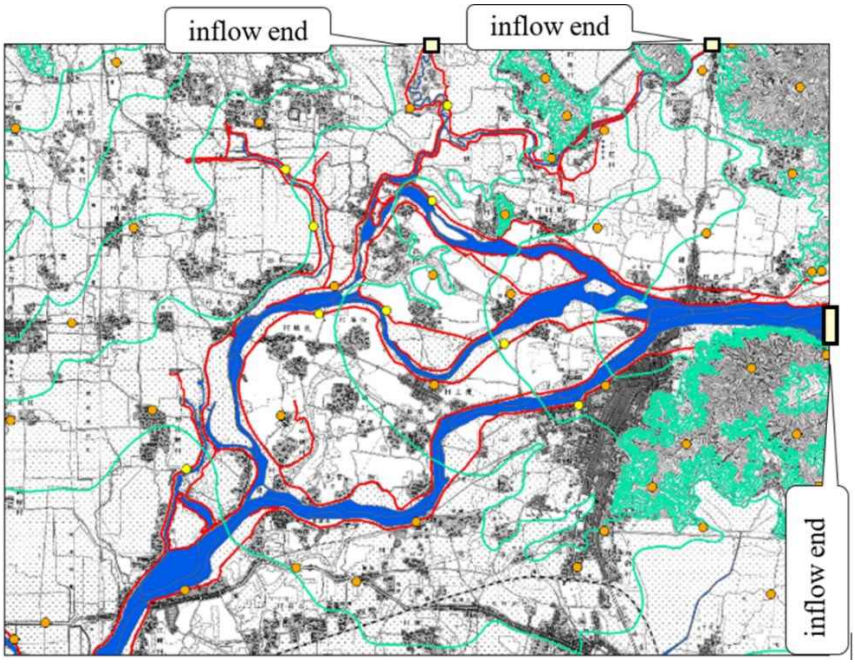

Figure 4.3 Digitized symbols in 1891 (Meiji era).

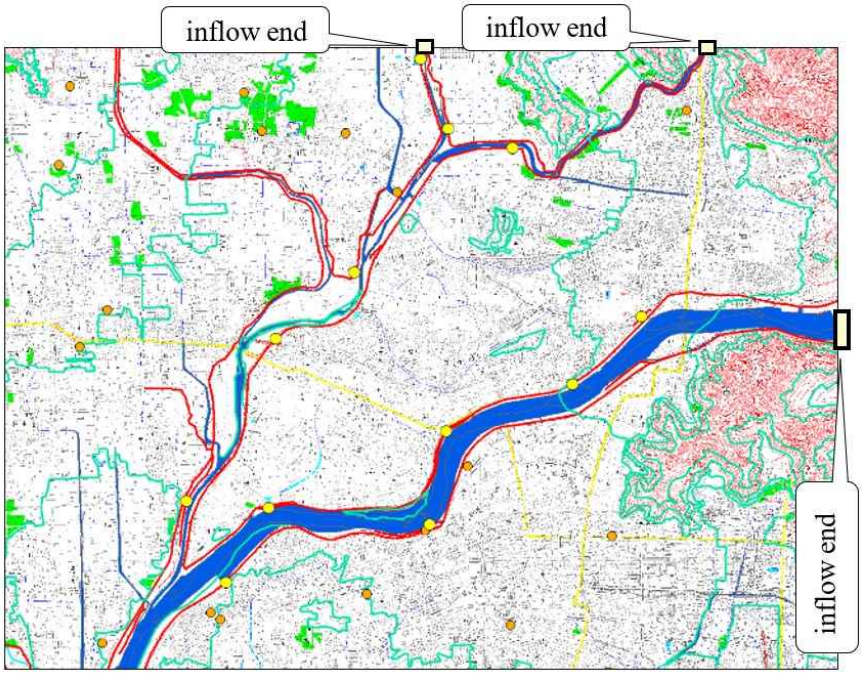

Figure 4.4 Digitized symbols in 2009 (Heisei era).

Figure 4.3 and Figure 4.4 show the digitized symbols for the past and current topographical maps. The digitized shapefiles are rasterized and interpolated to the 10 m grid by the method of Ohno and Tamura [Ohno 2002] in order to flood inundation analysis.

4.2.2. Land use data

Land use/cover in the study area are dramatically changed from 1891 to 2009. Figure 4.5 and Figure 4.6 are shown the land use changes from 1891 to 2009. These land use data are digitized from the topographical maps in the Meiji era and the Heisei era [Nakamura 2018]. The land use is categorized into 8 classes such as urban area, public, factory, forest, farmland, paddy field, wasteland, and water area. In the Meiji era, urban area extended to the left levee of the mainstream of the Nagara River. The almost area between the Nagara River and Ijira River is covered by farmland. On the other hand, the urban area extends to both sides of the mainstream of the Nagara River in the Heisei era. Figure 4.5 and 4.6 show that the urban area has dramatically developed in the last 100 years in the study area.

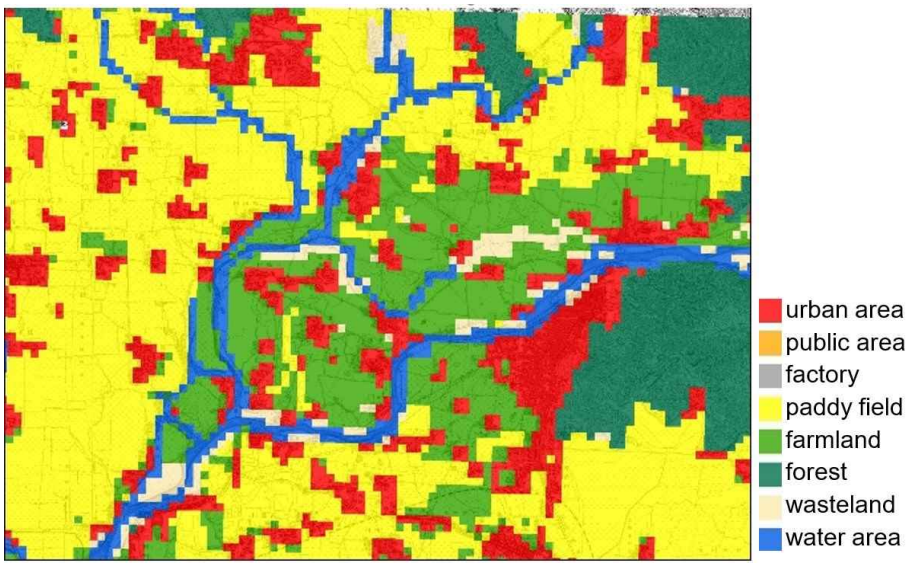

Figure 4.5 Land use map in 1891 (Meiji era).

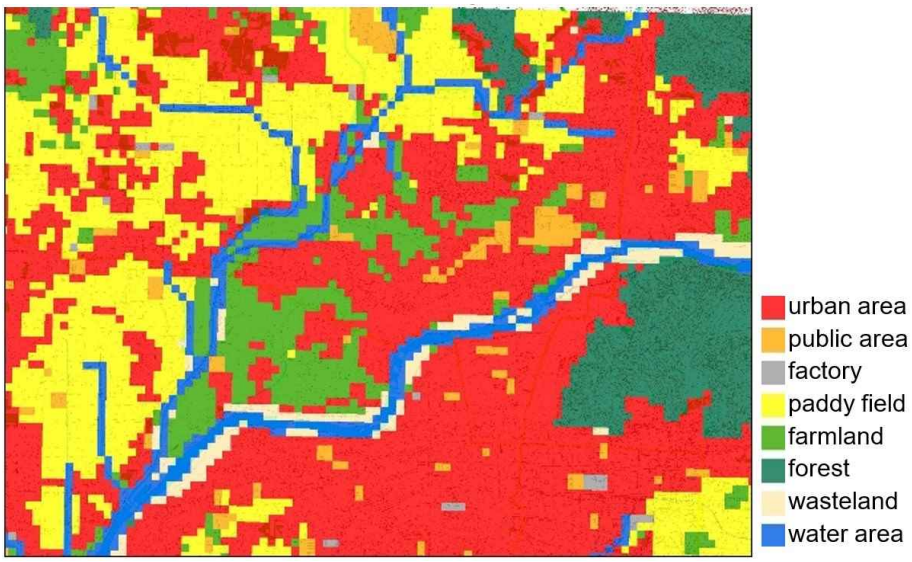

Figure 4.6 Land use map in 2009 (Heisei era).

4.3. Method

4.3.1. Flood simulation model

In this chapter, iRIC Nays 2D Flood [Shimizu 2014], an analytical solver for calculation of unsteady two-dimensional plane flow and riverbed deformation using boundary-fitted coordinates within general curvilinear coordinates is used to flood inundation simulation. In the above mentioned, which introduced about iRIC flood model. (See the section 3.3.1)

4.3.2. Computational conditions

When performing flooding calculation using iRIC Nays 2D Flood, in addition to the numerical elevation model created in the previous chapter, the setting of a hydrograph showing the inflow and flow rate from each river, boundary condition of calculation lattice and a time step of the calculation are necessary to set. The flood calculation was carried out with three hydrographs set in Section 3.3.1 for the two numerical elevation models of Gifu city in the past and the current time.

Hydrograph:

In this study, inflow hydrographs are set to the three rivers such as the Nagara River, Ijira River, and Toba River. The Nagara River basin is about 1620 km^2. On the other hand, the Ijira River and Toba River are relatively small basin as about 48 km^2 and 55 km^2. The inflow hydrograph of the Nagara River is defined with the basic high water which is used for the basic policy of river improvement announced on August 31, 2007, by the Ministry of Land, Infrastructure, and Transportation [Ministry of Land Infrastructure and Transport of Japan. 2007], and determined as Figure 4.7(a). The peak flow rate of the reference hydrograph of the Nagara River is 8900m^3/s. And its time series was referenced the heavy rainfall event on November 2000. There is no reference hydrograph for the Ijira and Toba River. Thus, the Ijira River hydrograph was prepared by the following procedure.

1） The peak flow rate Q_p (m^3/s) is set using the rational formula as Equation. (4.1).

$$Q_p = f_p \frac{1}{3.6} rA \tag{4.1}$$

where: f_p = peak runoff coefficient

r = average rainfall intensity (mm/h)

A = catchment area (km^2)

2） Set the time to reach the peak flow rate from the flood arrival time formula as Equation 4.2. The current data is used for the flow path length and average slope of the river.

$$T_p = 1.67 \times 10^{-3} \left(L / \sqrt{S} \right)^{0.7} \tag{4.2}$$

where: T_p = flood arrival time (s)

L = flow path length of the river (km)

S = mean slope

3） Make a hydrograph using the kinematic wave method's motion equation as Equation 4.3 and the decreasing curve equation as Equation 4.4. Use Equation 4.3 when the flow rate increases and Equation 4.4 when the flow rate decreases.

$$Q_t = \frac{\sqrt{\sin\theta}}{N} (rt)^{\frac{5}{3}} B \tag{4.3}$$

$$Q_t = Q_0 K^{-(t-t_0)} \tag{4.4}$$

where: Q_t = flow rate at time t (m^3/s)

B = river width (m)

θ = river bed slope

N = equivalent roughness of river bed

Q_0 = flow rate at the time t_0

K = constant

The base flow rate was defined as 5 hours from the start of inflow. Also, the base flow rate was 100 m^3/s of the Nagara River and 20 m^3/s of other small rivers. The inflow hydrographs created by the above method are shown in Figure 4.5. The peak flow rate of the Ijira and Toba Rivers are less than 100 m^3/s, so, the second panel of Figure 4.7(b) shows the detail of the hydrographs of the Ijira and Toba rivers.

As mentioned above, the basic inflow hydrographs are defined as Figure 4.7. In this study, we prepared three patterns of hydrograph with peak flow as 1/4, 1/6, and 1/10 of the basic hydrographs shown in Figure 4.7, due to evaluate several disaster scales. The new patterns of hydrograph are shown in figure 4.8. The peak flow rate of the basic hydrographs assumes the disaster scale with 100-y return period. The hydrographs with 1/4, 1/6 peak flow are assumed the middle scale disaster, and 1/10 peak flow is assumed the small-scale disaster.

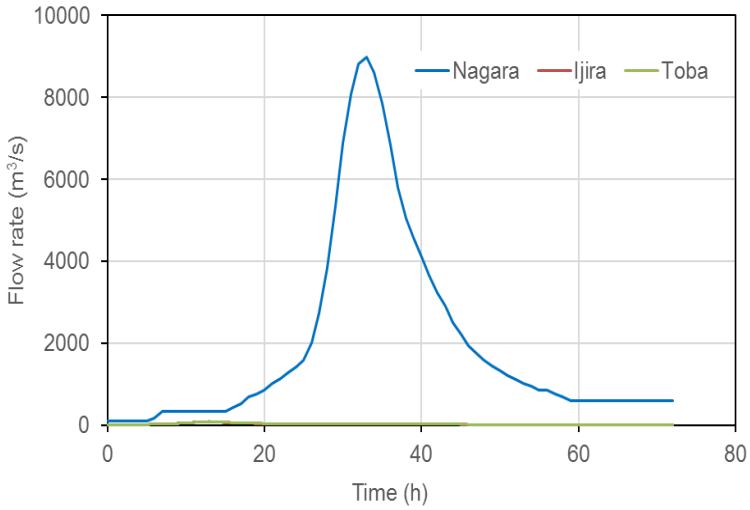

(a) Basic hydrographs of three rivers

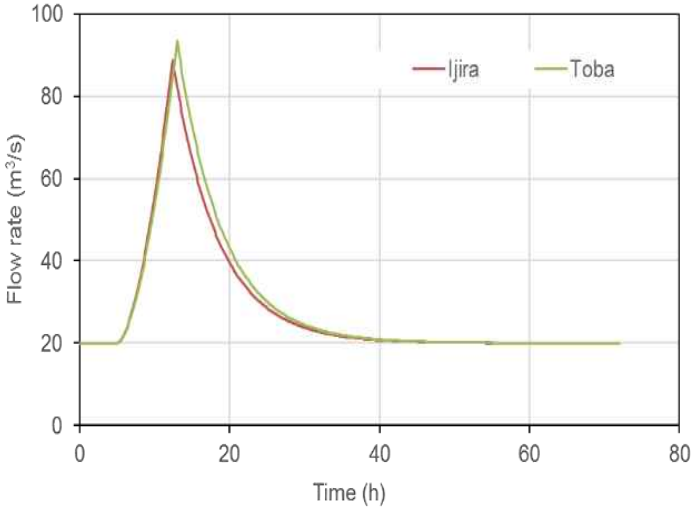

(b) Basic hydrographs of the Ijira and Toba Rivers

Figure 4.7. Basic inflow hydrographs for iRIC Simulation.

Parameter settings:

When performing flood inundation simulation, it is necessary to set boundary conditions, calculation grid, calculation time step, etc. The set parameters are summarized in Table 4.2. The inflow end of each river is set the upstream end of each river on the study area boundary line. The inflow ends are shown as black rectangle boxes in Figure 4.3 and Figure 4.4. Mentioned hydrographs are input from these inflow end into flood simulation boundary area. The boundary conditions are free-flowing at the southern and the western end of the grid, and the other flows are inflows. The following conditions must be taken into consideration in the size and time step of the calculation grid.

$$\Delta x > u\Delta t \tag{4.5}$$

where: u = flow rate in the x direction (m/s)

Δx = calculation grid size in the x direction (m)

Δt = calculation time step (s)

Table 4.2 Parameters

Number of grids	x direction	950
	y direction	700
Grid size (m)	x direction	10
	y direction	10
Method of difference method		Upwind difference
Calculation time step (s)		0.5
Boundary condition	East end	inflow
	West end	outflow
	North end	inflow
	South end	outflow
Roughness coefficient	Rivers	0.01
	Other than river	0.06
Land using type	Residential	0.5
	Non-residential	0

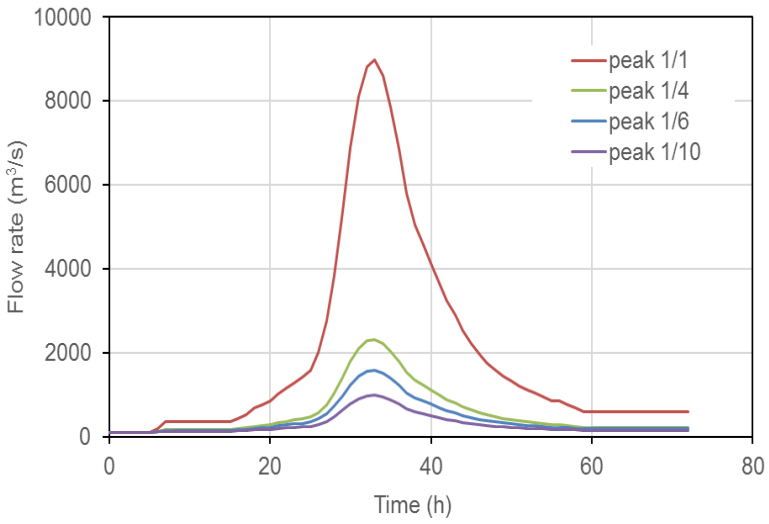

(a) The Nagara River

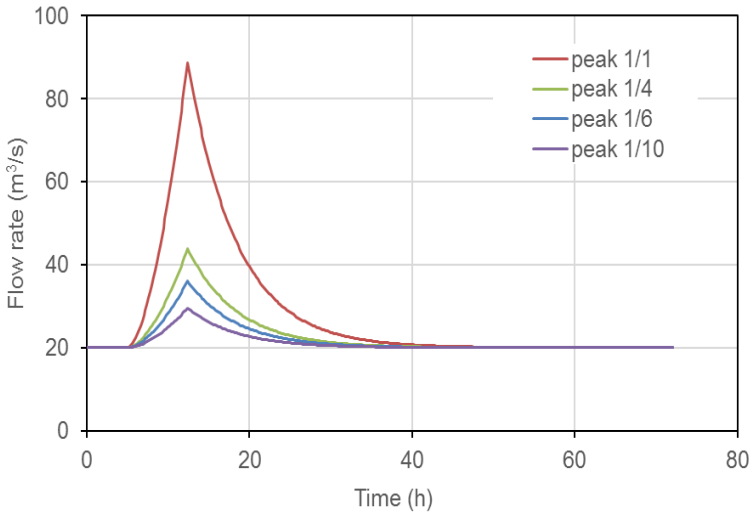

(b) The Ijira River

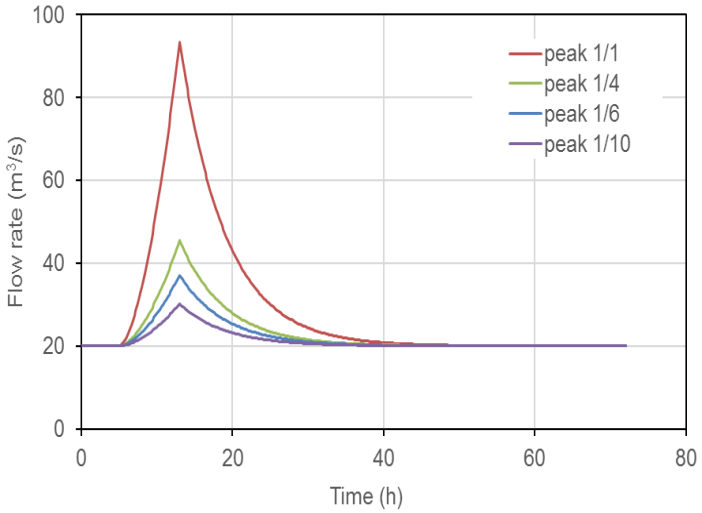

(c) The Toba River

Figure 4.8. Modified hydrographs for iRIC Simulation.

The grid size was 10m×10m, and the calculation time step was 0.5s. If the calculation time step is too small, the time required for the calculation becomes very long. To do all the flooding calculations, we set the calculation time step to this value.

4.3. Result and discussion

4.3.1. Flood inundation simulation

Flood simulation performed with the modified hydrographs for each era. The simulation result of the inundation area when using the basic hydrographs with 1/1 peak flow rate was covered over almost all of the study area. Because the differences of simulated flood inundation area between two eras were not so obviously from each other, we used the modified hydrographs to compare the disaster risks of two eras. Figure 4.9 shows the distribution of the maximum flood inundation depth simulated with the modified hydrographs with 1/4, 1/6, and 1/10 peak in 1890 (Meiji era). The simulation results with 1/4 and 1/6 peak have the almost same flood inundation area. Only the urban area on the left levee side of the Nagara River was not flooded. The area nearby the Mount Kinka is relatively higher elevation area. The almost all area between the branches of the Nagara River as the Furu and Furu-furu River were flooded. The simulation results with 1/10 peak showed relatively less flood inundation area than the other results. The many areas on the left levee side of the Nagara River were not flooded. This area became the urban area in 2009.

Figure 4.9 shows the distribution of the maximum flood inundation depth simulated with the modified hydrographs with 1/4, 1/6, and 1/10 peak in 2009 (Heise era). Figure 10 shows the flood inundation area reduced from the Meiji era.

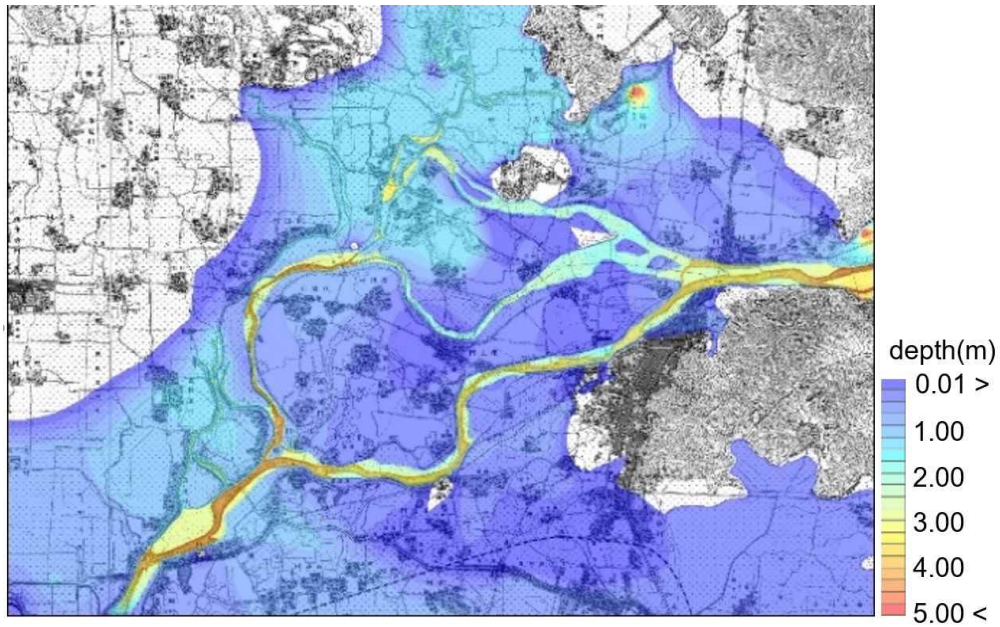

(a) Maximum flood inundation depth with 1/4 hydrograph

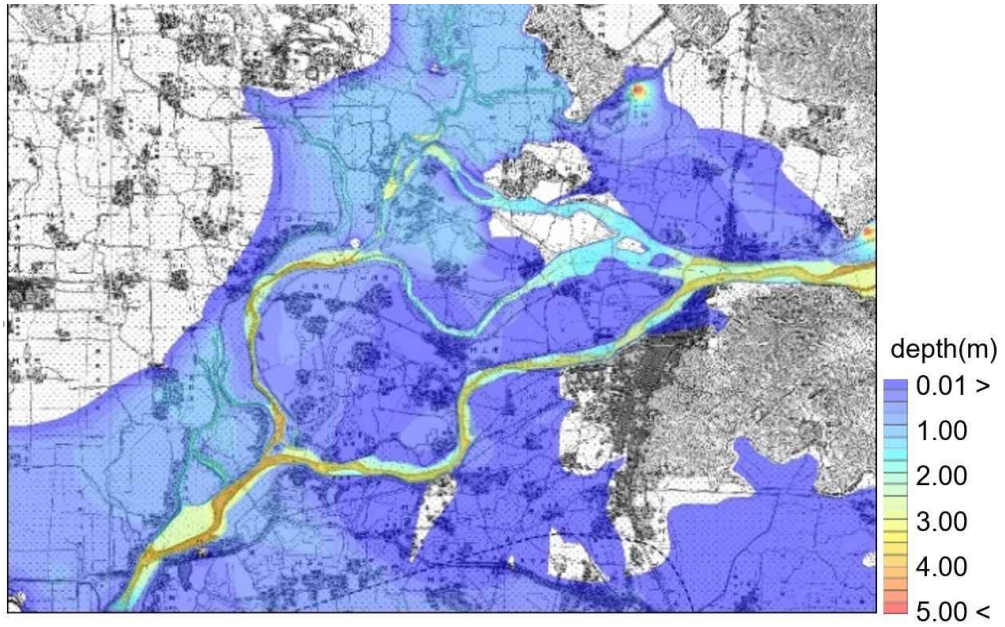

b) Maximum flood inundation depth with 1/6 hydrograph

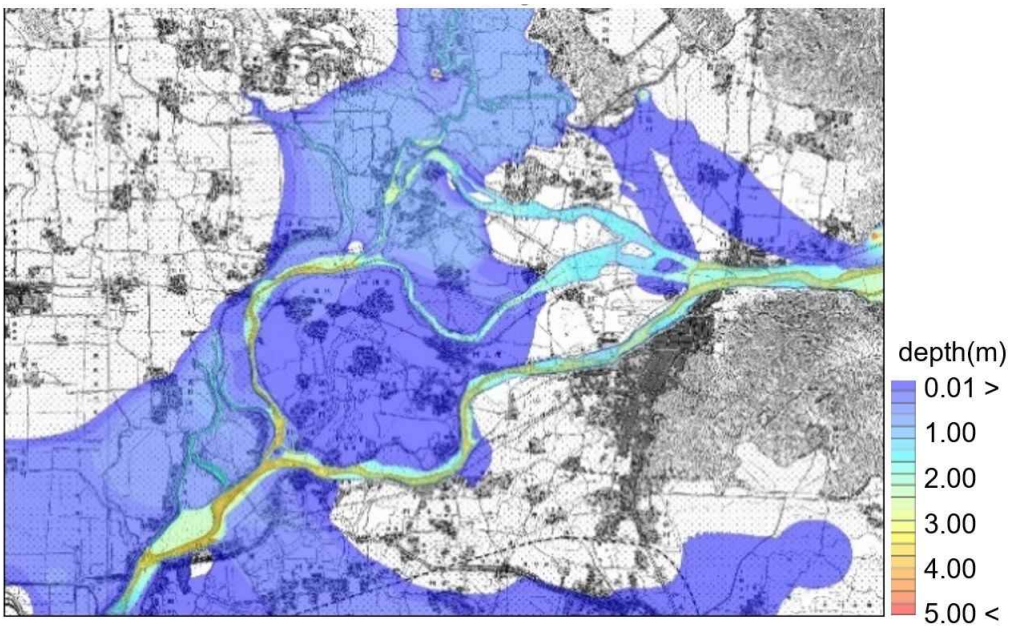

(c) Maximum flood inundation depth as 1/10 hydrograph

Figure 4.9. Distribution of maximum flood depth in 1891.

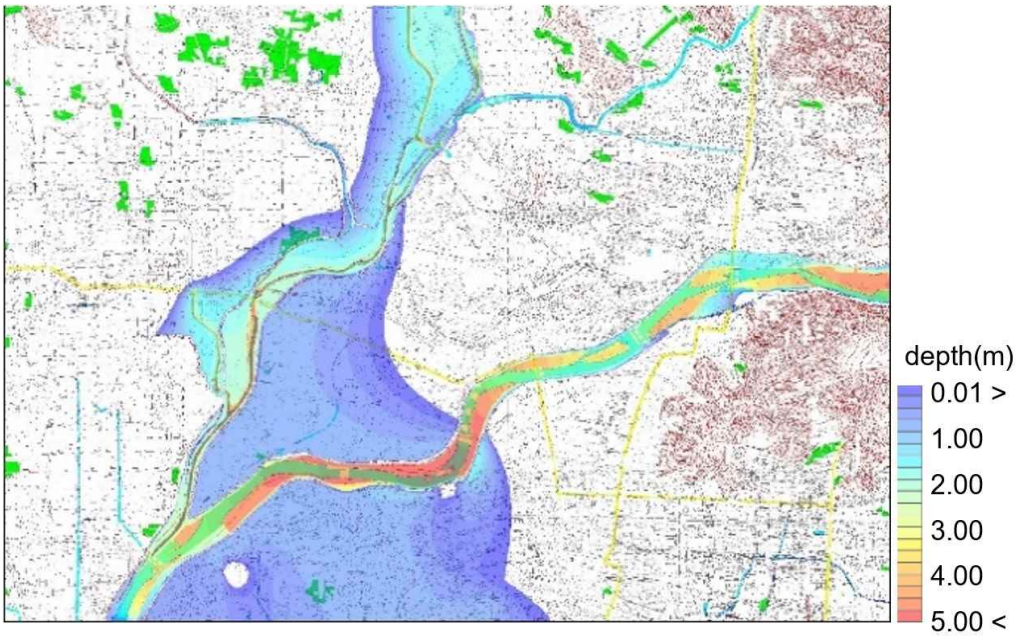

(a) Maximum flood inundation depth with 1/4 hydrograph

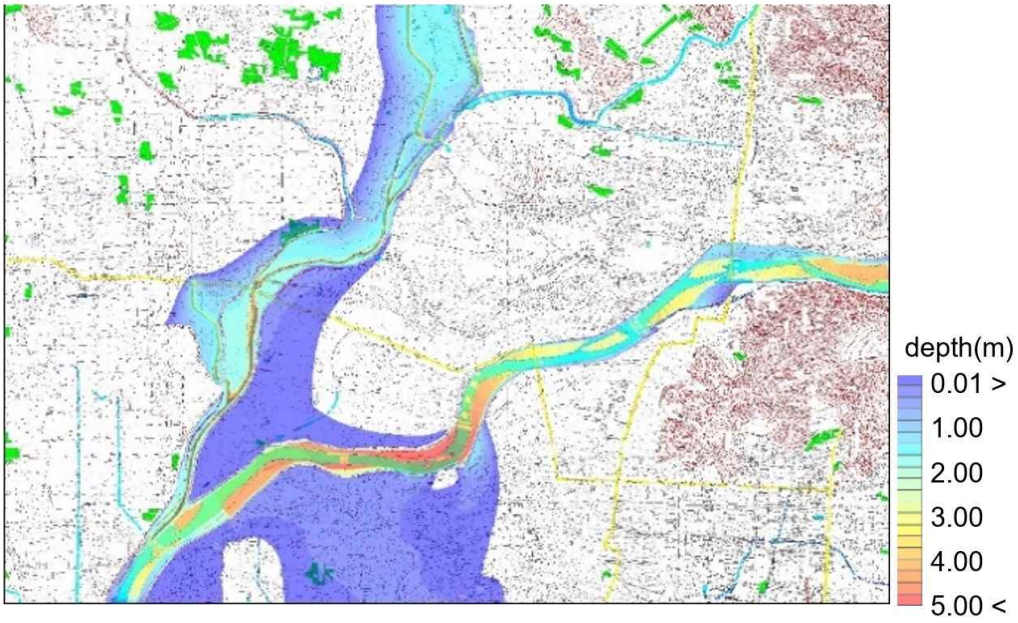

(b) Maximum flood inundation depth with 1/6 hydrograph

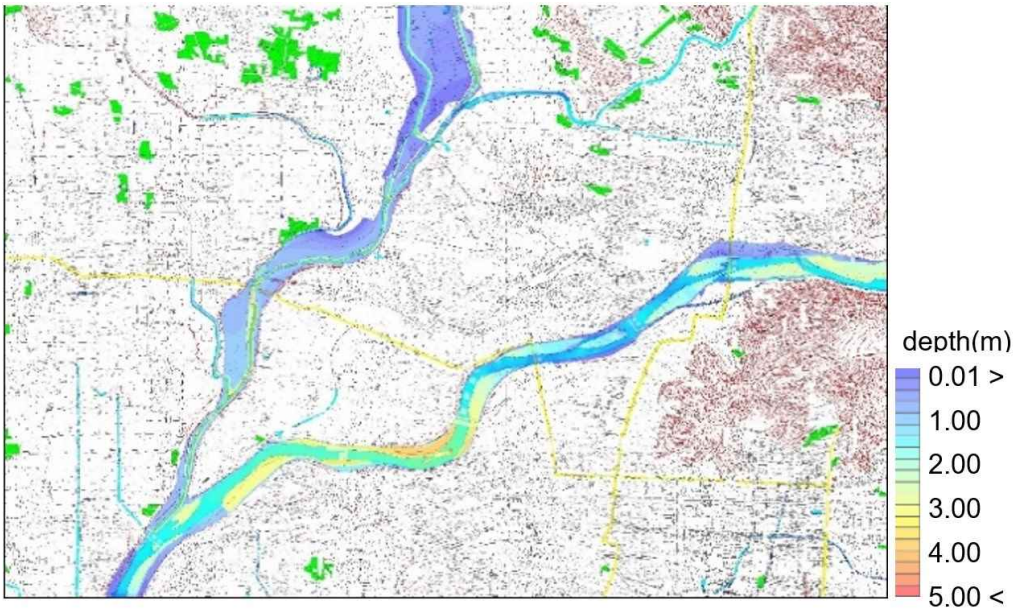

(c) Maximum flood inundation depth as 1/10 hydrograph

Figure 4.10. Distribution of maximum flood depth in 2009.

Figure 4.10 shows the comparison of the flood inundation area with each flood disaster scale as peak modification value. The flood inundation area with 1/4 peak in 2009 is less than 1/10 peak in 1891. The flood inundation area is significantly reduced. It is indicated that the river improvement has worked effectively for medium or less scale flood disaster.

4.3.2. Overlay with land use data

It is confirmed that the total flood inundation area is reduced by river improvement from 1891 to 2009. On the other hand, because the urban area is expanding in the last 100 years, as we mentioned in figures 4.5 and 4.6, the assessment of flood risk in the urban area is also essential. Therefore, we calculate the flood inundation area in the urban area as figure 4.12 with overlaying the flood inundation cover map and land use map. Figure 4.12 shows flood inundation area in the urban area for 1891 and 2009 are the almost same with 1/4 and 1/6 peak hydrographs. However, the results with 1/10 peak hydrograph are dramatically reduced from 3.82 km2 in 1891 to 0.48 km2 in 2009. For middle-scale flood disaster as 1/4 and 1/6 peak, it is suggested that flood risks in urban area are not decreased, because decreasing of flood risk by river improvement competed with urbanization around the river stream. However, for small scale flood disaster as 1/10 peak, the flood risk is dramatically reduced. It is suggested that the urban is hardly never flooded for small scale disaster. We also compared the maximum flood inundation depths in the urban area as figure 4.13. Maximum flood inundation depths are

slightly decreased from the Meiji era to the Heisei era. And the difference of flood inundation depth for small scale disaster is only a little, different from the results of flood inundation area.

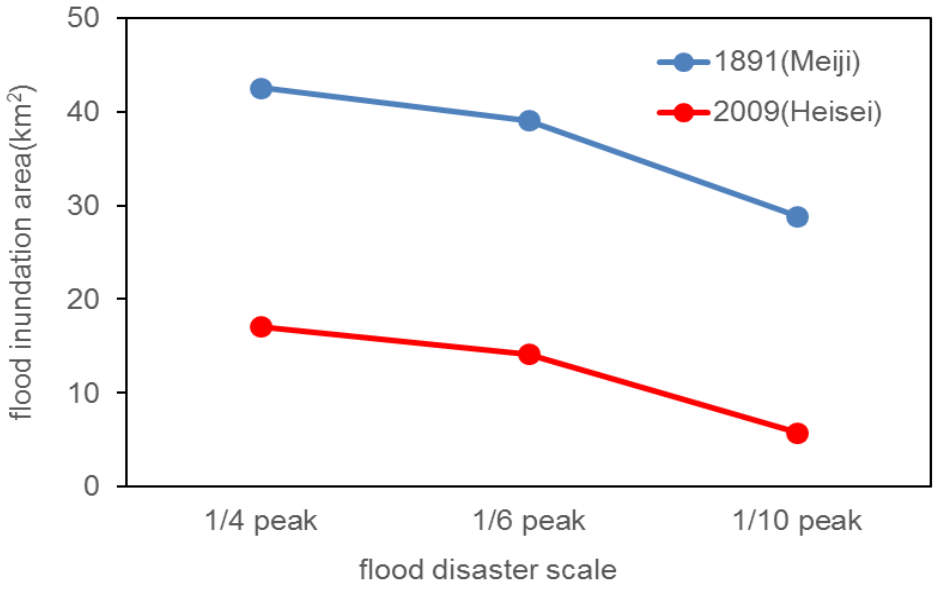

Figure 4.11 Comparison of flood inundation area for the whole of the study area.

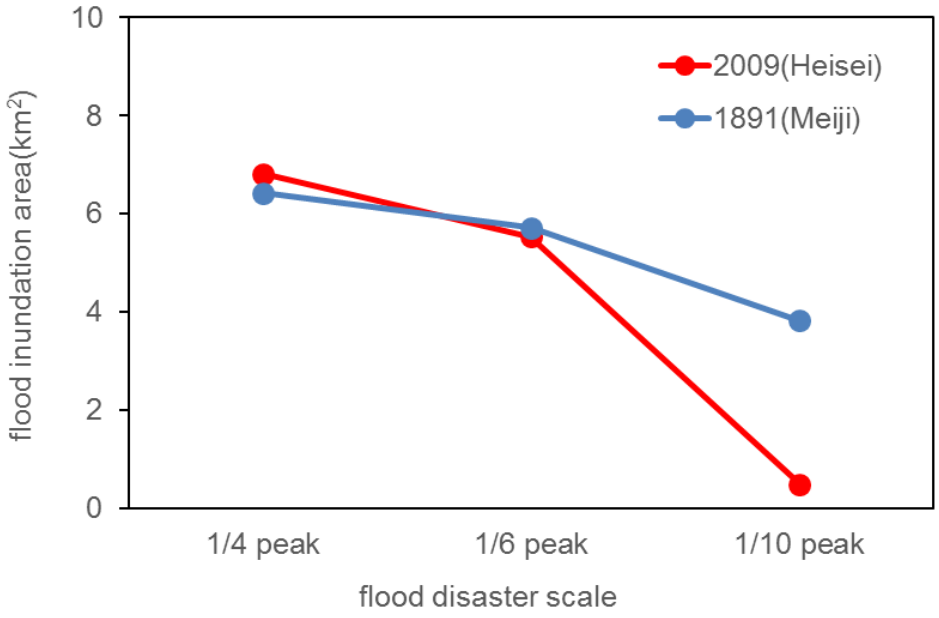

Figure 4.12. Comparison of flood inundation area for the urban area.

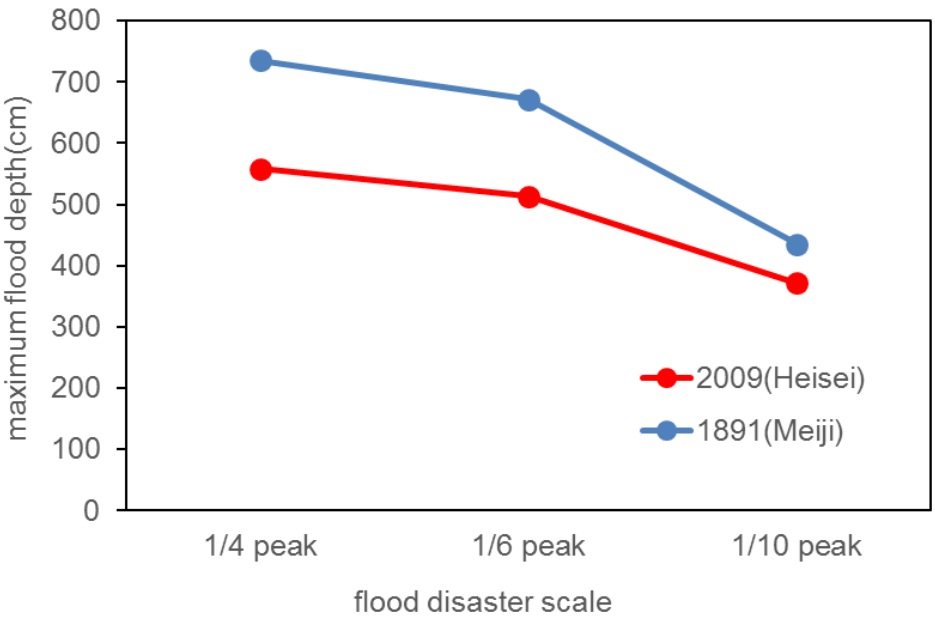

Figure 4.13 Comparison of maximum flood inundation depths for the urban area.

4.5. Summary

In this study, the authors investigate the relationship flood risk changes and land use changes with 2D flood inundation simulation in order to evaluate "Levee Effect" in Gifu City, Japan. The river infrastructures and stream networks of the Nagara River in Gifu City, Japan were improved in this past 100 years. The topographical maps in 1891 and 2009 are digitized in order to provide terrain data for flood inundation simulation. From the results of flood inundation simulation, it is shown that the flood inundation area for the same disaster scale has been decreased with the progress of river infrastructure improvement. However, only in the urban area, the flood inundation area for large and middle scale flood disaster are the almost same, the flood risks are not so much improved with the progress of river infrastructure improvement. On the other hands, the flooded area in the urban area for small scale flood disaster dramatically is reduced from 3.82 km² in the past time to 0.48 km² in the current time. The above results suggest that decreased of flood risk by river improvement for massive and middle disaster competed with urbanization around the river stream. Recent flood risk reduction by river infrastructures and improvement in the urban area mainly affects to small scale disaster and only small influence on large and middle scale disasters. These results provide essential knowledge for investigation of "Levee Effect".

CHAPTER 5. CONCLUSION

This chapter summarizes the results presented in this thesis for the purposes described in Section 1.3.

This research was made the following conclusions that described by each study of evaluation and assessment for long term changes in flooding using deep learning and flood simulation.

Firstly, Chapter 2 performed deep learning using CNN for the purpose of the classifying land use of highly accurate map images. Specifically, we aimed to put into practical use a method for classifying existing maps including map symbols by using deep learning. By the result, the overall accuracy (OA) is consistently 85% or higher, which provides a land use map of approximately 100 m of mesh in categories of 1: 25000 maps and it proposed a practical level land use classification method that can be shown.

The results obtained in this study are listed below.

- The number of samples to be taken per class must be 15,000 or more to show the actual level of accuracy of the classification. As for the number of learning samples, it is better to make the number of samples of each class uniform to some extent. If the number of training samples in each class is not balanced, the classification accuracy will decrease even if the total number of samples is large.
- Regarding the optimum number of learnings, the optimal number of surveys is approximately 5 times. When learning 10 or more times, the value of the loss function increases significantly and the effect of overfitting can be seen.
- There was no significant difference in the results of integration by the three proposed integration methods (Max method, Sum method, Mode method). When using the integrated method, it is recommended that the number of learning samples in each class be 10,000 or more.

Chapter 3 performed the temporal changes of flood risks from the Meiji era to the current time in Gifu city are investigated with an old topographical map, GIS analysis, and flood simulation.

The findings in this research are summarized as follows:

- Land use changes are investigated by the comparison of the old map and current map. The area of paddy fields in the target area decreased by 30% from the Meiji era to the current time.
- The flood simulation with the iRIC and 5-m DEM published by Japanese GSI is attempted using a sample hydrograph. It is showed that the iRIC and 5-m DEM have a good effect on the simulation of flood inundation. It showing the flood prevention system and other river improvements are working great.
- The DEM in Meiji era is produced by the interpolation technique with the contour lines from the old topographical map. However, the interpolation with contour lines could not produce good DEM, which is suitable for flood simulation. In a normal map, elevations on the river bed are uncertain. Therefore, the interpolated river bed is often not smooth from up to downstream, as the mentioned results in this chapter. In the simulation results, the discharge from upstream is blocked by the irregular grid, and the unexpected overflow occurs in the upstream. It is showed that iRIC and high-resolution DEM has an excellent performance to simulate the flood inundation. The improvement of the interpolation technique from contour lines is one of the essential tasks for the evaluation of flood inundation risks with old topographical maps.

Chapter 4. Moreover, understanding of "Levee Effect", land use changes and flood risk by flood inundation simulation have not yet been fully investigated. The river infrastructures and stream networks of the Nagara River were improved in this past 100 years.

From the results of flood inundation simulation, it is shown that the flood inundation area for the same disaster scale has been decreased with the progress of river infrastructure improvement. However, only in the urban area, the flood inundation area for large and middle scale flood disaster are the almost same, the flood risks are not so much improved with the progress of river infrastructure improvement. On the other hands, the flooded area in the urban area for small scale flood disaster dramatically is reduced from 3.82 km^2 in the past time to 0.48 km^2 in the current time. The above results suggest that decreased of flood risk by river improvement for massive and middle disaster competed with urbanization around the river stream. Recent flood risk reduction by river infrastructures and improvement in the urban area mainly affects to small scale disaster and only small influence on large and middle scale disasters. These results provide essential knowledge for investigation of "Levee Effect".

REFERENCES

1. Priess, J.A., et al., *The consequences of land-use change and water demands in Central Mongolia.* Land Use Policy, 2011. **28**(1): p. 4-10.
2. Mandakh, U., et al., *Impacts of rapid changes of land cover and intensive human activities on avarga toson lake area, Mongolia.* Sustainability, 2020. **12**(15): p. 6070.
3. Japan Aerospace Exploration Agency, J. *High-Resolution Land Use and Land Cover Map of Japan.* 2016 [cited 2021 November 23]; Available from: https://www.eorc.jaxa.jp/ALOS/a/en/dataset/lulc/lulc_jpn_e.htm.
4. Tateishi, R., et al., *Production of global land cover data-GLCNMO2008.* Journal of Geography and Geology, 2014. **6**(3): p. 99.
5. Nishikawa, Himiyama Y, *"Atlas - Environmental Change in Modern Japan (in Japanese)."*. Modernization and Lan Use Change, 1995: p. 2-3.
6. Ikemi, H., Tetsuro ESAKI, Yasuhiro MITANI and Tu Anh TRAN, *Spatial Distribution of Human Impacts on Terrain Based on Land-use Change Analysis -Development and GIS Analysis of Land-use Maps since 1900 in the Fukuoka Prefecture Area (in Japanese).* Journal of the Japan Society of Engineering Geology, 2011. **52**(3): p. 97-108.
7. Ohara, Y. and A. Ymashita, *Mesh Data Analysis on Land Use Change and Its Correlation with Topographic Condition in Sapporo, Tokyo and Osaka Metropolitan Areas.* Geographical Studies, 2011. **86**(1): p. 55-71.
8. Collenteur, R.A., et al., *The failed-levee effect: Do societies learn from flood disasters?* Natural Hazards, 2014. **76**(1): p. 373-388.
9. Heine, R.A., Pinter, Nicholas, *Levee effects upon flood levels: an empirical assessment.* Hydrological Processes, 2012. **26**(21): p. 3225-3240.
10. Baldassarre, G.D., et al., *Socio-hydrology: conceptualising human-flood interactions.* Hydrology and Earth System Sciences, 2013. **17**(8): p. 3295-3303.
11. Nakamura S, I.Y., *Development of long-term land use data in the Kiso River basin and quantitative evaluation of Levee Effect.* Proceedings of Japan Society of Hydrology and Water Resources, 2018: p. 298-299.
12. History of the Japanese and Gifu. *The history of Nagara River, water damage and water control*. 2010 [cited 2021 29 November]; Available from: https://gifurekisi.web.fc2.com/rekisi/no31.htm.

13. Ministry of Land Infrastructure and Transport of Japan. *国土交通省: 国土数値情報 土地利用細分メッシュ*. 2021 [cited 2021 April 09]; Available from: https://nlftp.mlit.go.jp/ksj/gml/datalist/KsjTmplt-L03-b.html.
14. Geospatial Information Authority of Japan, *国土交通省国土地理院: 細密数値情報 (10m メッシュ土地利用)*. 2020.
15. Geospatial Information Authority of Japan, *国土交通省国土地理院: 数値地図 5000(土地利用)*. 2020.
16. Center for Global Environmental Research, *国立環境研究所地球環境研究センター: 全国土地利用データベース*. 2020.
17. 山本勝利, *里地におけるランドスケープ構造と植物相の変容に関する研究*. 農業環境技術研究所報告, 2001. **20**: p. 1-105.
18. 児島利治, 寶., *土地被覆, 空間分解能と蒸発散の関係に関する研究 -衛星データと 2km メッシュ土地利用データを用いて*. 環境システム研究論文集, 土木学会, 2002. **30**: p. 85-90.
19. 松原彰子, 郭俊麟, 高田佳奈, *GIS を用いた土地利用変化の解析：慶応義塾大学日吉キャンパスを例にして*. 慶応義塾大学日吉紀要. 社会科学, 2007. **17**: p. 1-8.
20. 池見洋明, 江崎哲郎, 三谷泰浩, TRAN, T.A., *土地利用の変遷分析に基づく人為的な地形改変の空間分布－福岡県域を対象とした 1900 年以降の土地利用データの作成と GIS 分析—*. 応用地質, 2011. **52**(3): p. 97-108.
21. 大原譽丈, 山下亜紀郎, *メッシュデータを用いた札幌・東京・大阪圏における土地利用変化と地形の関係分析*. 地理学論集, 2011(86).
22. 伊藤悠一郎, 中., *木曽川における長期土地利用データの構築と Levee Effect の定量的評価,*. 水文・水資源学会 2018 年度研究発表会, 2018: p. 298-299.

23. ドニー・クスハルドノ, 福., 下田陽久, 坂田俊文, *マルチバンド画像を対象とした同時生起行列に基づくニューラルネットワーク土地被覆分類モデルの検討.* 日本リモートセンシング学会誌, 1996. **16**(1): p. 36-49.

24. Franklin, S.E., R. J. Hall, L. M. Moskal, A. J. Maudie and M. B. Lavigne, *Incorporating texture into classification of forest spe-cies composition from airborne multispectral images.* Int. J. Remote Sensing, 2000. **21**: p. 61-79.

25. Lobo, A., K. Moloney and N. Chiariello, *Fine-scale mapping of a grassland from digitized aerial photography: an approach using image segmentation and discriminant analysis.* Int. J. Remote Sensing, 1998. **19**: p. 65-84.

26. 小坂尚子, 秋., 蔡斌, 児島利治, *高分解能衛星画像のテクスチャ特徴量とスペクトル特徴量を用いたオブジェクト指向型林分タイプ分類.* 写真測量とリモートセンシング, 2007. **46**: p. 27-36.

27. 山本遼介, 泉., 松山洋, *都市域の土地被覆分類におけるピクセルベース手法とオブジェクトベース手法の比較—高解像度デジタル航空写真を用いて—.* 日本リモートセンシング学会誌, 2017. **37**: p. 236-247.

28. 伊東里保，飯野翔太，藤田藍斗，今泉友之，彦坂修平, *ディープラーニングを適用した衛星画像からの土地利用分類手法の評価.* 第 30 回人工知能学会全国大会論文集, 2016.

29. Tateishi, R., N. T. Hoan, T. Kobayashi, B. Alsaaideh, G. Tana and D. Xuan, *Production of Global Land Cover Data – GLCNMO2008.* J. Geography and Geology, 2014. **6**: p. 99-122.

30. 吉原篤, 滝., 有木康夫, *衛星画像における分類精度の向上を目的とした CNN の導入および非学習領域への応用検証.* 神戸大学都市安全研究センター研究報告, 2017. **21**: p. 151-156.

31. 平島景, 重., 杉本知史, 石塚洋一, 宮島廣美, *半教師あり学習を用いた空中写真からの CNN による土地利用分類.* 第 36 回ファジィシステムシンポジウム講演論文集, 2020: p. 277-282.
32. 岩崎亘典, 和., *Deep Learning での地図タイル活用の検討.* Proceedings of the 31st Annual Conference of the Japanese Socie-ty for Artificial Intelligence, 2017: p. 2B1-5.
33. 花島裕樹, *土地利用データにおける主題属性の誤差評価.* 第 18 回 GISA 学術研究発表大会梗概集, 2009: p. 77-80.
34. Thomlinson, J.R., P. V. Bolstad and W. B. Cohen, *Coordinating methodologies for scaling landcover classifications from site-specific to global: steps toward validating global map products.* Remote Sensing of Environment, 1999. **70**: p. 16-28.
35. 児島利治, 宝馨, *リモートセンシング画像の空間分解能と土地被覆分類精度の関係—4 種の画像と低分解能化アルゴリズムを用いて—.* 日本リモートセンシング学会誌, 1996. **16**(23-37).
36. Congalton, R.G., *A review of assessing the accuracy of classifications of remotely sensed data, .* Remote Sensing of Environment, 1991. **37**: p. 35-46.
37. 清水英範, 児島利治, *人工衛星画像のファジィ分類法への GMDH の適用可能性—ニューラルネットワークとの比較を中心として—.* 写真測量とリモートセンシング, 1994. **33**: p. 4-11.
38. Zhang, L., D. Li, Q. tong and L. Zheng, *Study of the spectral mixture model of soil and vegetation in PoYang Lake area, China.* Int. J. Remote Sensing, 1998. **19**: p. 2077-2084.
39. 石田晴海, 稲., *ミクセルデータに対する多重分校画像のカテゴリー分類性能評価.* 日本リモートセンシング学会誌, 2002. **22**: p. 2-11.
40. Omnimap East View Companies. *Japan Topographic Maps*. 2021 [cited 2021 30 November]; Available from: https://www.omnimap.com/catalog/int/japan2.htm#p5.
41. El Emary, I.M., Ramakrishnan, S, *Wireless sensor networks: from theory to applications*. 2019: CRC press.

42. Biodiversity Center of Japan, M.o.t.E. *Report of Vegetation Survey on 3rd National Basic Survey on Natural Environment* 2021 [cited 2021 November 23]; Available from: http://www.biodic.go.jp/copyright/index_e.html.
43. Bolstad, P., *GIS fundamentals: a first textbook on geographic information systems.* GIS fundamentals. A first text book on geographic information systems. White Bear Lake, Minnesota, 2008.
44. Childs, C. *Interpolating Surfaces in ArcGIS Spatial*. 2004.
45. Watson, R.T., et al., *Land use, land-use change and forestry: a special report of the Intergovernmental Panel on Climate Change*. 2000: Cambridge University Press.
46. Ministry of land Infrastructure Transport and Tourism. *Water Information system*. 2020 [cited 2021 1 December]; Available from: http://www1.river.go.jp.
47. Ministry of Land Infrastructure and Transport of Japan. *The Kiso River water system river improvement basic policy-a document about basic high water.* 2007 [cited 2021 April 09].
48. Bedient, P.B., W.C. Huber, and B.E. Vieux, *Hydrology and floodplain analysis*. Vol. 816. 2008: Prentice Hall Upper Saddle River, NJ. chapter 3
49. iRIC software. *Changing river science*. 2021 [cited 2021 1 December]; Available from: https://i-ric.org/en/download/.
50. Yasuyuki Shimizu, *iRIC Software Changing River Science Nays2D Flood Solver Manual*, E.S. Takuya Inoue, Satomi Kawamura, Toshiki Iwasaki, Michihiro Hamaki, Kensuke Omura, Eriko Kakegawa, Tomohiko Yoshida,, Editor. 2015.

ACKNOWLEDGMENTS

This work would not have been possible without the support of the people listed below and many others I appreciate.

First of all, the gratefully acknowledged supervisor Professor Toshiharu Kojima gave me a great opportunity to fulfill my doctoral study. This doctoral study has hugely benefited from his supervision and continuous guidance, professional advice in this research study as well as with various support and amicable cooperation during all of the stages.

At the same time, I am extremely thankful to Professor Shinoda Seirou and Keisuke Ohashi and all of the members of the Laboratory of River and Hydrology, Faculty of Engineering, Gifu University, for their direct guidance in carrying out this research.

We would also like to express our gratitude to the to the professors and all of the members of the Rearing Program for Basin Water Environmental Leaders, Gifu University, for providing me support in study and research whenever I needed.

Last but not least, I would like to express my deep gratitude to my dear son, mother, siblings and family for always giving me all the support and encouragement and thanks to everyone for your supports that make this research complete.

I feel incredibly fortunate knowing that all of your great love and affection will continue to be for my future.